Microvesicles in disease

Inauguraldissertation

zur

Erlangung der Würde eines Doktors der Philosophie

vorgelegt der

Philosophisch-Naturwissenschaftlichen Fakulät

der Universität Basel

von

Arun Čumpelik

aus Prag, Tschechische Republik

Basel, 2014

Genehmigt von der Philosophisch-Naturwissenschaftlichen Fakultät der Universität Basel auf Antrag von:

Prof. Dr. Jürg A. Schifferli

Prof. Dr. Jean Pieters

Prof. Dr. Ed Palmer

Basel, den 16. September 2014

Prof. Dr. Jörg Schibler, Dekan

Namensnennung-Keine kommerzielle Nutzung-Keine Bearbeitung 3.0 Schweiz
(CC BY-NC-ND 3.0 CH)

Sie dürfen: **Teilen** — den Inhalt kopieren, verbreiten und zugänglich machen

Unter den folgenden Bedingungen:

Namensnennung — Sie müssen den Namen des Autors/Rechteinhabers in der von ihm festgelegten Weise nennen.

Keine kommerzielle Nutzung — Sie dürfen diesen Inhalt nicht für kommerzielle Zwecke nutzen.

Keine Bearbeitung erlaubt — Sie dürfen diesen Inhalt nicht bearbeiten, abwandeln oder in anderer Weise verändern.

Wobei gilt:

- **Verzichtserklärung —** Jede der vorgenannten Bedingungen kann **aufgehoben** werden, sofern Sie die ausdrückliche Einwilligung des Rechteinhabers dazu erhalten.
- **Public Domain (gemeinfreie oder nicht-schützbare Inhalte) —** Soweit das Werk, der Inhalt oder irgendein Teil davon zur Public Domain der jeweiligen Rechtsordnung gehört, wird dieser Status von der Lizenz in keiner Weise berührt.
- **Sonstige Rechte —** Die Lizenz hat keinerlei Einfluss auf die folgenden Rechte:
    - Die Rechte, die jedermann wegen der Schranken des Urheberrechts oder aufgrund gesetzlicher Erlaubnisse zustehen (in einigen Ländern als grundsätzliche Doktrin des **fair use** bekannt);
    - Die **Persönlichkeitsrechte** des Urhebers;
    - Rechte anderer Personen, entweder am Lizenzgegenstand selber oder bezüglich seiner Verwendung, zum Beispiel für **Werbung** oder Privatsphärenschutz.
- **Hinweis —** Bei jeder Nutzung oder Verbreitung müssen Sie anderen alle Lizenzbedingungen mitteilen, die für diesen Inhalt gelten. Am einfachsten ist es, an entsprechender Stelle einen Link auf diese Seite einzubinden.

Quelle: http://creativecommons.org/licenses/by-nc-nd/3.0/ch/ Datum: 12.11.2013

Table of Contents

Section 3 Erythrocyte-derived microvesicles amplify systemic inflammation by thrombin-dependent activation of complement.

General Summary

On activation cells shed vesicles from their surface by the process of ectocytosis. These micro-vesicles or Ectosomes express phosphatidyl-serine (PS) on their surface, which can elicit a range of biological effects from immune-suppression to the activation of the clotting and complement pathways. While the full consequence of this phenomena is still subject of intensive research, it is clear that microvesicles, despite their size, can profoundly impact the immune system.

The aim of this thesis was to study clinically relevant scenarios where micro-vesicle release alters the course of inflammation. The conditions studied were:

1. The release of neutrophil microvesicles (PMN-Ecto) and spontaneous resolution of Gout.

   Gout is an inflammatory arthritis caused by mono-sodium urate crystals (MSU) precipitating in joints. When attempting to clear MSU, resident macrophages activate their inflammasome complex and release large amounts of highly inflammatory cytokine IL-1β. One of the intriguing features of gout is that acute attacks resolve spontaneously and leave minimal residual damage to the joint. The mechanism driving the resolution of gout is still poorly understood. We hypothesized that the early release of PMN-Ecto during acute gout contains the inflammatory response to MSU.

   In a murine peritonitis model of gout we found that the release of IL-1β following stimulation with MSU relied on the generation of C5a by MSU itself. Neutrophils infiltrating the peritoneum in response to C5a released phosphatidylserine (PS)-positive ectosomes early on in the course of inflammation. Treatment of the peritoneum with these PMN-Ecto in turn resulted in suppression of IL-1β release and translated in a decrease of PMN influx. Ectosome-mediated suppression could be reproduced using PS-expressing liposomes and required the presence of the PS-receptor MerTK. Finally, PMN-Ecto from joint aspirates of patients with gouty arthritis had similar anti-inflammatory properties. Ectosome-mediated control of inflammasome-driven inflammation is a compelling concept of autoregulation initiated early on during PMN activation in gout.

2. Platelet microvesicles (PLT-Ecto) and sub-clinical disseminated intravascular coagulopathy (DIC) during anti-thymoglobulin therapy (ATG).

   Anti-Thymo-Globulins (ATG) are T-cell depleting antibodies used for hematopoietic stem cell (HSCT) and kidney (NTX) transplant patients as an immuno-suppressant to prevention graft vs. host disease (GvHD). Although designed to target T-cell, ATG recognizes a wide range of epitopes, including those present on platelets. Consequently the rapid infusion of ATG frequently cause side effects that are associated with the overt activation of the clotting system called DIC. The mechanism relating ATG therapy to DIC remains unclear. We hypothesized that ATG induces DIC by the release of pro-coagulant PLT-Ecto.

   We could demonstrate that ATG induces platelet activation, degranulation and release of PLT-Ecto. The shedding of PLT-Ecto required the presence of complement and could be inhibited by an anti-C5 blocking antibody. PLT-Ecto exhibited high pro-thrombinase activity. The blocking of C5 during ATG treatment of platelets therefore indirectly inhibited thrombin generation. In HSCT and NTx patients, ATG treatment resulted in elevated levels of d-dimer and thrombin-anti-thrombin complexes indicating heightened state of clotting. Furthermore, we could confirm the presence of PLT-Ecto in patients plasma and ATG dose dependent complement fragment deposition on PLT-Ecto.
   In conclusion, ATG induced complement dependent release of pro-coagulant PLT-Ecto and the use of anti-C5 antibody may prove to be beneficial in preventing thrombotic complications during ATG therapy.

3. Red Blood cell microvesicles (RBC-Ecto) and transfusion related complication.

   Transfusion of RBC is known to exacerbate systemic inflammation and increase morbidity and mortality of critically ill patients. The adverse effect of RBC transfusions has been attributed to changes that occur during extended periods of RBC storage. The ageing process of RBC is accompanied by the shedding of RBC-Ecto, which accumulate in storage and are transfused along with RBC. We hypothesized that RBC-Ecto derived from aged RBCs amplify systemic inflammation and contribute to some of the deleterious effects of aged blood transfusions.

We established a murine transfusion model using RBC-Ecto purified from aged erythrocytes. While the injection of RBC-Ecto into healthy mice had no effect, transfusion of RBC-Ecto amplified systemic inflammation in endotoxemic mice. These effects were mediated by a thrombin depenedent activation of C5 complement factor on the surface of RBC-Ecto. Consequently, the treatment of mice with a thrombin anticoagulant prior to transfusion alleviated the proinflammatory effects of RBC-Ecto. The inhibition of thrombin in vivo lead to suppresion of systemic C5a generation, inflammatory cytokine release and subsequently lung neutrophil sequestration.

In conclusion, we could identify RBC-Ecto as potential mediators of transfusion related morbidity. RBC-Ecto mediated their effects by sequentially activating the coagulation and complement system, which then aggrevated systemic inflammation.

General introduction

Microvesicles, Ectosomes and Exosomes

Micro-vesicle (MV) is a general term used to describe sub-micron sized vesicles released by cells upon stimulation (1, 2). Based on their mechanism of release, MV's can be divided into two distinct subsets, Ecto-somes and Exo-somes. Ectosomes (Ecto) are vesicles shed directly from the surface of the cell. During ecto-cytosis small cytoplasmic protrusions bud outward from the plasma membrane and detach by fission of their stalk (Figure 1). Exosomes, unlike Ectosomes, are formed by the intra-cellular inward budding of the late endosomal compartment and released by the exocytosis of these multi-vesicular bodies (MVB) (Figure 1). The different mechanisms by which MVs are formed reflect in the way they convey their biological message. While Ectosome rely on direct cell-MV contact, Exosome alter cell behavior by delivering their cargo molecules (miRNA) to target cells (2, 3). The biological effect of MVs is therefore defined either by what they express on their surface (Ectosomes) or by what they contain and transfer to cells (Exosomes). MV release represents a new form of inter-cellular communication. Neutrophil (PMN), erythrocyte (RBC) and platelet (PLT) Ectosomes are the subject of this thesis.

Vesicles shed by ectocytosis maintain their right-side out orientation of their plasma membrane, but lose the asymmetrical distribution of membrane phospholipids characteristic for resting cells. The absence of lipid asymmetry and expression of phosphatidyl-serine (PS) is one of the defining features of ectosomes and is closely related to both their biological effect and mechanism of release (1).

Although resting cells release ectosomes constitutively, the rate of the process increases dramatically upon stimulation (4-6). Sub-lytic complement attack, C5a, fMLP, phorbol ester activation of protein kinase C and Ca^{2+} ionophores are known to induce strong shedding responses (7-11). The converging mechanism of these triggers, is the influx or release of Ca^{2+} accompanying cell stimulation. Ca^{2+} influx drives the translocation of PS, a phospholipid from the inner side of the plasma membrane, to the outer leaflet (12). PS exposure is followed by MV release allowed by cytoskeleton degeneration by Ca^{2+} dependent proteolysis. Membrane remodeling and MP shedding seems to be a fundamental process probably shared by virtually all cell types. Ectosomes released by activated PMN, RBC and PLT consequently stain positive for Annexin V (AnV), which binds PS. Microvesicles, unlike their parent cells, continue to stably express PS since they lack the energy necessary to restore asymmetric lipid distribution.

Neutrophil ectosomes (PMN-Ecto) were initially described as a means by which neutrophils confer resistance to a sub-lytic complement attack. During complement activation, neutrophils expel membrane attack complexes (MAC, C5b-9) by ectocytosis of vesicles (7). The shedding of vesicles has later been confirmed to be a generalized phenomena of neutrophil activation. C5a and fMLP induce one of the strongest shedding responses (9).

PMN-Ecto are heterogeneous, predominantly spherical vesicles that range 100-500nm in size. During ectocytosis PMN-Ecto acquire a select panel of proteins and lipids, from their parent cells (8, 9). This implied early on that ectocytosis is not a random event, but involves specific sorting mechanisms. PMN-Ecto express CD66b, CR1, selectins, integrins (CD11a,CD11b), complement regulators (CD46, CD55, CD59), HLA-1 and FcγRIII, but not CD14, FcγRII and CD87. The selective inclusion and exclusion of proteins is not specific to transmembrane or GPI-linked proteins. In addition, PMN-Ecto actively recruit neutrophil enzymes from azurophilic (MPO, PR3 and NE) and specific (MMP-9) granules to their surface. These enzymes retain their catalytic activity. As all ectosomes, PMN-Ecto express PS on their surface and consequently stain positive for Annexin V (AnV), Annexin A1 (AnA1), C1q and Gas6 (9, 13).

PMN-Ecto are anti-inflammatory. PMN-Ecto generated by C5a stimulated PMN attenuate the cytokine response (TNFα, IL-6,-8,-12) of human monocyte derived macrophages (HMDM) to TLR ligands (LPS, ZymA) in vitro (14). They achieve this by engaging the MerTK-PI3K/Akt pathway, which inhibits NFκB trans-activation upon TLR stimulation (15). The binding of PMN-Ecto to cells is sufficient to mediate suppression and PS containing liposomes can reproduce their effect. In addition to PS, PMN-Ecto foster these anti-inflammatory effects by inducing the release of TGFβ in target cells (16).

Erythrocyte ectosomes (RBC-Ecto) were first described to be released by erythrocyte under complement attack (11). As with PMN-Ecto, RBC-Ecto shedding allows erythrocytes to survive sub-lytic complement activation by removal of the MAC (C5b-9 complex). RBC-Ecto can also be released in a much slower and gradual process of erythrocyte senescence (17-19). The progressive decline in membrane fluidity, osmotic stability, lipid and protein oxidation is accompanied by the release of RBC-Ecto. This is particularly apparent during extended storage of erythrocyte transfusion units (storage lesion) where RBC-Ecto accumulate over time.

RBC-Ecto are homogenous spherical vesicles 50-200nm in size that express glycophorin A, complement regulators (CR1, CD55, CD59) and contain hemoglobin (19). RBC-Ecto are PS positive and bind both C1q and Annexin V (AnV). RBC-Ecto generated either from aged RBC or

induced by a Ca^{2+} ionophores suppress HMDM pro-inflammatory cytokine response to TLR ligands the same way as PMN-Ecto with exception of their inability to trigger TGFβ release.

Platelet ectosomes (PLT-Ecto) are released by activated platelets and constitute the dominant population of circulating MVs. Circulating PLT-Ecto are shed by activated platelets and support hemostasis by generating thrombin on their negatively charged PS expressing surface (20-22). As with all Ecto, PLT-Ecto can be induced by sub-lytic complement attack (10) and their release is triggered by the Ca^{2+} influx caused by C5b-9 deposition (23).
PLT-Ecto are 100-500nm in size and express platelet specific markers (CD36, CD41, CD47, CD61), complement inhibitors (CD55, CD59) and PS (24). In addition to membrane proteins, PLT-Ecto bind C1q and factor H from plasma. PLT-Ecto are known to down-modulate immune responses of HMDM in vitro.

Ectosomes, The Inflammasome and Gout

Gout is a type of inflammatory arthritis triggered by the precipitation of MSU crystals in joints (25). MSU crystals are a potent activator of the NLRP3 inflammasome complex, a molecular platform that is responsible for IL-1β secretion (26). IL-1β is a crucial mediator that drives gouty inflammation (25).

The NLRP3 inflammasome is primarily designed to integrate bacterial (pathogen associated molecular patterns, PAMP) and danger signals (danger associated molecular patterns, DAMP) (25, 27, 28) (Figure 2). The purpose behind this design is to ensure the inflammasome is active only in a circumstances when pathogenic microbes are causing tissue damage. This allows the immune system to mount a coordinated response to infection and injury, while remaining unresponsive to ‘harmless’ non-self. This ‘danger’ hypothesis has been first articulated by Matzinger who defined innate immunity as a danger sentinel (29-31). The dual requirement for concomitant PAMP and DAMP stimulation is inbuilt in innate cells, which express low levels of critical components of the inflammasome (pro-IL-1β, NLRP3), which in the absence of PAMP limits their activation potential (32-34). MSU and MSU crystals in this context represent danger signals (35). Uric acid is an end product of purine metabolism and high extracellular concentrations of MSU signify high cell turnover and cell damage. The precipitation of MSU crystals in joints has various triggers including infection and joint trauma. Resident macrophages attempt to clear these crystals, but ultimately fail due to absence of uricase and

the crystal size that greatly exceeds their own. This is followed by some form of MSU danger recognition, inflammasome activation and IL-1β release.

Specific recognition of MSU by the inflammasome is highly unlikely on account of the structural diversity of stimuli that have been shown to induce the NLRP3-dependent IL-1β secretion. It is hypothesized that all NLRP3 stimuli, including MSU, share the ability to trigger several intracellular events that result in NLRP3 activation (27) (Figure 3). Mitochondrial ROS is considered to be the most likely proximal signal for NLRP3 activation (36-38). The association of the inflammasome is purposeful, since mitochondria are sensitive to metabolic stress and ROS are evolutionary conserved signals of danger. In fact, any mitochondrial stressor can induce the NLRP3 inflammasome assembly and recently thioredoxin-interacting protein (TXNIP) has been identified as the ROS sensitive regulator of the NLRP3 inflammasome (37). Phagocytosis is essential for particulate inflammasome activators (25, 39-41). Another model suggest that the uptake of particulates stimuli (AL, MSU) causes disruption of lysosomal membrane and the release of putative NLRP3-activating lysosomal contents (cathepsin B) into the cytosol causing cleavage of NLRP3 or its inhibitor (40, 42). Alternatively, ionic perturbations (K^+ efflux, Na^+ and H_20 influx) due to endogenous ion channel ($P2X_7$ channel for ATP) or pore-forming bacterial toxins (nigericin) lead to intracellular hypo-kalemia and NLRP3 activation (43-46). All three mechanisms are non-exclusive. Considering that: K+ efflux can lead to ROS production and ROS positively modulates K^+ efflux (47, 48); K+ efflux is involved in the initiation of phagocytosis (49); ROS is a major promoter of lysosomal rupture and lysosomal permeabilization can induce ROS (50, 51), it is plausible to assume that some form of signal integration takes place and likely converges on the ROS-TXNIP-NLRP3 axis. The NLRP3 inflammasome essentially detects a combination of loss of membrane stability (K+ efflux and lysosomal destabilization) and heightened metabolic stress (mitochondrial ROS).

Inflammasome activation involves the assembly of the NLRP3 complex and caspase-1 activation. NLRP3 consists of three components: the central nucleotide-binding and oligomerization domain (NACHT) flanked by the C-terminal leucine-rich repeats (LRRs) and N-terminal pyrin domain (PYD). Activation signals are sensed by the LRR domain, which normally in an auto-repressed state obscuring access to the NACHT and PYD domain with the assistance of the SGT1 and HSP90 chaperones (26, 52). Upon sensing of intracellular danger signals, LRR auto-repression is relieved and the PYD and NACHT domain is exposed. This allows NLRP3 oligomerization by homotypic association of NACHT domains and the recruitment of the PYD-CARD adaptor ASC, which then recruits pro-caspsae-1 molecules. Pro-caspase-1

clustering leads to auto-activation to caspase-1 and subsequent cleavage of pro-IL-1β to IL-1β and its release.

IL-1β has a wide range of biological effects (53). Systemically IL-1β acts as an endogenous pyrogen, induces an acute phase response, vasodilation and hypotension. Locally, IL-1β is a strong neutrophil and monocyte chemo-attractant, activates endothelial cells and facilitates neutrophil rolling and extravasation, enhances leakiness of capillaries and mediates sensation of pain. Consequently joints undergoing a gout attack present with swelling, redness, warmth and are extremely painful to touch. A gout attack typically escalates within an hour and can be even accompanied by systemic symptoms of fever and hypotension.

In addition to IL-1β complement activation contributes to the inflammatory response to MSU crystals. High levels of active complement fragments are present in synovial fluids of patients with acute gout (54-56). The functional importance of complement has also been illustrated in animal models of acute gout, where depletion of, or deficiency in, complement components resulted in abrogation of MSU crystal-induced inflammation (57-59). Experiments with human serum in vitro have shown that MSU crystals activate complement by the classical and alternative pathway (56, 60-62). Although IgG can be found coating MSU crystals, the activation of C1q and the classical pathway was independent of IgG (60). In fact, the activation of many of the complement proteins appears to involve direct interactions with the negatively charged crystal surface, including assembly of a functional C5 convertase complex at the crystal surface resulting in the generation of active C5a (63). In vitro, C5a generated by MSU treated human sera, acted as a strong neutrophil chemo-attractant (63). C5a could be potentially responsible for amplifying neutrophil recruitment and licensing the inflammasome by C5aR mediated activation of NFκB (64-66). Concurrently, C5a induces a strong vesiculation response in neutrophils, which consequently release large amounts of PMN-Ecto (9, 14).

The acute gouty inflammatory response is typically self-limiting within 7-10 days and leaves minimal residual damage to the joint (67). While there is no conclusive model on how gout resolution occurs, a range of potential mechanisms have been suggested and include: release of TGFβ, clearance of apoptotic cells and desensitization of caspase-1.

TGFβ is regarded as the prime mediator in the active resolution of gout. In clinical studies elevated levels of TGFβ have been reported in the synovial fluid of patients in the late stages of gout, suggesting that TGFβ may be involved in maintaining inflammatory quiescence during

asymptomatic periods (68-70). Furthermore, patients carrying functional polymorphisms of TGFβ had a higher incidence of a more aggressive forms of gout (tophaceous gout) (71). In vivo, extraneous administration of TGFβ attenuated neutrophil recruitment in response to MSU in a rat air-pouch model (72). In vitro studies have shown that as monocytes differentiate into macrophages they progressively lose their ability to release IL-1β and gain the capacity to release TGFβ in response to MSU (73). This implied that the resolution of gout is the consequence of monocyte differentiation. TGFβ in this model also suppressed the release of TNFα by LPS stimulated monocytes and inhibited endothelial cell activation in response to inflammatory cytokines (74). In monocytes TGFβ was shown to suppress IL-6 release by in response to IL-1β. Despite the indication of TGFβ involvement in gout, the mechanism of suppression remains unknown and cellular sources of endogenous TGFβ undefined.

Another possible mechanism that may initiate resolution of gout is the clearance of apoptotic neutrophils. Neutrophils are the dominant cell population infiltrating the joint space during gout. They typically have a short life span and undergo apoptotic cell death in later phases of inflammation (75). Apoptotic neutrophils convey their anti-inflammatory signals by at least three mechanisms. PS expressed by apoptotic cells can activate various PS receptors including the family of TAM receptors (consisting of Tyro, Axl, Mer). The MerTK receptor is the most extensively studied and has been shown to suppress the inflammatory response of macrophages and DCs to TLR ligands (76). Furthermore, apoptotic cells are known to induce the synthesis and release of TGFβ (77, 78). The mechanisms of TGFβ release is not yet understood and may be associated with PS expression (78). Finally, the uptake of apoptotic cells alters the behavior of macrophages by inducing the so called alternative activation or M2 phenotype (79, 80). Alternatively activated macrophages release anti-inflammatory cytokines (IL-10), pro-resolving lipid mediators (resolvins) and take part in connective tissue repair (Arginase) (81, 82).

Lastly, the activation of the inflammasome complex can be restricted by two basic means that reflect the inherent/inbuilt limitations of the system. Low pro-IL-1β and NLRP3 expression in myeloid cells are the limiting factors of the inflammasome complex and therefore, prior to activation, the inflammasome requires licensing (32). Once primed, however, inflammasome activation is not self-sustaining and requires continuous pro-IL-β synthesis. The clearance or inactivation (C5a) of the priming agent may lead to a decline in inflammasome activation as the synthesis of pro-IL-1β starts to lag behind the rapid pace of IL-1β release. Furthermore caspase-1 is a protease prone to inactivation by changes in redox potential (83). ROS

generated during mitochondrial stress were identified as one of the ‘danger’ signals necessary for inflammasome assembly and caspase-1 activation. Superoxide radicals are also known to modify redox-sensitive cysteines and can inadvertently inactivate caspase-1. This may provide temporal or dose dependent negative feedback of caspase-1 activity.
We hypothesized that the timely and efficient resolution of gout is initiated early on by PMN-Ecto released by infiltrating neutrophils.

Ectosomes, Complement and Coagulation

Platelet ectosomes (PLT-Ecto) represent the largest population of circulating MV in blood (84). In the presence of plasma, PS expressed on the surface of PLT-Ecto can provide a catalytic surface for the assembly of the pro-thrombinase enzyme complex and initiate the coagulation cascade (85). Furthermore, thrombin can serve as an alternate C3/C5 convertase activating the complement system (86). Due to the cross-talk between coagulation and complement system, more clotting can translate to more inflammation.

Platelets are responsible for primary hemostasis. The activation of platelet is accompanied by the translocation of PS to the membrane surface and the release of PLT-Ecto. PS on PLT-Ecto significantly enhances the pro-coagulant activity of platelets by binding components of the clotting cascade. The association of PS and clotting factors is based on the electrostatic interaction between positively charged γ-carboxyglutamic acid (GLA) domains of clotting factors and negatively charged PS on PLT-Ecto. Clotting factors that contain the GLA domain include VIIa (initiating complex), FIXa (intrinsic tenase complex) and FXa (pro-thrombininase complex). Collectively these factors initiate the intrinsic coagulation pathway resulting in the generation of thrombin. Systemic activation of clotting can lead to disseminated intravascular coagulopathy (DIC) which is initially characterized by overactive clotting system and compromised microcirculation (thrombotic microangiopathy) followed by overt bleeding due to the consumption of clotting factors and loss of clotting potential.
Early studies demonstrated that the MV depletion prolonged the clotting time of human plasma and that activated platelets generated MV capable of supporting thrombin generation in platelet-poor plasma (87, 88). The functional significance of PS and PLT-Ecto release for efficient clotting can be illustrated on patients with Scotts syndrome. These patients have a primary bleeding disorder caused by the inability of platelets to translocate PS to their surface and release PLT-Ecto (22).

The release of PLT-Ecto can be induced by platelet stimuli such as thrombin or ADP. The vesiculation response is, however, much stronger during complement activation on the surface of platelets (10). Platelets exposed to sub-lytic concentration of C5b-9 were shown to release large amounts of small membrane vesicles capable of binding factor Va and assembling the pro-thrombinase enzyme complex (23). This form of platelet activation may be relevant in idiopathic thrombocytopenic purpura (ITP), an autoimmune condition with antibodies against platelet surface antigens that would initiate classical complement pathway activation and C5b-9 deposition (89). Alternatively, during T-cell depletion therapy with anti-thymoglobuins (ATG) which cross-react with platelet antigens (90).

ATG is the purified IgG fraction of sera from rabbits immunized with thymocytes (Thymoglobulin, Genzyme) or Jurkat cells (ATG Fresenius, Fresenius-Biotech). It is used in hematopoietic stem cell transplantation (HSCT) conditioning regimens to prevent graft vs. host disease (GvHD) or in kidney transplantation (NTX) as prevention or rescue treatment of acute rejection. ATG therapy is accompanied by various complications that include systemic activation of the coagulation system. Given that ATG recognizes platelet antigens, we hypothesized that ATG activates complement on the surface of platelets and induces the release of pro-coagulant PLT-Ecto, which accelerate clotting and cause thrombophilia.

Erythrocytes (RBC) release RBC-Ecto under same conditions. Clinically antibody recognition of RBC and subsequent complement attack is an unlikely event that would only occur when ABO incompatible blood was transfused. During the storage of RBC in transfusion units RBC undergo a range of biochemical and structural changes that include the formation of RBC-Ecto (18, 91, 92). In fact, RBC lose 20% of their hemoglobin content in the form of RBC-Ecto during storage and these vesicles that accumulate are given in significant amounts to patients along with RBC at the time of transfusion (17).

Clotting abnormalities with RBC transfusion are rare, but can be severe (93-96). Transfusion related acute lung injury (TRALI) is the most common cause of major morbidity and death after transfusion (97). The underlying mechanism of TRALI can be explained by the presence of contaminating leukocyte antibodies in the plasma of donor blood directed against human leukocyte antigens (HLA). The transfused anti-HLA antibodies target and activate neutrophils, which subsequently migrate to the lungs and compromise the pulmonary microcirculation. The

release of radicles and proteolytic enzymes by activated neutrophils damage the endothelial cells of lung capillaries. A pulmonary capillary leak syndrome develops resulting in pulmonary edema (98). Clinically TRALI presents as acute respiratory distress syndrome within 6h of transfusion. In 40% of TRALI patients, however, anti-leukocyte antibodies are absent in both the donor and recipient (99). The trigger for neutrophil activation in non-immune TRALI remains unknown.

We hypothesized that the transfusion of pro-coagulant RBC-Ecto brings about a state of heightened clotting and inflammation due to systemic thrombin activation and C5a generation, which triggers neutrophil sequestration in lung microcirculation.

Aims and Objectives

The aim of this thesis was to establish in vivo models of clinically relevant scenarios where micro-vesicle release alters the course of inflammation and provide mechanistic insights into disease pathophysiology. Specifically the aims were:

1. To investigate the role of neutrophil microvesicles (PMN-Ecto) and complement activation in the initiation and resolution of gout.

   In the first project the aim was to establish a murine peritonitis model of gouty arthritis and determine whether PMN-Ecto are released by infiltrating neutrophils and whether they have an anti-inflammatory effect in vivo. Furthermore, we aimed to investigate the role of complement activation in gout. Specifically the ability of C5a to trigger PMN-Ecto release and in turn suppress the potentially priming effect of C5a on the inflammasome. Finally, we aimed to verify the presence of PMN-Ecto in joint exudates of patients undergoing an acute gout attack and confirm their anti-inflammatory effect in vitro.
   We hypothesized that PMN-Ecto constitute an early counter-regulatory signal that helps initiate the resolution of gouty inflammation and explain its self-limiting nature.

2. To investigate the role of complement-induced platelet microvesicles (PLT-Ecto) release in the context of anti-thymoglobulin (ATG) induced coagulopathy.

   In the second project we set out to analyze whether ATG can induce complement dependent platelet activation, aggregation and PLT-Ecto release. Furthermore, we aimed to assess the ability of PLT-Ecto to activate the clotting cascade by assembling the pro-thrombinase complex. Finally, the aim was to correlate the activation of the complement and clotting system with the release of PLT-Ecto in patients receiving ATG.
   We hypothesize that ATG induces complement dependent platelet activation and release of PLT-Ecto. The release of these PLT-Ecto expressing PS then initiates systemic activation of the clotting system.

3. To investigate the mechanism by which Red Blood Cell microvesicles (RBC-Ecto) induce activation of the complement system and amplify inflammation in the context of transfusion related complications.

In the third project, the aim was to establish a murine transfusion model using RBC-Ecto purified from aged erythrocytes and measure the degree of inflammation after transfusion. Specifically we aimed at measuring systemic thrombin and C5a generation, IL-6 release and pulmonary leukocyte sequestration.

We hypothesized that RBC-Ecto derived from aged RBCs amplify systemic inflammation by thrombin dependent activation of C5 complement factor.

Figures

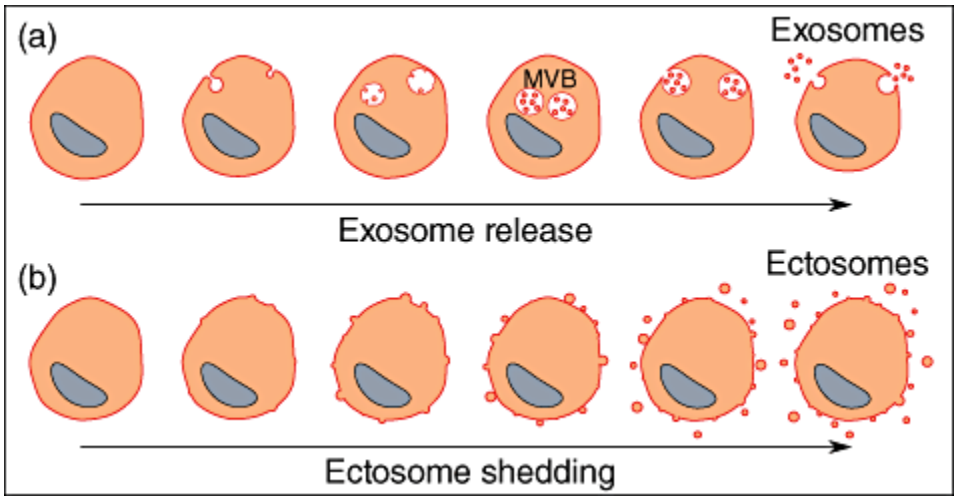

Figure 1.

Exosomes and ectosomes are microvesicles budding from a membrane. (a) Exosomes are produced by inward budding into the late endosomal compartment, called multi-vesicular bodies (MVB). When MVB fuse with the cell membrane, exosomes are released as preformed vesicles. (b) Ectosomes are small membrane vesicles shed by many cells by budding directly from the cell membrane. (100)

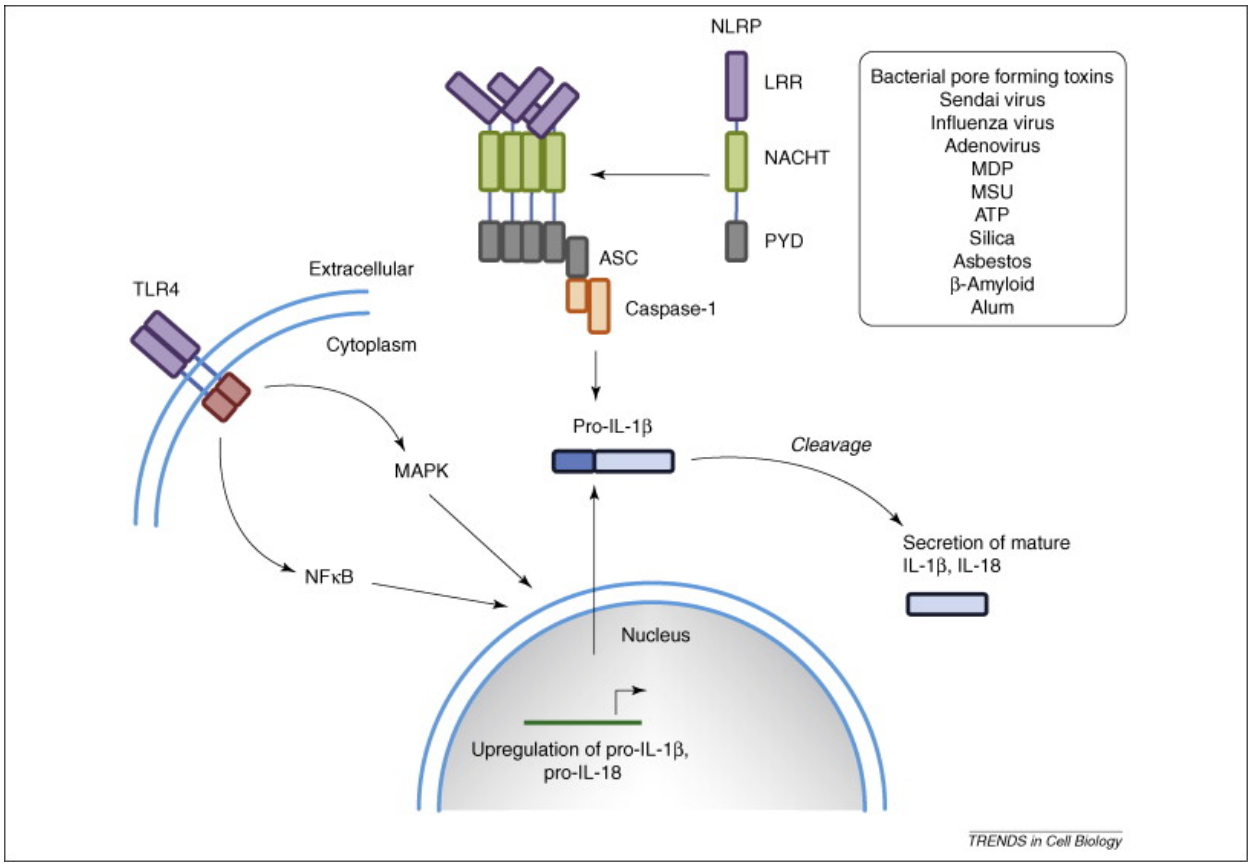

Figure 2.

Mechanisms regulating IL-1β production. Generation of IL-1β requires a priming signal, often from PRRs such as TLRs that activate NF-κB and NF-κB-dependent transcription of pro-IL-1β. The pro-IL-1β is then cleaved into the active, mature 17 kDa cytokine by caspase-1. NLR containing inflammasomes activate caspase-1. NLRs such as NLRP3 oligomerize upon activation (by danger signals such as those shown in the box) and recruit the adapter molecule ASC that subsequently recruits and activates caspase-1.(101)

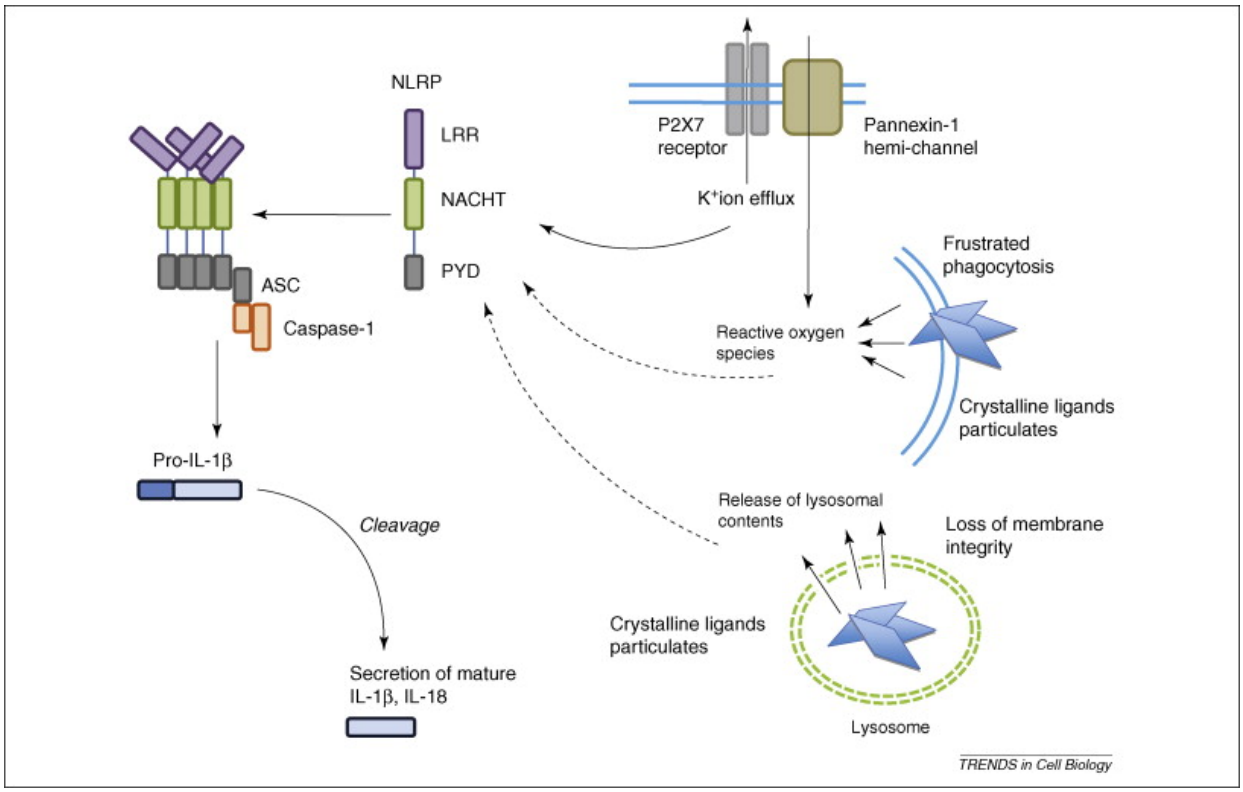

Figure 3.

Models of NLRP3 inflamamsome activation. The activation of NLRP3 has been shown to involve the ATP-gated P2X7R, pore-forming molecules or particulate ligands. Stimulation of P2X7R by extracellular ATP induces the activation of a cation channel that mediates potassium efflux. In addition, P2X7R activation promotes opening of the pannexin-1 pore, which may enable the cytosolic delivery of microbial molecules such as MDP. How particulate ligands activate NLRP3 is less clear. There is evidence that it may involve generation of ROS and additional studies suggest that destabilization of the lysosomal membrane and activation of the lysosomal protease cathepsin B (in the case of silica, urate crystals and fibrillar β amyloid) are critical. (101)

References

1. Cocucci E, Racchetti G, and Meldolesi J. Shedding microvesicles: artefacts no more. *Trends Cell Biol.* 2009;19(2):43-51.
2. Théry C, Ostrowski M, and Segura E. Membrane vesicles as conveyors of immune responses. *Nat Rev Immunol.* 2009;9(8):581-93.
3. Johnstone RM. Exosomes biological significance: A concise review. *Blood Cells Mol Dis.* 2006;36(2):315-21.
4. Moskovich O, and Fishelson Z. Live cell imaging of outward and inward vesiculation induced by the complement c5b-9 complex. *J Biol Chem.* 2007;282(41):29977-86.
5. Pilzer D, Gasser O, Moskovich O, Schifferli JA, and Fishelson Z. Emission of membrane vesicles: roles in complement resistance, immunity and cancer. *Springer Semin Immunopathol.* 2005;27(3):375-87.
6. Ratajczak J, Wysoczynski M, Hayek F, Janowska-Wieczorek A, and Ratajczak MZ. Membrane-derived microvesicles: important and underappreciated mediators of cell-to-cell communication. *Leukemia.* 2006;20(9):1487-95.
7. Stein JM, and Luzio JP. Membrane sorting during vesicle shedding from neutrophils during sublytic complement attack. *Biochem Soc Trans.* 1989;17(6):1082-3.
8. Stein JM, and Luzio JP. Ectocytosis caused by sublytic autologous complement attack on human neutrophils. The sorting of endogenous plasma-membrane proteins and lipids into shed vesicles. *Biochem J.* 1991;274 (Pt 2)(381-6.
9. Gasser O, Hess C, Miot S, Deon C, Sanchez JC, and Schifferli JA. Characterisation and properties of ectosomes released by human polymorphonuclear neutrophils. *Exp Cell Res.* 2003;285(2):243-57.
10. Sims PJ, Faioni EM, Wiedmer T, and Shattil SJ. Complement proteins C5b-9 cause release of membrane vesicles from the platelet surface that are enriched in the membrane receptor for coagulation factor Va and express prothrombinase activity. *J Biol Chem.* 1988;263(34):18205-12.
11. Iida K, Whitlow MB, and Nussenzweig V. Membrane vesiculation protects erythrocytes from destruction by complement. *J Immunol.* 1991;147(8):2638-42.
12. Bevers EM, Comfurius P, Dekkers DW, and Zwaal RF. Lipid translocation across the plasma membrane of mammalian cells. *Biochim Biophys Acta.* 1999;1439(3):317-30.

13. Dalli J, Norling LV, Renshaw D, Cooper D, Leung KY, and Perretti M. Annexin 1 mediates the rapid anti-inflammatory effects of neutrophil-derived microparticles. *Blood.* 2008;112(6):2512-9.
14. Gasser O, and Schifferli JA. Activated polymorphonuclear neutrophils disseminate anti-inflammatory microparticles by ectocytosis. *Blood.* 2004;104(8):2543-8.
15. Eken C, Martin PJ, Sadallah S, Treves S, Schaller M, and Schifferli JA. Ectosomes released by polymorphonuclear neutrophils induce a MerTK-dependent anti-inflammatory pathway in macrophages. *J Biol Chem.* 2010;285(51):39914-21.
16. Eken C, Sadallah S, Martin PJ, Treves S, and Schifferli JA. Ectosomes of polymorphonuclear neutrophils activate multiple signaling pathways in macrophages. *Immunobiology.* 2013;218(3):382-92.
17. Tissot JD, Rubin O, and Canellini G. Analysis and clinical relevance of microparticles from red blood cells. *Curr Opin Hematol.* 2010;17(6):571-7.
18. Lutz HU, Liu SC, and Palek J. Release of spectrin-free vesicles from human erythrocytes during ATP depletion. I. Characterization of spectrin-free vesicles. *J Cell Biol.* 1977;73(3):548-60.
19. Sadallah S, Eken C, and Schifferli JA. Erythrocyte-derived ectosomes have immunosuppressive properties. *J Leukoc Biol.* 2008;84(5):1316-25.
20. Wiedmer T, Esmon CT, and Sims PJ. Complement proteins C5b-9 stimulate procoagulant activity through platelet prothrombinase. *Blood.* 1986;68(4):875-80.
21. Wiedmer T, Esmon CT, and Sims PJ. On the mechanism by which complement proteins C5b-9 increase platelet prothrombinase activity. *J Biol Chem.* 1986;261(31):14587-92.
22. Sims PJ, Wiedmer T, Esmon CT, Weiss HJ, and Shattil SJ. Assembly of the platelet prothrombinase complex is linked to vesiculation of the platelet plasma membrane. Studies in Scott syndrome: an isolated defect in platelet procoagulant activity. *J Biol Chem.* 1989;264(29):17049-57.
23. Sims PJ, and Wiedmer T. Repolarization of the membrane potential of blood platelets after complement damage: evidence for a Ca++ -dependent exocytotic elimination of C5b-9 pores. *Blood.* 1986;68(2):556-61.
24. Sadallah S, Eken C, Martin PJ, and Schifferli JA. Microparticles (ectosomes) shed by stored human platelets downregulate macrophages and modify the development of dendritic cells. *J Immunol.* 2011;186(11):6543-52.
25. Martinon F, Pétrilli V, Mayor A, Tardivel A, and Tschopp J. Gout-associated uric acid crystals activate the NALP3 inflammasome. *Nature.* 2006;440(7081):237-41.

26. Martinon F, Burns K, and Tschopp J. The inflammasome: a molecular platform triggering activation of inflammatory caspases and processing of proIL-beta. *Mol Cell.* 2002;10(2):417-26.
27. Gross O, Thomas CJ, Guarda G, and Tschopp J. The inflammasome: an integrated view. *Immunol Rev.* 2011;243(1):136-51.
28. Schroder K, and Tschopp J. The inflammasomes. *Cell.* 2010;140(6):821-32.
29. Matzinger P. Introduction to the series. Danger model of immunity. *Scand J Immunol.* 2001;54(1-2):2-3.
30. Matzinger P. An innate sense of danger. *Ann N Y Acad Sci.* 2002;961(341-2.
31. Matzinger P. The danger model: a renewed sense of self. *Science.* 2002;296(5566):301-5.
32. Bauernfeind FG, Horvath G, Stutz A, Alnemri ES, MacDonald K, Speert D, Fernandes-Alnemri T, Wu J, Monks BG, Fitzgerald KA, et al. Cutting edge: NF-kappaB activating pattern recognition and cytokine receptors license NLRP3 inflammasome activation by regulating NLRP3 expression. *J Immunol.* 2009;183(2):787-91.
33. Franchi L, Eigenbrod T, and Núñez G. Cutting edge: TNF-alpha mediates sensitization to ATP and silica via the NLRP3 inflammasome in the absence of microbial stimulation. *J Immunol.* 2009;183(2):792-6.
34. Guarda G, Zenger M, Yazdi AS, Schroder K, Ferrero I, Menu P, Tardivel A, Mattmann C, and Tschopp J. Differential expression of NLRP3 among hematopoietic cells. *J Immunol.* 2011;186(4):2529-34.
35. Shi Y, Evans JE, and Rock KL. Molecular identification of a danger signal that alerts the immune system to dying cells. *Nature.* 2003;425(6957):516-21.
36. Shimada K, Crother TR, Karlin J, Dagvadorj J, Chiba N, Chen S, Ramanujan VK, Wolf AJ, Vergnes L, Ojcius DM, et al. Oxidized mitochondrial DNA activates the NLRP3 inflammasome during apoptosis. *Immunity.* 2012;36(3):401-14.
37. Zhou R, Tardivel A, Thorens B, Choi I, and Tschopp J. Thioredoxin-interacting protein links oxidative stress to inflammasome activation. *Nat Immunol.* 2010;11(2):136-40.
38. Zhou R, Yazdi AS, Menu P, and Tschopp J. A role for mitochondria in NLRP3 inflammasome activation. *Nature.* 2011;469(7329):221-5.
39. Hornung V, Bauernfeind F, Halle A, Samstad EO, Kono H, Rock KL, Fitzgerald KA, and Latz E. Silica crystals and aluminum salts activate the NALP3 inflammasome through phagosomal destabilization. *Nat Immunol.* 2008;9(8):847-56.

40. Dostert C, Pétrilli V, Van Bruggen R, Steele C, Mossman BT, and Tschopp J. Innate immune activation through Nalp3 inflammasome sensing of asbestos and silica. *Science.* 2008;320(5876):674-7.
41. Dostert C, Guarda G, Romero JF, Menu P, Gross O, Tardivel A, Suva ML, Stehle JC, Kopf M, Stamenkovic I, et al. Malarial hemozoin is a Nalp3 inflammasome activating danger signal. *PLoS One.* 2009;4(8):e6510.
42. Hornung V, and Latz E. Critical functions of priming and lysosomal damage for NLRP3 activation. *Eur J Immunol.* 2010;40(3):620-3.
43. Kahlenberg JM, and Dubyak GR. Mechanisms of caspase-1 activation by P2X7 receptor-mediated K+ release. *Am J Physiol Cell Physiol.* 2004;286(5):C1100-8.
44. Schorn C, Frey B, Lauber K, Janko C, Strysio M, Keppeler H, Gaipl US, Voll RE, Springer E, Munoz LE, et al. Sodium overload and water influx activate the NALP3 inflammasome. *J Biol Chem.* 2011;286(1):35-41.
45. Pétrilli V, Papin S, Dostert C, Mayor A, Martinon F, and Tschopp J. Activation of the NALP3 inflammasome is triggered by low intracellular potassium concentration. *Cell Death Differ.* 2007;14(9):1583-9.
46. Perregaux D, and Gabel CA. Interleukin-1 beta maturation and release in response to ATP and nigericin. Evidence that potassium depletion mediated by these agents is a necessary and common feature of their activity. *J Biol Chem.* 1994;269(21):15195-203.
47. Avshalumov MV, and Rice ME. Activation of ATP-sensitive K+ (K(ATP)) channels by H2O2 underlies glutamate-dependent inhibition of striatal dopamine release. *Proc Natl Acad Sci U S A.* 2003;100(20):11729-34.
48. Sesti F, Liu S, and Cai SQ. Oxidation of potassium channels by ROS: a general mechanism of aging and neurodegeneration? *Trends Cell Biol.* 2010;20(1):45-51.
49. Link TM, Park U, Vonakis BM, Raben DM, Soloski MJ, and Caterina MJ. TRPV2 has a pivotal role in macrophage particle binding and phagocytosis. *Nat Immunol.* 2010;11(3):232-9.
50. Boya P, and Kroemer G. Lysosomal membrane permeabilization in cell death. *Oncogene.* 2008;27(50):6434-51.
51. Ghosh M, Carlsson F, Laskar A, Yuan XM, and Li W. Lysosomal membrane permeabilization causes oxidative stress and ferritin induction in macrophages. *FEBS Lett.* 2011;585(4):623-9.

52. Mayor A, Martinon F, De Smedt T, Pétrilli V, and Tschopp J. A crucial function of SGT1 and HSP90 in inflammasome activity links mammalian and plant innate immune responses. *Nat Immunol.* 2007;8(5):497-503.
53. Dinarello CA. A clinical perspective of IL-1β as the gatekeeper of inflammation. *Eur J Immunol.* 2011;41(5):1203-17.
54. Pekin Jr TJ, and Zvaifler NJ. Hemolytic complement in synovial fluid. *J Clin Invest.* 1964;43(1372-82.
55. Hunder GG, McDuffie FC, and Mullen BJ. Activation of complement components C3 and factor B in synovial fluids. *J Lab Clin Med.* 1977;89(1):160-71.
56. Hasselbacher P. Immunoelectrophoretic assay for synovial fluid C3 with correction for synovial fluid globulin. *Arthritis Rheum.* 1979;22(243-50.
57. Webster ME, Maling HM, Zweig MH, Williams MA, and Anderson Jr W. Urate crystal induced inflammation in the rat: evidence for the combined actions of kinins, histamine and components of complement. *Immunol Commun.* 1972;1(185-98.
58. Kellermeyer RW, and Naff GB. Chemical mediators of inflammation in acute gouty arthritis. *Arthritis Rheum.* 1975;18(765-70.
59. Tramontini N, Huber C, Liu-Bryan R, Terkeltaub RA, and Kilgore KS. Central role of complement membrane attack complex in monosodium urate crystal-induced neutrophilic rabbit knee synovitis. *Arthritis Rheum.* 2004;50(2633-9.
60. Giclas PC, Ginsberg MH, and Cooper NR. Immunoglobulin G independent activation of the classical complement pathway by monosodium urate crystals. *J Clin Invest.* 1979;63(4):759-64.
61. Naff GB, and Byers PH. Complement as a mediator of inflammation in acute gouty arthritis. I. Studies on the reaction between human serum complement and sodium urate crystals. *J Lab Clin Med.* 1973;81(5):747-60.
62. Fields TR, Abramson SB, Weissmann G, Kaplan AP, and Ghebrehiwet B. Activation of the alternative pathway of complement by monosodium urate crystals. *Clin Immunol Immunopathol.* 1983;26(2):249-57.
63. Russell IJ, Mansen C, Kolb LM, and Kolb WP. Activation of the fifth component of human complement (C5) induced by monosodium urate crystals: C5 convertase assembly on the crystal surface. *Clin Immunol Immunopathol.* 1982;24(2):239-50.
64. Pan ZK. Anaphylatoxins C5a and C3a induce nuclear factor kappaB activation in human peripheral blood monocytes. *Biochim Biophys Acta.* 1998;1443(1-2):90-8.

65. Kastl SP, Speidl WS, Kaun C, Rega G, Assadian A, Weiss TW, Valent P, Hagmueller GW, Maurer G, Huber K, et al. The complement component C5a induces the expression of plasminogen activator inhibitor-1 in human macrophages via NF-kappaB activation. *J Thromb Haemost.* 2006;4(8):1790-7.
66. Laudisi F, Spreafico R, Evrard M, Hughes TR, Mandriani B, Kandasamy M, Morgan BP, Sivasankar B, and Mortellaro A. Cutting edge: the NLRP3 inflammasome links complement-mediated inflammation and IL-1β release. *J Immunol.* 2013;191(3):1006-10.
67. Neogi T. Clinical practice. Gout. *N Engl J Med.* 2011;364(5):443-52.
68. Fava R, Olsen N, Keski-Oja J, Moses H, and Pincus T. Active and latent forms of transforming growth factor beta activity in synovial effusions. *J Exp Med.* 1989;169(1):291-6.
69. Lotz M, Kekow J, and Carson DA. Transforming growth factor-beta and cellular immune responses in synovial fluids. *J Immunol.* 1990;144(4189-94.
70. Scanu A, Oliviero F, Ramonda R, Frallonardo P, Dayer JM, and Punzi L. Cytokine levels in human synovial fluid during the different stages of acute gout: role of transforming growth factor β1 in the resolution phase. *Ann Rheum Dis.* 2012;71(4):621-4.
71. Chang SJ, Chen CJ, Tsai FC, Lai HM, Tsai PC, and Tsai MH. Associations between gout tophus and polymorphisms 869T/C and -509C/T in transforming growth factor beta1 gene. *Rheumatology (Oxford).* 2008;47(617-21.
72. Lioté F, Prudhommeaux F, Schiltz C, Champy R, Herbelin A, Ortiz-Bravo E, and Bardin T. Inhibition and prevention of monosodium urate monohydrate crystal-induced acute inflammation in vivo by transforming growth factor beta1. *Arthritis Rheum.* 1996;39(7):1192-8.
73. Yagnik DR, Evans BJ, Florey O, Mason JC, Landis RC, and Haskard DO. Macrophage release of transforming growth factor beta1 during resolution of monosodium urate monohydrate crystal-induced inflammation. *Arthritis Rheum.* 2004;50(2273-80.
74. Yagnik DR, Evans BJ, Florey O, Mason JC, Landis RC, and Haskard DO. Macrophage release of transforming growth factor beta1 during resolution of monosodium urate monohydrate crystal-induced inflammation. *Arthritis Rheum.* 2004;50(7):2273-80.
75. Rose DM, Sydlaske AD, Agha-Babakhani A, Johnson K, and Terkeltaub R. Transglutaminase 2 limits murine peritoneal acute gout-like inflammation by regulating macrophage clearance of apoptotic neutrophils. *Arthritis Rheum.* 2006;54(10):3363-71.
76. Rothlin CV, Ghosh S, Zuniga EI, Oldstone MB, and Lemke G. TAM receptors are pleiotropic inhibitors of the innate immune response. *Cell.* 2007;131(6):1124-36.

77. Fadok VA, Bratton DL, Konowal A, Freed PW, Westcott JY, and Henson PM. Macrophages that have ingested apoptotic cells in vitro inhibit proinflammatory cytokine production through autocrine/paracrine mechanisms involving TGF-beta, PGE2, and PAF. *J Clin Invest.* 1998;101(890-8.
78. Huynh ML, Fadok VA, and Henson PM. Phosphatidylserine-dependent ingestion of apoptotic cells promotes TGF-beta1 secretion and the resolution of inflammation. *J Clin Invest.* 2002;109(1):41-50.
79. Gordon S. Alternative activation of macrophages. *Nat Rev Immunol.* 2003;3(1):23-35.
80. Mosser DM, and Edwards JP. Exploring the full spectrum of macrophage activation. *Nat Rev Immunol.* 2008;8(12):958-69.
81. Dalli J, and Serhan CN. Specific lipid mediator signatures of human phagocytes: microparticles stimulate macrophage efferocytosis and pro-resolving mediators. *Blood.* 2012;120(15):e60-72.
82. Edwards JP, Zhang X, Frauwirth KA, and Mosser DM. Biochemical and functional characterization of three activated macrophage populations. *J Leukoc Biol.* 2006;80(6):1298-307.
83. Meissner F, Molawi K, and Zychlinsky A. Superoxide dismutase 1 regulates caspase-1 and endotoxic shock. *Nat Immunol.* 2008;9(8):866-72.
84. Berckmans RJ, Nieuwland R, Böing AN, Romijn FP, Hack CE, and Sturk A. Cell-derived microparticles circulate in healthy humans and support low grade thrombin generation. *Thromb Haemost.* 2001;85(4):639-46.
85. Sinauridze EI, Kireev DA, Popenko NY, Pichugin AV, Panteleev MA, Krymskaya OV, and Ataullakhanov FI. Platelet microparticle membranes have 50- to 100-fold higher specific procoagulant activity than activated platelets. *Thromb Haemost.* 2007;97(3):425-34.
86. Huber-Lang M, Sarma JV, Zetoune FS, Rittirsch D, Neff TA, McGuire SR, Lambris JD, Warner RL, Flierl MA, Hoesel LM, et al. Generation of C5a in the absence of C3: a new complement activation pathway. *Nat Med.* 2006;12(6):682-7.
87. Wolf P. The nature and significance of platelet products in human plasma. *Br J Haematol.* 1967;13(3):269-88.
88. CHARGAFF E, and WEST R. The biological significance of the thromboplastic protein of blood. *J Biol Chem.* 1946;166(1):189-97.
89. van Leeuwen EF, van der Ven JT, Engelfriet CP, and von dem Borne AE. Specificity of autoantibodies in autoimmune thrombocytopenia. *Blood.* 1982;59(1):23-6.

90. Beiras-Fernandez A, Walther S, Muenzing S, Thein E, and Hammer C. In vitro assessment of dose-dependent platelet activation by polyclonal antithymocyte globulins: a flow-cytometric analysis. *Transplantation.* 2004;78(5):751-4.
91. Latham JT, Bove JR, and Weirich FL. Chemical and hematologic changes in stored CPDA-1 blood. *Transfusion.* 1982;22(2):158-9.
92. Salzer U, Zhu R, Luten M, Isobe H, Pastushenko V, Perkmann T, Hinterdorfer P, and Bosman GJ. Vesicles generated during storage of red cells are rich in the lipid raft marker stomatin. *Transfusion.* 2008;48(3):451-62.
93. Wang D, Cortés-Puch I, Sun J, Solomon SB, Kanias T, Remy KE, Feng J, Alimchandani M, Quezado M, Helms C, et al. Transfusion of older stored blood worsens outcomes in canines depending on the presence and severity of pneumonia. *Transfusion.* 2014;54(7):1712-24.
94. Weinberg JA, McGwin G, Griffin RL, Huynh VQ, Cherry SA, Marques MB, Reiff DA, Kerby JD, and Rue LW. Age of transfused blood: an independent predictor of mortality despite universal leukoreduction. *J Trauma.* 2008;65(2):279-82; discussion 82-4.
95. Koch CG, Li L, Sessler DI, Figueroa P, Hoeltge GA, Mihaljevic T, and Blackstone EH. Duration of red-cell storage and complications after cardiac surgery. *N Engl J Med.* 2008;358(12):1229-39.
96. Spinella PC, Carroll CL, Staff I, Gross R, Mc Quay J, Keibel L, Wade CE, and Holcomb JB. Duration of red blood cell storage is associated with increased incidence of deep vein thrombosis and in hospital mortality in patients with traumatic injuries. *Crit Care.* 2009;13(5):R151.
97. Toy P, Gajic O, Bacchetti P, Looney MR, Gropper MA, Hubmayr R, Lowell CA, Norris PJ, Murphy EL, Weiskopf RB, et al. Transfusion-related acute lung injury: incidence and risk factors. *Blood.* 2012;119(7):1757-67.
98. Bux J, and Sachs UJ. The pathogenesis of transfusion-related acute lung injury (TRALI). *Br J Haematol.* 2007;136(6):788-99.
99. Bux J. Transfusion-related acute lung injury (TRALI): a serious adverse event of blood transfusion. *Vox Sang.* 2005;89(1):1-10.
100. Sadallah S, Eken C, and Schifferli JA. Ectosomes as modulators of inflammation and immunity. *Clin Exp Immunol.* 2011;163(1):26-32.
101. Bryant C, and Fitzgerald KA. Molecular mechanisms involved in inflammasome activation. *Trends Cell Biol.* 2009;19(9):455-64.

Neutrophil microvesicles suppress inflammasome-driven gouty inflammation.

Arun Cumpelik, MD[1], Barbara Ankli, MD[3], Daniel Zecher, MD[1,2*], Jürg A. Schifferli, MD, PhD[1,2*]

[1]Department of Biomedicine, [2]Department of Medicine, [3]Department of Rheumatology, University Hospital Basel, Switzerland

* these authors contributed equally to this work

Abstract

Gout is a highly inflammatory but self-limiting joint disease induced by the precipitation of monosodium urate crystals (MSU). While it is well established that inflammasome activation by MSU mediates acute inflammation, little is known about the mechanisms controlling its spontaneous resolution. Here we found in a murine peritonitis model that neutrophil-derived microvesicles (ectosomes) resolve acute MSU-driven inflammation. The release of IL-1β following MSU stimulation was dependend on generation of complement C5a. Neutrophils (PMN) infiltrating the peritoneum in response to C5a released phosphatidylserine (PS)-positive ectosomes early on in the course of inflammation. Treatment of the peritoneum with these ectosomes in turn resulted in suppression of IL-1β release and translated in a decrease in PMN influx. Ectosome-mediated suppression could be reproduced using PS-expressing liposomes and required the presence of the PS-receptor MerTK. In addition, ectosomes triggered the release of TGFβ independent of MerTK. TGFβ, however, was not sufficient to control MSU-driven inflammation in vivo. Finally, neutrophil-derived microvesicles from joint aspirates of patients with gouty arthritis had similar anti-inflammatory properties. Ectosome-mediated control of inflammasome-driven inflammation is a compelling concept of autoregulation initiated early on during PMN activation in gout.

Introduction

Gout is a highly inflammatory arthritis induced by the precipitation of monosodium urate crystals (MSU) in articular joints. Even without intervention, an acute gouty arthritis usually resolves spontaneously within a few days leaving minimal residual damage to the joint. What drives this timely resolution of gout, however, is not yet clear.

The early inflammatory phase of gout is characterized by the production of the pro-inflammatory cytokine IL-1β and the infiltration of neutrophils into the joint space. IL-1β is the principle driving force of gouty inflammation and is released as a consequence of NALP3 inflammasome assembly and caspase 1 activation (1). The underlying mechanism behind the resolution of gout must therefore interfere with the release of IL-1β.

Previous studies indicate that the generation of apoptotic leukocytes and their clearance by macrophages may play a key role in resolving gout (2, 3). Both the recognition of phosphatidylserine (PS) on the surface of apoptotic cells and the release of TGFβ upon their clearance are strong anti-inflammatory cues that can suppress an inflammatory response (4). PS-positive surfaces can engage the MerTK receptor initiating the transcription of suppressor of cytokine signaling (SOCS) 3 (5-7). High levels of SOCS3 expression in synovial tissues as well as elevated levels of TGFβ in the synovial fluids of patients during the resolution phase of gout have been reported (8). Little is however known about how and where the inflammasome is regulated.

We previously established that human neutrophils stimulated by complement C5a or bacterial peptide (formyl-Methionyl-Leucyl-Phenylalanine, fMLP) in vitro release microvesicles (ectosomes) from their surface (9). These ectosomes express PS and are capable of inducing the release of TGFβ by monocyte-derived macrophages. In vitro, neutrophil-derived ectosomes have been shown to suppress the response to TLR ligands in monocyte-derived macrophages and dendritic cells (10).

The aim of this study was to determine whether the anti-inflammatory effects of ectosomes extend to the NALP3 inflammasome, whether ectosomes are found in vivo and whether they take part in the early resolution of gouty inflammation.

Results

Bone marrow-derived ectosomes (BM-Ecto) suppress inflammasome activation in vitro. We first set out to find a source of murine ectosomes using B6 wild-type bone marrow cells as a close approximation of neutrophils. BM-Ecto were isolated by sequentially centrifuging supernatants of bone marrow cells stimulated with fMLP. Flow cytometric analysis identified intact vesicles that were able to retain CFSE. Further characterization revealed the expression of the neutrophil marker Gr-1 and surface exposure of phosphatidylserine (PS, assessed by staining with annexin V) on approximately 70-80% of intact BM-Ecto (Figure 1A). Consistent with data from human neutrophil-derived ectosomes (9), electron microscopy of BM-Ecto preparations revealed round shaped vesicles with a size of 50-500 nm (Figure 1B).

We next asked whether BM-Ecto suppress MSU-induced inflammasome activation of resident peritoneal macrophages in vitro. Inflammasome activation in vitro is a two-step process that requires priming with a TLR ligand (LPS) (11) prior to stimulation with a specific inflammasome activator (MSU) (Figure 1C). Whereas up-regulation of pro-IL-1β and NALP3 components in cells is the measure of successful priming (Figure 1D), release of mature IL-1β along with the caspase 1 sub-units p20 or p10 defines efficient inflammasome stimulation (1, 12, 13). To determine whether BM-Ecto interfere with inflammasome activation, BM-Ecto were given to macrophages either prior to LPS priming or prior to stimulation with MSU (Figure 1E) once all LPS priming events (pro-ILβ and NALP3 upregulation) had taken place (Figure 1D).

The release of IL-1β into culture supernatants was significantly suppressed when macrophages received BM-Ecto either prior to LPS priming or MSU stimulation (Figure 1F), indicating that BM-Ecto acted on both phases of inflammasome activation. Immunoblots of cell extracts (Figure 1G, XT) and cell culture supernatants (Figure 1G, SN) revealed that when macrophages were co-incubated with BM-Ecto prior to LPS, they did not undergo efficient priming (less NALP3 and pro-IL-1β expression) and subsequently failed to respond to MSU stimulation (no Caspase 1 p20/10 and IL-1β release). The addition of BM-Ecto after LPS priming resulted in partial suppression of the MSU response (no Caspase 1 p20 and less IL-1β), consistent with data obtained by ELISA (Figure 1F). These results indicated that BM-Ecto contain inflammasome activation in vitro by suppressing LPS priming and MSU stimulation independently of each other.

The anti-inflammatory effects of Ecto have been attributed to their surface expression of PS (14) analogous to what has been reported for apoptotic cells (4, 5, 7). We therefore asked the question whether the in vitro effects of BM-Ecto could be reproduced by size-matched

liposomes expressing PS. Following our in vitro stimulation protocol (Figure 1E) macrophages were treated with equimolar (75nM) amounts of PS or control phosphatidylcholine (PC) liposomes prior to stimulation with MSU crystals. While PS liposomes interfered with LPS priming (Figure 1H and I, XT) and MSU stimulation (Figure 1H and I, SN), PC liposomes failed to attenuate the inflammasome response at any level. These results suggested that PS is involved in the inhibition of inflammasome activation by BM-Ecto.

Inflammasome activation in macrophages is functionally limited by low expression of pro-IL-1β and therefore requires some form of priming (1, 13, 15). During gout, the activation of the NALP3 inflammasome, however, occurs in a sterile environment and has been shown to be independent of Toll-Like-Receptor 4 (16). Therefore the use of LPS as a priming agent may be purposeful in vitro, but does not accurately reflect what occurs in vivo.

C5a and MSU-induced inflammation. MSU crystals are known to activate complement by assembling a functional C5 convertase complex at the crystal surface, which results in the generation of active C5a (17). C5a fragments have been reported to activate NFκB (18-20). Given that the injection of MSU alone can trigger IL-1β release, we hypothesized that C5a generated by MSU is responsible for inflammasome priming in vivo.

Following the previously outlined in vitro protocol (Figure 1E), BM-Ecto were capable of suppressing IL-1β release from macrophages primed with C5a and stimulated with MSU (Figure 2A) or macrophages stimulated by MSU in the presence of normal mouse plasma (NMP) (Figure 2B). MSU crystals in the presence of normal mouse plasma (NMP) generated C5a, which in turn primed the inflammasome via the C5aR leading to the release of IL-1β upon MSU stimulation of macrophages in vitro (Figure 2C). These results suggested that C5a is essential for inflammasome activation by MSU and that BM-Ecto inhibit C5a-mediated inflammasome priming.

To study inflammasome activation in vivo, we next adopted a murine model of MSU-induced peritonitis (21). First we set out to analyze the course of the inflammatory response following intraperitoneal injection of MSU. We identified an almost immediate and steep rise of C5a 15min after introducing MSU into the peritoneum (Figure 2D). The generation of C5a was followed by the release of IL-1β into both the peritoneum and peripheral blood peaking 4 hours after MSU injection (Figure 2D-E). The release of C5a and IL-1β triggered a rapid rise in blood neutrophils (Figure 2E), which then infiltrated the peritoneal compartment reaching a maximum 14 hours after stimulation (Figure 2D). In accordance with our in vitro results, the release of IL-1β in response to MSU was significantly impaired in C5aR deficient mice (Figure 2F).

Our second objective was to determine whether Ecto are released by infiltrating neutrophils during MSU-induced peritonitis. At various time points following MSU stimulation, Ecto were isolated from peritoneal lavages by sequential centrifugation. Using flow cytometry, surface staining with annexin V and anti-Gr-1 identified them as PS-positive microvesicles of neutrophil origin (Figure 2G). These neutrophil ectosomes (PMN-Ecto) were found to be present in significant numbers, reaching up to $1{,}5x10^7$ in the peritoneum 8 hours after MSU stimulation (Figure 2D). The kinetics of PMN-Ecto suggested that their release is an early event of neutrophil activation.

Administration of Ecto attenuates MSU-induced inflammation in vivo. To determine whether Ecto have anti-inflammatory properties in vivo, the peritoneal compartment was pre-treated with $2x10^7$ Ecto 2 hours prior to the intraperitoneal injection of MSU. The Ecto used to pre-condition the peritoneum were either BM-Ecto isolated from ex vivo stimulated bone marrow cells or PMN-Ecto isolated from the lavage fluid of MSU-inflamed peritonea. The quantity ($2x10^7$) of pre-injected BM- and PMN-Ecto corresponded to the maximum number of PMN-Ecto recovered during MSU-induced peritoneal inflammation (Figure 2D).
Pre-treatment with PMN- or BM-Ecto resulted in a two to threefold suppression of IL-1β (Figure 3) release in response to MSU in the peritoneum (Figure 3A) and peripheral blood (Figure 3B). This early suppression of inflammation translated into less pronounced neutrophilia in blood (Figure 3C) and subsequently a threefold decrease in the number of neutrophils infiltrating the peritoneum 14 hours after stimulation (Figure 3D). Taken together, these results indicated that Ecto from two independent sources can suppress local and systemic inflammation induced by MSU.

The in vivo effects of Ecto can be mimicked by liposomes expressing phosphatidylserine (PS). To confirm that PS liposomes can act as a surrogate for Ecto in vivo, approximately $1x10^8$ PS or control PC liposomes were injected intraperitoneally instead of Ecto 2 hours prior to stimulation with MSU. Pre-treatment with PS liposomes resulted in suppression of pro-inflammatory cytokines (Figure 4A-B), blood neutrophilia (Figure 4C) and neutrophil influx into the peritoneum (Figure 4D) in response to MSU. Injection of control PC liposomes failed to achieve an anti-inflammatory effect.

Suppression by BM-Ecto is MerTK-dependent in vivo. To directly test the involvement of PS in Ecto-mediated immunosuppression, we next applied our model to mice lacking the MerTK

receptor (*MerTK*$^{-/-}$) which is known to bind PS and relay its signal by inducing suppressor of cytokine signaling (SOCS) 3 (7).

The peritonea of *MerTK*$^{-/-}$ and control B6129S wild-type mice were pre-treated with BM-Ecto prior to MSU stimulation. Whereas pre-treatment of wild-type mice with BM-Ecto led to suppression of cytokines in both peritoneum (Figure 5A) and peripheral blood (Figure 5B), the anti-inflammatory effects of BM-Ecto were absent in *MerTK*$^{-/-}$ mice. The same pattern emerged with regard to blood neutrophilia (Figure 5C) and peritoneal accumulation of neutrophils (Figure 5D). Furthermore, 4 hours after intraperitoneal BM-Ecto injection, we observed a MerTK-dependent induction of SOCS3 in peritoneal macrophages (Figure 5E). Of note, inflammation induced by MSU in *MerTK*$^{-/-}$ mice was significantly higher compared to background-matched wild-type mice (Figure 5A-D), suggesting that in wild-type mice endogenously released PMN-Ecto limit the magnitude of MSU-induced inflammation via MerTK.

BM-Ecto induce the release of TGFβ. It has been suggested that TGFβ participates in the resolution of gout in its late stages (22). Therefore, we next asked whether Ecto induce the release of TGFβ in vivo. Injection of BM-Ecto induced the release of TGFβ in the peritoneum (Figure 6A). The release of TGFβ was further enhanced when BM-Ecto primed mice received MSU (Figure 6A). Since BM-Ecto themselves were not the source of TGFβ (Figure 6B) and the amount of TGFβ released in vitro by peritoneal macrophages remained the same regardless of inflammasome activation (Figure 6C), we hypothesized that the additive effect of MSU and BM-Ecto on TGFβ release could be due to infiltrating cells responding to BM-Ecto. Indeed, monocytes and neutrophils isolated from MSU inflamed peritonea were able to release TGFβ in response to BM-Ecto in vitro (Figure 6D). To determine which of these cells contributes the most to the TGFβ pool in vivo, resident macrophages, infiltrating monocytes and neutrophils from BM-Ecto-treated peritonea were stained for latency associated peptide (LAP). LAP is part of latent TGFβ and remains tethered to the surface of macrophages (23) and monocytes (24) once TGFβ is released and cleaved into its active form. Whereas expression of LAP in naive resident peritoneal macrophages (F480^{+}, CD115^{+}, Ly6C^{-}) was low, LAP progressively increased over time after intraperitoneal injection of BM-Ecto, indicating continuous TGFβ release (Figure 6E). Monocytes and neutrophils are not present in untreated peritonea. Upon i.p. MSU stimulation, however, infiltrating monocytes (Ly6C^{+}, F480^{-}, Ly6G^{-}) and, to a lesser extent, neutrophils (Ly6C^{+}, F480^{-}, Ly6G^{+}) up-regulated LAP when the peritoneum was pre-treated with BM-Ecto prior to MSU (Figure 6E).

Ecto suppress MSU-induced peritonitis independent of TGFβ. We next asked whether TGFβ was necessary for the suppressive effects of Ecto. In vitro, TGFβ release was found to be independent of MerTK (Figure 6F). Significant increases in TGFβ were consistently measured in the peritoneum of both wild-type and *MerTK*$^{-/-}$ mice pre-treated with BM-Ecto (Figure 6G). Of note, PS liposomes did not induce TGFβ release in vivo (Figure 7H). Since PS liposomes attenuated the response to MSU (Figure 4) without inducing TGFβ and BM-Ecto failed to inhibit inflammation in MerTK$^{-/-}$ mice (Figure 5) despite releasing TGFβ (Figure 6G), TGFβ did not seem to be necessary for BM-Ecto-mediated resolution of acute gouty inflammation. To confirm that the effect of BM-Ecto was independent of TGFβ, neutralizing anti-TGFβ1 antibody (100μg) was given i.p. 30min prior to BM-Ecto. In the presence of TGFβ1-blocking antibody, BM-Ecto still retained their capacity to suppress inflammation (Figure 6I). Although the blocking of TGFβ1 slightly increased neutrophil influx in response to MSU suggesting that TGFβ may play a role (Figure 6I), the injection of 1μg recombinant mouse TGFβ1 instead of BM-Ecto had not effect (Figure 6J).

Taken together, these data suggested that Ecto inhibit the acute inflammatory response to MSU predominantly via the PS-MerTK pathway rather than TGFβ. Although Ecto induced the release of TGFβ by macrophages and monocytes, MerTK alone was necessary and sufficient for Ecto to suppress inflammasome activation in vivo.

PMN-Ecto are present in synovial exudates during gouty inflammation in humans. Lastly, we sequentially centrifuged synovial exudates of gouty arthritis (GA) and control osteoarthritis (OA) patients to verify the presence of microvesicles during gouty attacks in humans. Arthrocenthesis was performed within 1 day after the onset of symptoms. Using flow cytometry, we found annexin V-positive vesicles expressing the granulocyte marker CD66b and the neutrophil-specific enzyme myeloperoxidase (MPO) (Figure 7A). Electron micrographs (Figure 7B) of exudates confirmed the presence of intact vesicles that were approximately 50 nm in size.

The amount of PMN-Ecto isolated from gout exudates correlated with the number of infiltrating PMN (Figure 7C) and gouty arthritis (GA) exudates had significantly higher numbers of PMN-Ecto compared to osteoarthritis exudates (Figure. 7D). Recovery of neutrophil-derived microvesicles from synovial exudates of patients during gouty inflammation suggested that PMN-Ecto release occurs and is relevant in vivo.

In vitro, PMN-Ecto from gout exudates (Gout-Ecto) were able to induce the release of TGFβ from human monocyte-derived macrophages (Figure 7E) and inhibited the release of IL-1β by macrophages (Figure 7F) treated as outlined in Figure 1E. Furthermore, in the presence of

normal human plasma (NHP), MSU crystals were able to simultaneously prime and stimulate the inflammasome. Consistently, MSU failed to prime the inflammasome in the presence of heat inactivated or C5-blocked plasma, confirming that priming is C5-dependent (Figure 7G). Finally, Gout-Ecto suppressed IL-1β release in macrophages stimulated by MSU in the presence of NHP (Figure 7H).

Discussion

The major finding of the present study is that PMN-Ecto are rapidly released by infiltrating neutrophils in a murine model of gout and that these ectosomes participate in the control of inflammation induced by MSU crystals. Ectosomes achieve their anti-inflammatory effect by engaging the MerTK receptor. The regulation induced by PMN-Ecto starts almost immediately after the influx of cells into the peritoneum, indicating that the control of inflammation starts much earlier than presumed until now. Interestingly, the very cells that are responsible for acute inflammation (i.e. neutrophils), act also as its regulator due to the shedding of ectosomes.

The release of PMN-Ecto is an early phenomenon of neutrophil activation (9). In our gout model, PMN-Ecto were released as early as 2 hours after intraperitoneal injection of MSU and their concentration peaked at 8 hours. To analyze the effect of Ecto on gouty inflammation, Ecto were given intraperitoneally prior to MSU injection. The number of Ecto injected was physiological and the amount was set at the maximum number of PMN-Ecto recovered from the peritoneum after MSU stimulation. Since Ecto bind back to cells (9) and are continuously cleared (25), the recovery of $1.5x10^7$ Ecto is likely an underestimation of the total amount of PMN-Ecto shed during the course of MSU peritonitis. Ecto were generated from two alternate sources, from bone marrow cells and neutrophils. Although BM-Ecto were an approximation of neutrophil-derived Ecto, they shared the same phenotype as PMN-Ecto (not shown) and were equally effective in suppressing inflammation. In addition to isolating Ecto from peritoneal exudates in our gout model (Figure 2D), the presence of PMN-Ecto was confirmed in synovial aspirates of patients undergoing an acute gouty attack (Figure 8), further supporting their in vivo relevance.

Previous studies have already suggested that PS expressed on apoptotic cells (3-5, 7) and ectosomes (26) contribute to the resolution of inflammation. PS has been shown to mediate anti-inflammatory signals via the MerTK receptor (5, 7). MerTK activation leads to induction of SOCS3 (6) and in turn to suppression of TLR-induced cytokine release (5, 7, 14). Whether the NALP3 inflammasome is subject to the same regulatory mechanism has not yet been shown. In accordance with these studies, we could confirm that PS-expressing Ecto suppress LPS priming of the NALP3 inflammasome in vitro (Figure 1F-G). LPS priming, however, is not required for the inflammatory response to MSU in vivo and is merely used to model inflammasome activation in vitro (27). In addition to activating the inflammasome, MSU crystals activate the complement cascade by assembling a C5 convertase on their surface (17). We could identify

C5a generated by MSU as the main inflammasome priming agent in gout. The anti-inflammatory effect of PMN-Ecto was therefore not limited to the inhibition of TLR stimuli, but extended to C5a and C5aR signaling as well. Furthermore, C5a was able to both prime the inflammasome and limit its activation by inducing the release of PMN-Ecto, thus forming the basis of an auto-regulatory negative feedback loop in gout (9).

Whereas studies using liposomes suggested that PS-positive vesicles could down-regulate inflammation, involvement of PS was confirmed in mice deficient for the PS receptor MerTK. Furthermore, the higher degree of inflammation in *MerTK*$^{-/-}$ compared to wild-type mice suggested that PS expressed on Ecto provides baseline suppression in gouty inflammation. Of note, high expression of SOCS3 in synovial tissue has been found in patients during the acute phase of gout (8), further supporting the notion that the PS-MerTK axis plays a role in limiting gouty inflammation.

TGFβ is regarded as the prime mediator in the active resolution of gout (8, 28, 29). Levels of TGFβ have been found to progressively increase in synovial fluids of gout patients after an attack, suggesting that TGFβ may be involved in late phases of resolution (8, 22). We demonstrated that Ecto trigger the release of TGFβ in vitro and in vivo. These findings are consistent with other studies that have shown release of TGFβ by macrophages (4) or neutrophils (3) in response to apoptotic cells and Ecto (26). In vivo, however, neither treatment with recombinant mouse TGFβ1 (Figure 6J), nor the release of TGFβ by Ecto in the absence of PS-MerTK activation (Figure 5D,6G) was sufficient to control the acute inflammatory response to MSU. Furthermore PS-liposomes alone could reproduce the Ecto effect without inducing the release of TGFβ (Figure 4,6H) and TGFβ blocking did not compromise the ability of BM-Ecto to suppress inflammation (Figure I). These findings argue against a role for TGFβ in the early phase of gout. Given that gout patients with TGFβ polymorphisms frequently progress to more advanced disease states, TGFβ may play a role in chronic gout and affect the rate of progression rather than resolution of acute attacks (30).

Aside from Ecto affecting macrophages, other cell types may have been involved in the observations made in our model. For instance, endothelial cells are critically involved in mediating neutrophil extravasation. Recent studies have demonstrated a crucial role for IL-1β-induced endothelial cell activation for neutrophil transmigration in MSU peritonitis (27). As MerTK is expressed on endothelial cells (31) and TGFβ is known to inhibit endothelial cell activation in vitro (28), it cannot be ruled out that the effect of Ecto on inhibiting neutrophil influx in vivo was in part mediated by the suppression of endothelial cell activation. Furthermore, other

mediators associated with PMN-Ecto, such as Annexin A1 and resolvins, may contribute to the resolution of gouty inflammation (Dalli et al., 2008; Dalli and Serhan, 2012).

The motivation behind this work was to better understand the self-limiting nature of gout. This study supports the notion that resolution of gout is initiated with the release of PMN-Ecto early on during neutrophil activation. In a broader context, PMN-Ecto release may limit excessive inflammation in response to both exogenous and endogenous danger signals and their pathophysiological relevance likely extends to conditions other than gout.

Materials and Methods

Mice. C57BL/6 (B6) and Balb/c mice were bred at the institution's animal facility or purchased from Charles River (Sulzfeld, Germany). B6;129-Mertktm1Grl/J (*MerTK*$^{-/-}$) and the respective wild-type strain B6;129SF2/J were obtained from The Jackson Laboratories (Bar Harbour, MN, USA). C.129S4(B6)-C5ar1tm1Cge/J (C5aR-/-) mice on a Balb/c background were a generous gift from Prof. van den Broek (Institute of Experimental Immunology, University of Zürich). All mice were housed in a specific pathogen-free environment and were used between 6 and 12 weeks of age. Animal care and experimentation were performed in accordance with national guidelines (Federal Veterinary Office) and had been approved by the local government authorities.

Reagents and Antibodies. Fluorochrome-conjugated antibodies against CD11b (clone M1/70), Gr-1 (RB6-8C5), Ly6C (AL-21), Ly6G (1A8), CD115 (AFS98), F4/80 (BM8), CD45 (30F11), CD66b (G10F5), MPO (MPO455-8E6) and LAP were from Biolegend (San Diego, CA, USA). Purified anti-CD16/32 (Fc-Block, 2.4G2) was from BD Pharmingen (Allschwill, Switzerland) and AnnexinV-APC was from Immunotools (Friesoyte, Germany). 7-AAD and CFSE were from Invitrogen (Zug, Switzerland), monosodium urate and fMLP from Sigma (Schnelldorf, Germany). Anti-IL1β (AF-401-NA), anti-TGFβ (9016) was from R&D, anti-NALP3 (Cryo-2) and anti-caspase 1 p20 (Casper-1) antibodies were from Adipogen (Liestal, Switzerland), anti-actin (C4), anti-TGFβ (H-112), anti-SOCS3 (H-103) and HRP conjugated anti-mouse (sc-2005), -rabbit (sc-2004) and -goat (sc-2020) antibodies were from Santa Cruz Biotechnology (Muttenz, Switzerland). Anti-C5 antibody (Eculizumab®) was a generous gift from Alexion Pharmaceuticals (Lausanne, Switzerland).

Generation of MSU crystals. MSU crystals were prepared by dissolving 0.5g of MSU in 90ml de-ionized H_20 and 600µl of 5M NaOH. This MSU solution was heated to 90°C, passed across a 0.2µm filter and allowed to precipitate into crystals over-night at room temperature. The slurry was subsequently washed with ethanol twice and acetone once, which was then allowed to evaporate leaving crystals behind. Crystals were stored at -20°C and dissolved in 0.9% NaCl at 6mg/ml prior to use. Size of MSU crystals was verified by transmission light microscope (Olympus, IX50) at room temperature and acquired by Cell Sense Standard software.

Generation and analysis of PMN-Ecto and BM-Ecto. Mouse PMN-Ecto were derived from inflamed peritonea. 6-10h after i.p. injection of 3mg MSU crystals, the peritoneal cavity was lavaged with 5ml PBS-1%FCS and the lavage fluid was then sequentially centrifuged to separate cells (350g/10'/4°C), cell debris (3000g/10'/4°C) and finally PMN-Ecto (50.000g/40'/4°C). The final pellet was diluted in 0.2µm filtered PBS or AnnexinV-staining buffer (BD), stained with fluorochrome-tagged AnnexinV and anti-Gr-1 and phenotyped by flow cytometry. In some experiments SSC threshold above Annexin buffer background was applied. To quantify PMN-Ecto, defined amounts of 4.3 µm fluorescent beads (Trucount tubes, BD) were added to the staining solution. The number of PMN-Ecto was determined as follows: (% of total microvesicles / % of Trucount beads) x (absolute no. of beads) x (% of $AnnexinV^+$, $Gr\text{-}1^+$ double positive events). Flow cytometric analysis was performed using a CyanADP cytometer (Beckaman Coulter, Nyon, Switzerland) and data were analyzed using FlowJo Software (TreeStar, San Jose, CA, USA). Mouse BM-Ecto were prepared from bone marrow cells, which were obtained by flushing femurs and tibias of B6 mice. Erythrocytes were removed by hypotonic lysis and the remaining myeloid cells stimulated with 1µM fMLP in RPMI for 30min at 37°C. The supernatant was sequentially centrifuged as above and BM-Ecto were phenotyped by flow cytometry with fluorochrome-tagged AnnexinV and anti-Gr-1. Alternatively, BM-Ecto were pre-stained with CFSE and only $CFSE^+$ vesicles were further analyzed. Human PMN-Ecto were isolated by sequentially centrifuging synovial exudates from patients with confirmed gouty attacks. These PMN-Ecto were phenotyped as $AnnexinV^+$, $CD66b^+$, MPO^+ vesicles.

Generation of PS/PC liposomes. Unilamelar liposomes, composed of either L-α-phosphatidyl-choline (PC, derived from bovine liver) alone or PC together with equimolar concentrations of L-α-phosphadityl-serine (PSPC, derived from porcine brain, both Avanti Polar Lipids, Alabaster, USA) were prepared according to the repeated freeze-thawing method (32). Briefly, the individual phospholipids, stored in chloroform, were added to glass tubes and the chloroform was evaporated. After adding PBS, the lipid mixture was vortexed for 5 min, subjected to five freeze-thaw cycles, and subsequently extruded eight times using a nucleopore polycarbonate filter (0.2 mm; VWR, San Diego, CA). Final liposome concentration of each preparation was adjusted at 16 mM as measured by a standard phosphate assay. This protocol yielded liposomes of 100 nm diameter as determined by electron microscopy and zetasizer (Delsa™ NanoC).

Electron microscopy. Microvesicles were fixed in 1% glutaraldehyde (final concentration) for 1 min at room temperature. They were then adsorbed to parlodion-coated copper grids. After washing, samples were stained with 2% uranylacetate before being observed in a Philips Morgani 268 D transmission electron microscope operated at 80 kV.

Cell culture conditions, ELISA and western blot. Resident peritoneal macrophages were harvested from the indicated mouse strains by peritoneal lavage and plated at a density of $2x10^6$/well. To achieve full inflammasome activation in vitro, cells were first primed with 10ng/ml ultra-pure LPS (Invivogen, catalogue code: tlrl-3pelps) or 10ng/ml mouse recombinant C5a (BD) for 10h, washed and subsequently stimulated with 100µg/ml MSU. Macrophages were treated with BM-Ecto ($1x10^8$/$2x10^6$ macrophages), PS- or PC-liposomes (75nM, approximately $1x10^8$/$2x10^6$ macrophages) for 10min either prior to LPS priming or prior to MSU stimulation. Cell extracts and cell culture supernatants were prepared for western blotting as described previously (33). Cells were lysed with RIPA buffer and lysates denatured at 95°C/10min in reducing sample buffer (Pierce). Cell supernatants were concentrated by TCA/Acetone protein precipitation and denatured in Laemmli buffer with added 2-ME. All samples were resolved with Tris-Gly SDS PAGE (Any-KD™ TGX™ precast gels, Biorad) and transferred to PVDF membrane (Immobilon PSQ, Millipore). Proteins were probed in blocking buffer (PBS, 0.05% Tween 5% non-fat milk) and developed by ECL detection reagents (Pierce). Pro-IL-1β, NALP3 and SOCS3 (Figure 1D, 5E) protein expression was analyzed by densitometry using Image Lab™ software (Biorad) and normalized to actin.

Cell culture supernatants, peritoneal lavages and serum samples were harvested at the indicated time points and cytokines analyzed by ELISA according to the manufacturer's instructions. IL-1β and IL-6 OptEIA® kits were from BD Pharmingen and TGFβ1 was from eBiosciences.

Human monocyte derived macrophages (HMDM) were isolated from buffy coats of healthy blood donors as described (26). Briefly, buffy coats were diluted 1/1(vol/vol) in HBSS, layered over Ficol-Histopaque (Sigma, St Louis, USA) and centrifuged 350g/25min/25°C with no breaks. The PBMC's were collected at the ficol gradient interphase, washed with PBS-2mMEDTA and MACS buffer (Miltenyi, Bergisch Gladbach, Germany). Monocytes were enriched by anti-CD14 magnetic beads (Miltenyi) according to manufacturer's instructions and allowed to mature into macrophages in tissue culture plates over 6-7days in DMEM 10% normal human serum.

Complement assays. C5a ELISA consisted of rat anti-mouse C5a IgG capture antibody (BD, 558027) and rat anti-mouse C5a biotinylated detection antibody (BD, 558028) both used at 5 µg/ml. PBS 10% FCS was the assay diluent and C5a was revealed with SA-HRP (BD). Recombinant mouse C5a (BD, 622597) was used as an ELISA standard and priming agent in vitro at 10ng/ml. Blood for the purpose of Normal mouse and human plasma were anti-coagulated with Refludan (Celgene, Boudry, Switzerland) at final concentration of 2.5µg/ml. Human plasma was heat inactivated at 56°C for 30min and C5 was inhibited with 50µg/ml anti-C5 blocking antibody (Eculizumab®) at 4°C for 30min.

Experimental peritonitis. Mice were pre-treated with an intraperitoneal (i.p.) injection of either $2x10^7$ BM- or PMN-Ecto 2 hours prior to i.p. stimulation with 3mg MSU-crystals in 500µl of 0.9% NaCl. Control groups were given ectosomes followed by 0.9% NaCl or received the stimulus preceded by an injection of 0.9% NaCl instead of ectosomes. At the indicated time points following induction of peritonitis, mice were sacrificed by CO_2-inhalation and peritoneal lavage was performed with 5 ml PBS 1% FCS. The lavage fluid was passed over a 70 µm filter, washed and contaminating red blood cells were removed by hypotonic lysis. Leukocytes were then counted with an automated cell counter (Beckman Coulter). Peripheral blood was obtained by cardiac puncture following sacrifice. Blood was drawn into 1ml syringes containing 100 U heparin, washed and red blood cells removed by hypotonic lysis. Blood leukocytes were counted using GLASSTIC slides (Hycor, CA, USA). Cellular phenotype of peritoneal and peripheral blood leukocytes was determined by flow cytometry following surface staining with the indicated antibodies (Figure S1).

Patient samples. Synovial arthrocenthesis samples were obtained from patients included in the Basel COUGAR cohort study. The study had been approved by the local ethics committee. All patients had given written informed consent prior to inclusion in the study.

Statistical analysis. All data are presented as mean ± SEM. Comparisons between treatment groups were performed using one-way ANOVA with Bonferroni's multiple comparison post-testing (Prism version 6; GraphPad Software). Significance was set at $P < 0.05$.

Acknowledgments

We thank Prof. Broz and Dr. Etienne Meunier (Biozentrum, University of Basel) for technical assistance, Prof. van den Broek and Dr. Laura Surace (Institute of Experimental Immunology, University of Zürich) for providing the $C5aR^{-/-}$ mice, Prof. Ed Palmer (Departement of Biomedicine, University Hospital Basel) for helpful discussions and Vesna Olivieri (Microscopy Core Facility, Biozentrum, University of Basel) for performing electron microscopy.

Authorship

A.C. designed, performed and analyzed all experiments. B.A. provided clinical samples from the COUGAR gout cohort. A.C., D.Z. and J.A.S. wrote the manuscript.

References

1. Martinon F, Pétrilli V, Mayor A, Tardivel A, and Tschopp J. Gout-associated uric acid crystals activate the NALP3 inflammasome. *Nature.* 2006;440(7081):237-41.
2. Rose DM, Sydlaske AD, Agha-Babakhani A, Johnson K, and Terkeltaub R. Transglutaminase 2 limits murine peritoneal acute gout-like inflammation by regulating macrophage clearance of apoptotic neutrophils. *Arthritis Rheum.* 2006;54(10):3363-71.
3. Steiger S, and Harper JL. Neutrophil cannibalism triggers transforming growth factor β1 production and self regulation of neutrophil inflammatory function in monosodium urate monohydrate crystal-induced inflammation in mice. *Arthritis Rheum.* 2013;65(3):815-23.
4. Huynh ML, Fadok VA, and Henson PM. Phosphatidylserine-dependent ingestion of apoptotic cells promotes TGF-beta1 secretion and the resolution of inflammation. *J Clin Invest.* 2002;109(1):41-50.
5. Yi Z, Li L, Matsushima GK, Earp HS, Wang B, and Tisch R. A novel role for c-Src and STAT3 in apoptotic cell-mediated MerTK-dependent immunoregulation of dendritic cells. *Blood.* 2009;114(15):3191-8.
6. Rothlin CV, Ghosh S, Zuniga EI, Oldstone MB, and Lemke G. TAM receptors are pleiotropic inhibitors of the innate immune response. *Cell.* 2007;131(6):1124-36.
7. Sen P, Wallet MA, Yi Z, Huang Y, Henderson M, Mathews CE, Earp HS, Matsushima G, Baldwin AS, and Tisch RM. Apoptotic cells induce Mer tyrosine kinase-dependent blockade of NF-kappaB activation in dendritic cells. *Blood.* 2007;109(2):653-60.
8. Chen YH, Hsieh SC, Chen WY, Li KJ, Wu CH, Wu PC, Tsai CY, and Yu CL. Spontaneous resolution of acute gouty arthritis is associated with rapid induction of the anti-inflammatory factors TGFβ1, IL-10 and soluble TNF receptors and the intracellular cytokine negative regulators CIS and SOCS3. *Ann Rheum Dis.* 2011;70(9):1655-63.
9. Gasser O, Hess C, Miot S, Deon C, Sanchez JC, and Schifferli JA. Characterisation and properties of ectosomes released by human polymorphonuclear neutrophils. *Exp Cell Res.* 2003;285(2):243-57.
10. Eken C, Gasser O, Zenhaeusern G, Oehri I, Hess C, and Schifferli JA. Polymorphonuclear neutrophil-derived ectosomes interfere with the maturation of monocyte-derived dendritic cells. *J Immunol.* 2008;180(2):817-24.
11. Bauernfeind FG, Horvath G, Stutz A, Alnemri ES, MacDonald K, Speert D, Fernandes-Alnemri T, Wu J, Monks BG, Fitzgerald KA, et al. Cutting edge: NF-kappaB activating

pattern recognition and cytokine receptors license NLRP3 inflammasome activation by regulating NLRP3 expression. *J Immunol.* 2009;183(2):787-91.

12. Guarda G, Dostert C, Staehli F, Cabalzar K, Castillo R, Tardivel A, Schneider P, and Tschopp J. T cells dampen innate immune responses through inhibition of NLRP1 and NLRP3 inflammasomes. *Nature.* 2009;460(7252):269-73.
13. Gross O, Thomas CJ, Guarda G, and Tschopp J. The inflammasome: an integrated view. *Immunol Rev.* 2011;243(1):136-51.
14. Eken C, Martin PJ, Sadallah S, Treves S, Schaller M, and Schifferli JA. Ectosomes released by polymorphonuclear neutrophils induce a MerTK-dependent anti-inflammatory pathway in macrophages. *J Biol Chem.* 2010;285(51):39914-21.
15. Gross O, Thomas CJ, Guarda G, and Tschopp J. The inflammasome: an integrated view.
16. Chen CJ, Shi Y, Hearn A, Fitzgerald K, Golenbock D, and Reed G. MyD88-dependent IL-1 receptor signaling is essential for gouty inflammation stimulated by monosodium urate crystals. *J Clin Invest.* 2006;116(2262-71.
17. Russell IJ, Mansen C, Kolb LM, and Kolb WP. Activation of the fifth component of human complement (C5) induced by monosodium urate crystals: C5 convertase assembly on the crystal surface. *Clin Immunol Immunopathol.* 1982;24(2):239-50.
18. Kastl SP, Speidl WS, Kaun C, Rega G, Assadian A, Weiss TW, Valent P, Hagmueller GW, Maurer G, Huber K, et al. The complement component C5a induces the expression of plasminogen activator inhibitor-1 in human macrophages via NF-kappaB activation. *J Thromb Haemost.* 2006;4(8):1790-7.
19. Pan ZK. Anaphylatoxins C5a and C3a induce nuclear factor kappaB activation in human peripheral blood monocytes. *Biochim Biophys Acta.* 1998;1443(1-2):90-8.
20. Laudisi F, Spreafico R, Evrard M, Hughes TR, Mandriani B, Kandasamy M, Morgan BP, Sivasankar B, and Mortellaro A. Cutting edge: the NLRP3 inflammasome links complement-mediated inflammation and IL-1β release. *J Immunol.* 2013;191(3):1006-10.
21. Martin WJ, Walton M, and Harper J. Resident macrophages initiating and driving inflammation in a monosodium urate monohydrate crystal-induced murine peritoneal model of acute gout. *Arthritis Rheum.* 2009;60(1):281-9.
22. Scanu A, Oliviero F, Ramonda R, Frallonardo P, Dayer JM, and Punzi L. Cytokine levels in human synovial fluid during the different stages of acute gout: role of transforming growth factor β1 in the resolution phase. *Ann Rheum Dis.* 2012;71(4):621-4.

23. Doherty TA, Soroosh P, Khorram N, Fukuyama S, Rosenthal P, Cho JY, Norris PS, Choi H, Scheu S, Pfeffer K, et al. The tumor necrosis factor family member LIGHT is a target for asthmatic airway remodeling. *Nat Med.* 2011;17(5):596-603.
24. Slobodin G, Kaly L, Peri R, Kessel A, Rosner I, Toubi E, Rimar D, Boulman N, Rozenbaum M, and Odeh M. Higher expression of latency-associated peptide on the surface of peripheral blood monocytes in patients with rheumatoid arthritis may be protective against articular erosions. *Inflammation.* 2013;36(5):1075-8.
25. Willekens FL, Werre JM, Kruijt JK, Roerdinkholder-Stoelwinder B, Groenen-Döpp YA, van den Bos AG, Bosman GJ, and van Berkel TJ. Liver Kupffer cells rapidly remove red blood cell-derived vesicles from the circulation by scavenger receptors. *Blood.* 2005;105(5):2141-5.
26. Gasser O, and Schifferli JA. Activated polymorphonuclear neutrophils disseminate anti-inflammatory microparticles by ectocytosis. *Blood.* 2004;104(8):2543-8.
27. Chen CJ, Shi Y, Hearn A, Fitzgerald K, Golenbock D, Reed G, Akira S, and Rock KL. MyD88-dependent IL-1 receptor signaling is essential for gouty inflammation stimulated by monosodium urate crystals. *J Clin Invest.* 2006;116(8):2262-71.
28. Yagnik DR, Evans BJ, Florey O, Mason JC, Landis RC, and Haskard DO. Macrophage release of transforming growth factor beta1 during resolution of monosodium urate monohydrate crystal-induced inflammation. *Arthritis Rheum.* 2004;50(7):2273-80.
29. Lioté F, Prudhommeaux F, Schiltz C, Champy R, Herbelin A, Ortiz-Bravo E, and Bardin T. Inhibition and prevention of monosodium urate monohydrate crystal-induced acute inflammation in vivo by transforming growth factor beta1. *Arthritis Rheum.* 1996;39(7):1192-8.
30. Chang SJ, Chen CJ, Tsai FC, Lai HM, Tsai PC, and Tsai MH. Associations between gout tophus and polymorphisms 869T/C and -509C/T in transforming growth factor beta1 gene. *Rheumatology (Oxford).* 2008;47(617-21.
31. Png KJ, Halberg N, Yoshida M, and Tavazoie SF. A microRNA regulon that mediates endothelial recruitment and metastasis by cancer cells. *Nature.* 2012;481(7380):190-4.
32. Szoka F, Olson F, Heath T, Vail W, Mayhew E, and Papahadjopoulos D. Preparation of unilamellar liposomes of intermediate size (0.1-0.2 mumol) by a combination of reverse phase evaporation and extrusion through polycarbonate membranes. *Biochim Biophys Acta.* 1980;601(3):559-71.
33. Broz P, and Monack DM. Measuring inflammasome activation in response to bacterial infection. *Methods Mol Biol.* 2013;1040(65-84.

Figure legends

Figure 1. **Characterization and in vitro properties of BM-Ectosomes.**

(**A**) Bone marrow-derived ectosomes (BM-Ecto) were generated as indicated in Methods. Following labeling with CFSE, CFSE-positive events (representing intact vesicles) were further analyzed for surface expression of Gr-1 and phosphatidylserine (via annexin V binding) by flow cytometry (upper lane, left to right). BM-Ecto are CFSE-, Gr-1, annexin V-positive. Controls (lower lane, left to right) are: annexin buffer alone, CFSE threshold set on sonicated BM-Ecto previously stained with CFSE, isotype control for BM-Ecto stained with annexin V and IgG1 isotype in PBS. Numbers are % positive events (**B**) Transmission electron microscopy of BM-Ecto. Size bar is 100 nm. (**C**) MSU crystals in light microscope. Size bar 50µm. (**D**) Pro-IL1β and NALP3 expression in B6 peritoneal macrophages during LPS priming (10 ng/ml) in vitro assessed by immunoblot. Expression in arbitrary units of band intensity normalized to actin. (**E**) In vitro stimulation protocol. B6 peritoneal macrophages were primed with LPS for 10h, washed and subsequently stimulated with 100µg/ml MSU for 4h. BM-Ecto ($1x10^8$/$2x10^6$ macrophages) were given either prior (BM-Ecto+LPS>MSU) or after (LPS>BM-Ecto+MSU) LPS priming as outlined. Alternatively, PS- or control PC-liposomes ($1x10^8$/$2x10^6$ macrophages) were given instead of BM-Ecto. (**F, H**) IL-1β in supernatants determined by ELISA. n=4 per group. Mean ± SEM is shown. (**G, I**) Cell extracts (XT) and supernatants (SN) were analyzed for the presence of NALP3, pro-IL-1β, IL-1β and active caspase 1 (p20 and p10). Data are representative for 3 independent experiments. ***P<0.001 using 1-way ANOVA and Bonferroni post test.

Figure 2. C5a and MSU-induced inflammation.

(**A-B**) Peritoneal macrophages of B6 mice were subjected to the inflammasome stimulation protocol as outlined in Figure 1E. For inflammasome priming, recombinant mouse C5a at 10ng/ml (**A**) or 25% normal mouse plasma (NMP) (**B**) was used instead of LPS. IL-1β release, pro-IL-1β and NALP3 expression were analyzed by ELISA and western blot, respectively. n=6 per group pooled from 2 independent experiments (ELISA), western blots representative of 2 independent experiments. (**C**) C5a generation and IL-1β release by C5aR+/+ or C5aR-/- peritoneal macrophages stimulated with 100µg/ml MSU + 25% NMP for 10h in vitro. n=6 per group pooled from 2 independent experiments. ***P<0.001 using Students t-test. (**D-E**) B6 mice were injected with 3mg MSU intraperitoneally. At the indicated time points thereafter, peritonea were lavaged and infiltrating cells isolated. Peripheral blood was obtained by cardiac puncture. Concentrations of C5a and IL-1β were determined by ELISA in (**D**) peritoneal lavage fluid and

(**E**) plasma. PMN were phenotyped by flow cytometry as $CD45^+$, $CD11b^+$, $Ly6C^+$, $Ly6G^+$ cells in both (**D**) peritoneal lavage and (**E**) blood. n=4/time point pooled from 2 independent experiments. (**F**) IL-1β concentration in the peritoneal lavage of C5aR+/+ and C5aR-/- mice 4h after 3mg MSU i.p. injection. n=5 pooled from 2 independent experiments. (**G**) PMN-Ecto were identified as Annexin V^+, Gr-1^+ events by flow cytometry after sequential centrifugation of peritoneal lavage fluid. Counting of PMN-Ecto was carried out with beads as indicated in Methods. Mean ± SEM is shown. ***P<0.001 using 1-way ANOVA and Bonferroni post test.

Figure 3. Administration of ectosomes attenuates MSU-driven peritoneal inflammation.
B6 mice were injected intraperitoneally with 3mg MSU. Where indicated, mice were pre-injected i.p. with $2x10^7$ BM- or PMN-Ecto 2h prior to MSU stimulation. Control groups received BM-/PMN-Ecto injections i.p. followed by NaCl instead of MSU. IL-1β was determined by ELISA 4h after MSU stimulation in (**A**) peritoneal lavage fluid and (**B**) plasma. PMN counts in peripheral blood (**C**) and peritoneum (**D**) 4h and 14h after MSU stimulation, respectively, were determined as indicated in Figure 2D-E. n=6-8 per group pooled from at least 3 independent experiments, *P<0.05, **P<0.01, ***P<0.001 using 1-way ANOVA and Bonferroni post test. Mean ± SEM is shown.

Figure 4. PS-liposomes mimic the anti-inflammatory effect of ectosomes in vivo.
B6 mice were injected intraperitoneally with 3mg MSU. Where indicated, mice were pre-injected with 75 nM (approximately $1x10^8$) of PS- or PC-liposomes i.p. 2h prior to MSU stimulation. Control groups received PS- or PC-liposome injections followed by NaCl instead of MSU. IL-1β was determined 4h after MSU stimulation in (**A**) peritoneal lavage fluid and (**B**) plasma. PMN counts in peripheral blood (**C**) and peritoneum (**D**) 4h and 14h after MSU stimulation, respectively, were determined as indicated in Figure 2D-E. n=6-8 per group pooled from at least 3 independent experiments, *P<0.05, **P<0.01, ***P<0.001 using 1-way ANOVA and Bonferroni post test. Mean ± SEM is shown. n.s. = not significant.

Figure 5. Ecto-mediated immunosuppression requires MerTK in vivo.
B6/129S (WT) or *MerTK*$^{-/-}$ mice were injected i.p. with 3mg MSU. Where indicated, mice were pre-injected with $2x10^7$ BM-Ecto i.p. 2h prior to MSU stimulation. IL-1β was determined 4h after MSU stimulation in (**A**) peritoneal lavage fluid and (**B**) plasma. PMN counts in (**C**) peripheral blood and (**D**) peritoneum 4h and 14h after MSU stimulation, respectively, were determined as in Figure 2D-E. n=6-8 per group, pooled from at least 3 independent experiments. (**E**) SOCS3

expression in peritoneal macrophages of B6/129S (WT) and *MerTK*$^{-/-}$ mice determined by immunoblot 4h after i.p. BM-Ecto injection. Expression of SOCS3 in arbitrary units of band intensity normalized to actin. n=2 per group pooled from 2 independent experiments. *P<0.05, **P<0.05 using 1-way ANOVA and Bonferroni post test. Mean ± SEM is shown. n.s. = not significant.

Figure 6. Ecto induce the release of TGF-β.

TGFβ in peritoneal lavage fluids of (**A**) B6 mice treated as outlined in Figure 3 was determined by ELISA. n=6-8 pooled from 3 independent experiments. (**B**) BM-Ecto lysates were assessed for TGFβ content by immunoblot. Recombinant mouse TGFβ was used as control. Release of TGFβ by B6 (**C**) resident peritoneal macrophages or (**D**) monocytes and neutrophils isolated from MSU-inflamed peritonea following treatment with C5a, MSU and/or BM-Ecto in vitro as outlined in Figure 2A. (**E**) Expression of latency associated peptide (LAP) on B6 macrophages, monocytes and neutrophils isolated either 4h after i.p. injection of BM-Ecto or 4h after i.p. injection of MSU with BM-Ecto pre-treatment. Controls received NaCl i.p. (untreated). (**F**) The release of TGFβ by WT and *MerTK*$^{-/-}$ macrophages treated with BM-Ecto in vitro. n=6/group. TGFβ in peritoneal lavage fluids of (**G**) B6/129S (WT) and MerTK$^{-/-}$ mice treated with BM-Ecto or (**H**) B6 mice treated with liposomes as outlined in Figures 3 and 4 ,respectively. n=6-8/group. (**I**) The effect of neutralizing TGFβ1 on peritoneal PMN influx using 100µg anti-TGFβ1 injected i.p. 15min prior to MSU or 15min prior to BM-Ecto pre-treatment. *P<0.05, **P<0.01, ***P<0.001 using 1-way ANOVA and Bonferroni post test. Mean ± SEM is shown. n.s. = not significant.

Figure 7. PMN-Ecto are present in gout exudates in humans.

Gout-Ecto isolated from joint aspirates of patients undergoing a gout attack. (**A**) Flow cytometric characterization of Gout-Ecto using annexin V, anti-CD66b and anti-myeloperoxidase (MPO) antibodies identified them to be of neutrophil origin. Counting was performed using microbeads. (**B**) Electron micrograph of Gout-Ecto. Size bar 1µm (left) and 100nm (right). (**C**) Correlation between the number of infiltrating PMN and Gout-Ecto found in gouty (GA) and osteoarthritis (OA) exudates. Each dot represents a single patient. Linear regression line and 95% confidence bands are indicated. (**D**) Concentration of Gout-Ecto in gout and osteoarthritis exudates. (**E**) Release of TGFβ by human monocyte-derived macrophages (HMDM) treated with Gout-Ecto ($1x10^8$ Gout-Ecto/$2x10^6$ macrophages). n=7 pooled from 2 independent experiments. (**F**) Suppression of IL-1β release by HMDM treated with Gout-Ecto following the in vitro protocol outlined in Figure 1E. (**G**) IL-1β release upon 14h stimulation of HMDM with 100ug/ml MSU in

25% normal human plasma (NHP), heat inactivated NHP (hiNHP) or C5-blocked NHP (αC5). (F-G) n=6 pooled from 3 independent experiments. ***P<0.001 using 1-way ANOVA and Bonferroni post test. (**H**) Suppression of IL-1β release by HMDM treated with Gout-Ecto and stimulated as outlined in (G). (D,E,H) ***P<0.001 using Student's t-test. Mean ± SEM is shown.

Figure S1. Peritoneal exudate cells phenotype and gating strategy

Phenotype of peritoneal exudate cells and blood leukocytes was determined by flow cytometry following surface staining of the indicated antibodies. Leukocyte populations were defined as follows: macrophages ($F480^+$, $CD115^+$, $Ly6C^-$), neutrophils ($Ly6C^+$, $F480^-$, $Ly6G^+$) and monocytes ($Ly6C^+$, $F480^-$, $Ly6G^-$).

Figure 1.

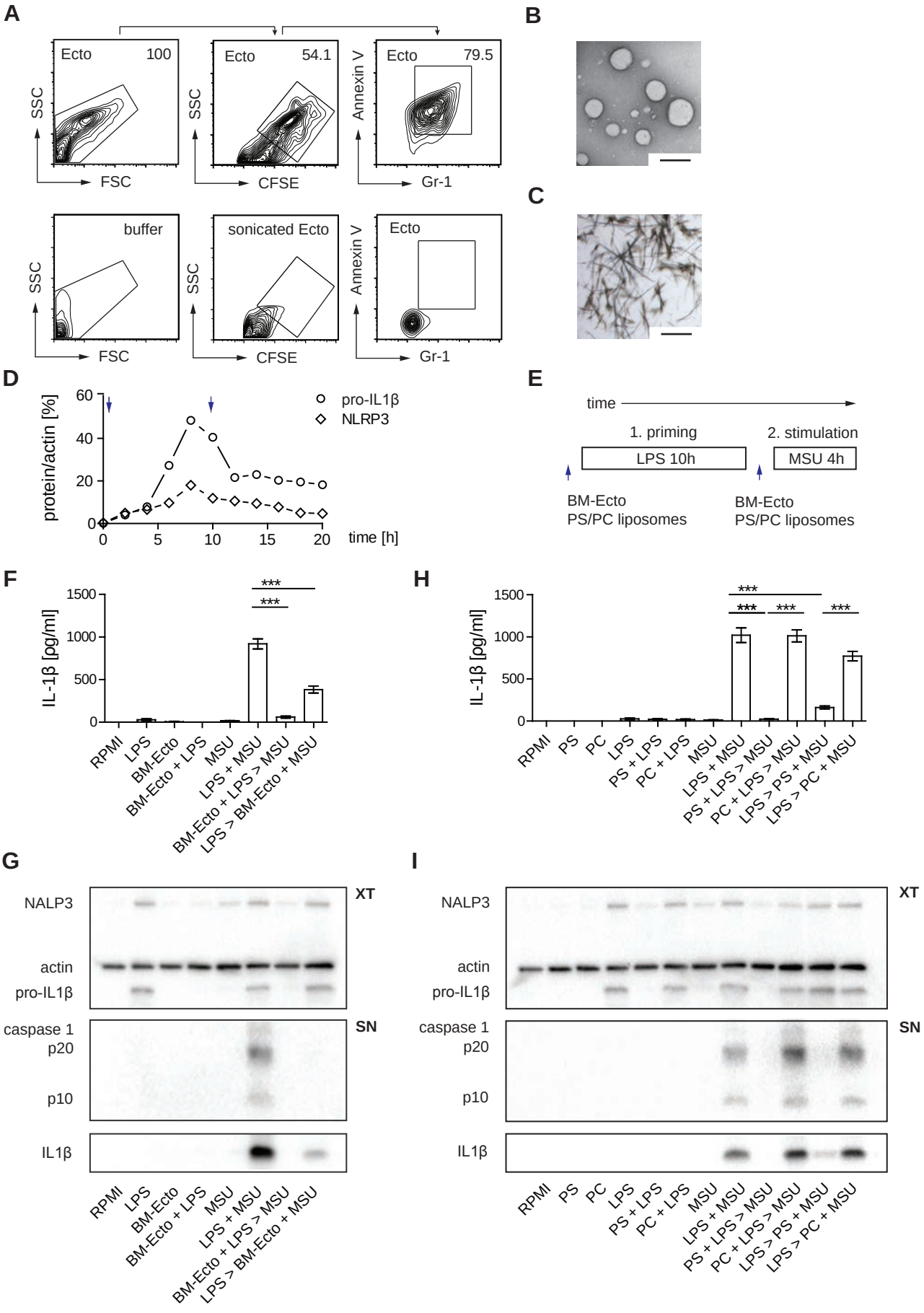
A
Ecto 100
Ecto 54.1
Ecto 79.5
SSC
FSC
CFSE
Annexin V
Gr-1
buffer
sonicated Ecto
Ecto
B
C
D
protein/actin [%]
time [h]
pro-IL1β
NLRP3
E
time
1. priming
2. stimulation
LPS 10h
MSU 4h
BM-Ecto
PS/PC liposomes
F
IL-1β [pg/ml]
RPMI
LPS
BM-Ecto
BM-Ecto + LPS
MSU
LPS + MSU
BM-Ecto + LPS > MSU
LPS > BM-Ecto + MSU
H
PS
PC
PS + LPS
PC + LPS
PS + LPS > MSU
PC + LPS > MSU
LPS > PS + MSU
LPS > PC + MSU
G
NALP3
actin
pro-IL1β
caspase 1
p20
p10
IL1β
XT
SN
I

Figure 2.

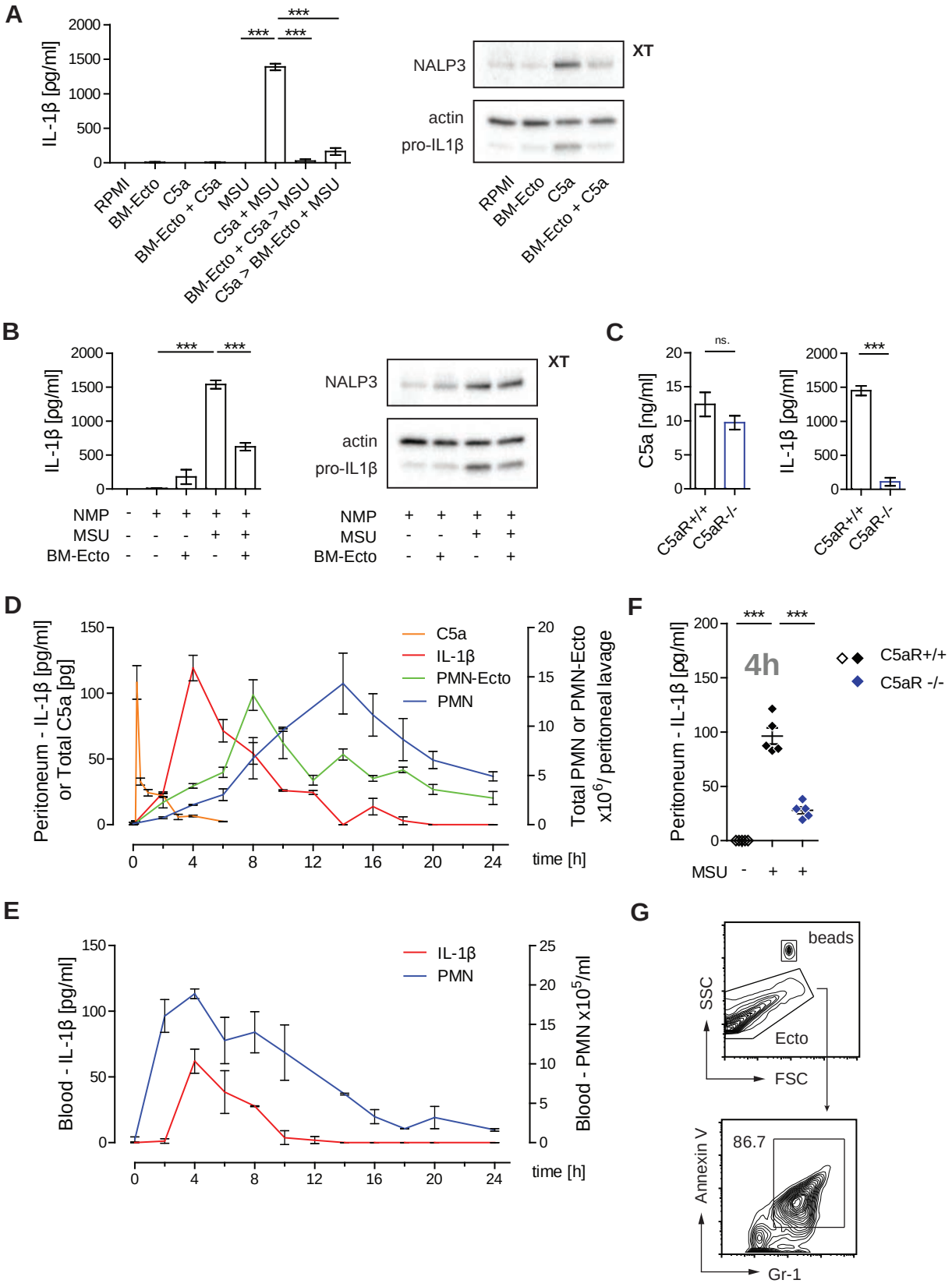
A
IL-1β [pg/ml]
RPMI
BM-Ecto
C5a
BM-Ecto + C5a
MSU
C5a + MSU
BM-Ecto + C5a > MSU
C5a > BM-Ecto + MSU
NALP3
actin
pro-IL1β
XT
B
NMP
MSU
BM-Ecto
C
C5a [ng/ml]
ns.
C5aR+/+
C5aR-/-
D
Peritoneum - IL-1β [pg/ml] or Total C5a [pg]
Total PMN or PMN-Ecto x10^6/ peritoneal lavage
C5a
IL-1β
PMN-Ecto
PMN
time [h]
E
Blood - IL-1β [pg/ml]
Blood - PMN x10^5/ml
F
4h
C5aR+/+
C5aR -/-
G
beads
SSC
Ecto
FSC
86.7
Annexin V
Gr-1

Figure 3.

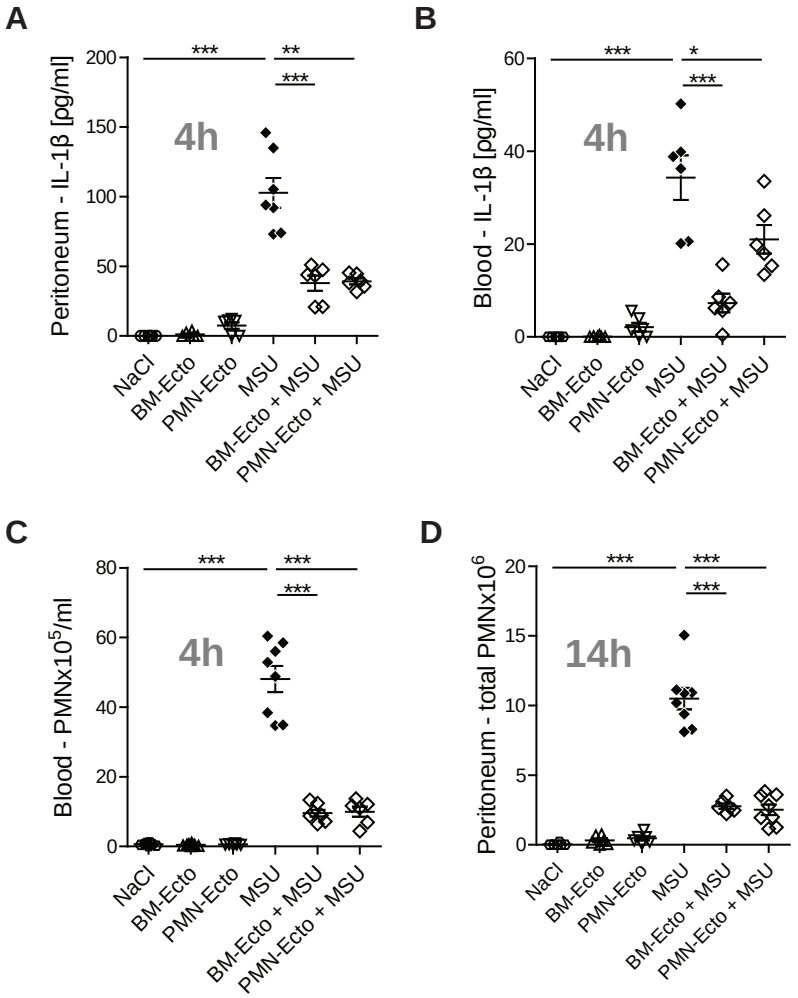
A
B
C
D
Peritoneum - IL-1β [pg/ml]
Blood - IL-1β [pg/ml]
Blood - PMNx10^5/ml
Peritoneum - total PMNx10^6
4h
14h
***
**
*
NaCl
BM-Ecto
PMN-Ecto
MSU
BM-Ecto + MSU
PMN-Ecto + MSU

Figure 4.

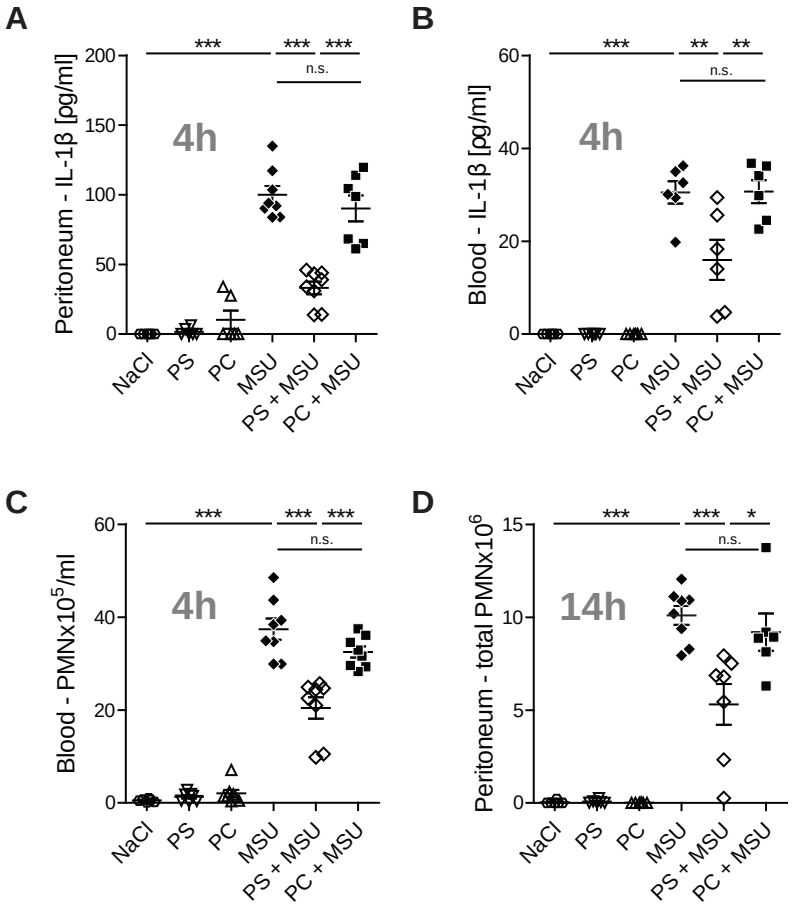
A
B
C
D
4h
4h
4h
14h
Peritoneum - IL-1β [pg/ml]
Blood - IL-1β [pg/ml]
Blood - PMNx10^5/ml
Peritoneum - total PMNx10^6
***
**
*
n.s.
NaCl
PS
PC
MSU
PS + MSU
PC + MSU

Figure 5.

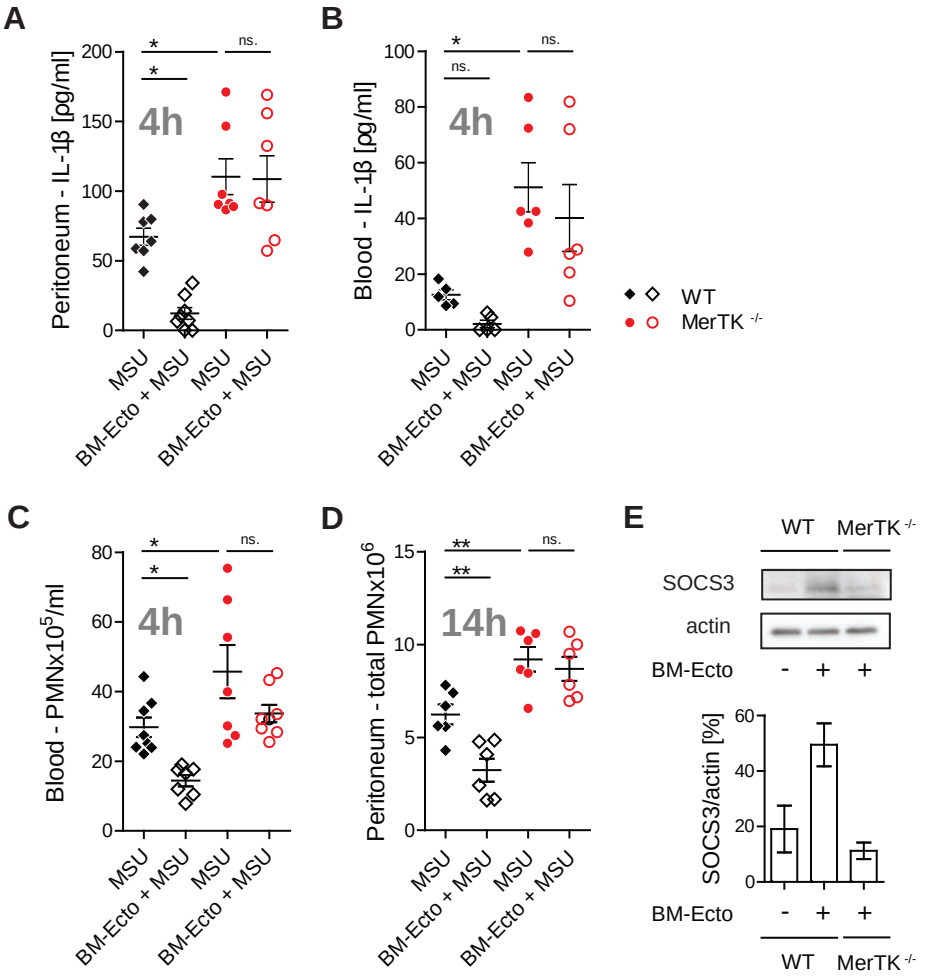
A
B
C
D
E
Peritoneum - IL-1β [pg/ml]
Blood - IL-1β [pg/ml]
Blood - PMNx10^5/ml
Peritoneum - total PMNx10^6
4h
14h
ns.
MSU
BM-Ecto + MSU
WT
MerTK -/-
SOCS3
actin
BM-Ecto
SOCS3/actin [%]

Figure 6.

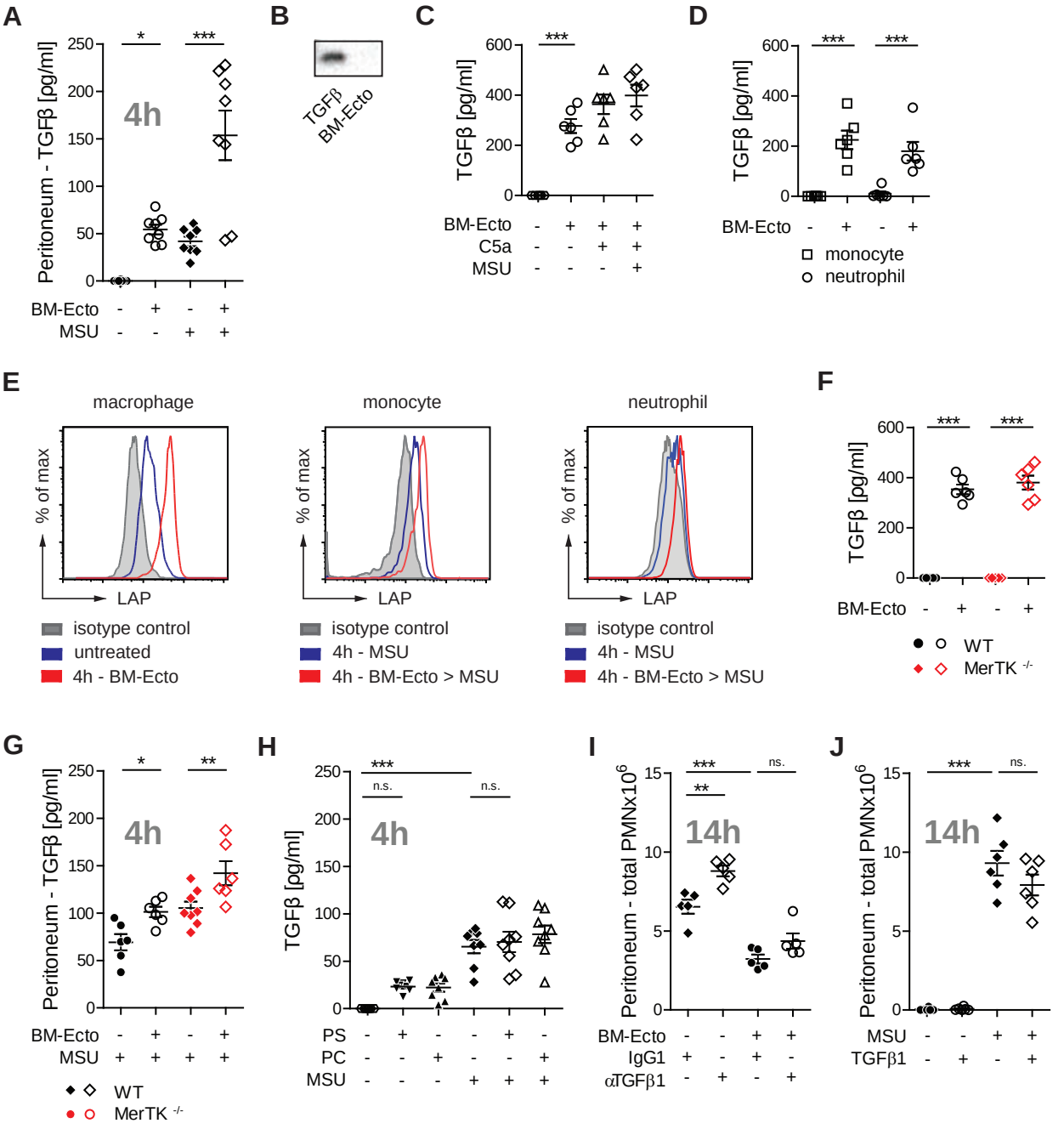
A
Peritoneum - TGFβ [pg/ml]
4h
BM-Ecto
MSU
B
TGFβ
BM-Ecto
C
TGFβ [pg/ml]
BM-Ecto
C5a
MSU
D
TGFβ [pg/ml]
BM-Ecto
monocyte
neutrophil
E
macrophage
monocyte
neutrophil
% of max
LAP
isotype control
untreated
4h - BM-Ecto
4h - MSU
4h - BM-Ecto > MSU
F
TGFβ [pg/ml]
BM-Ecto
WT
MerTK -/-
G
Peritoneum - TGFβ [pg/ml]
4h
BM-Ecto
MSU
WT
MerTK -/-
H
TGFβ [pg/ml]
4h
n.s.
PS
PC
MSU
I
Peritoneum - total PMNx10^6
14h
BM-Ecto
IgG1
αTGFβ1
ns.
J
Peritoneum - total PMNx10^6
14h
MSU
TGFβ1

Figure 7.

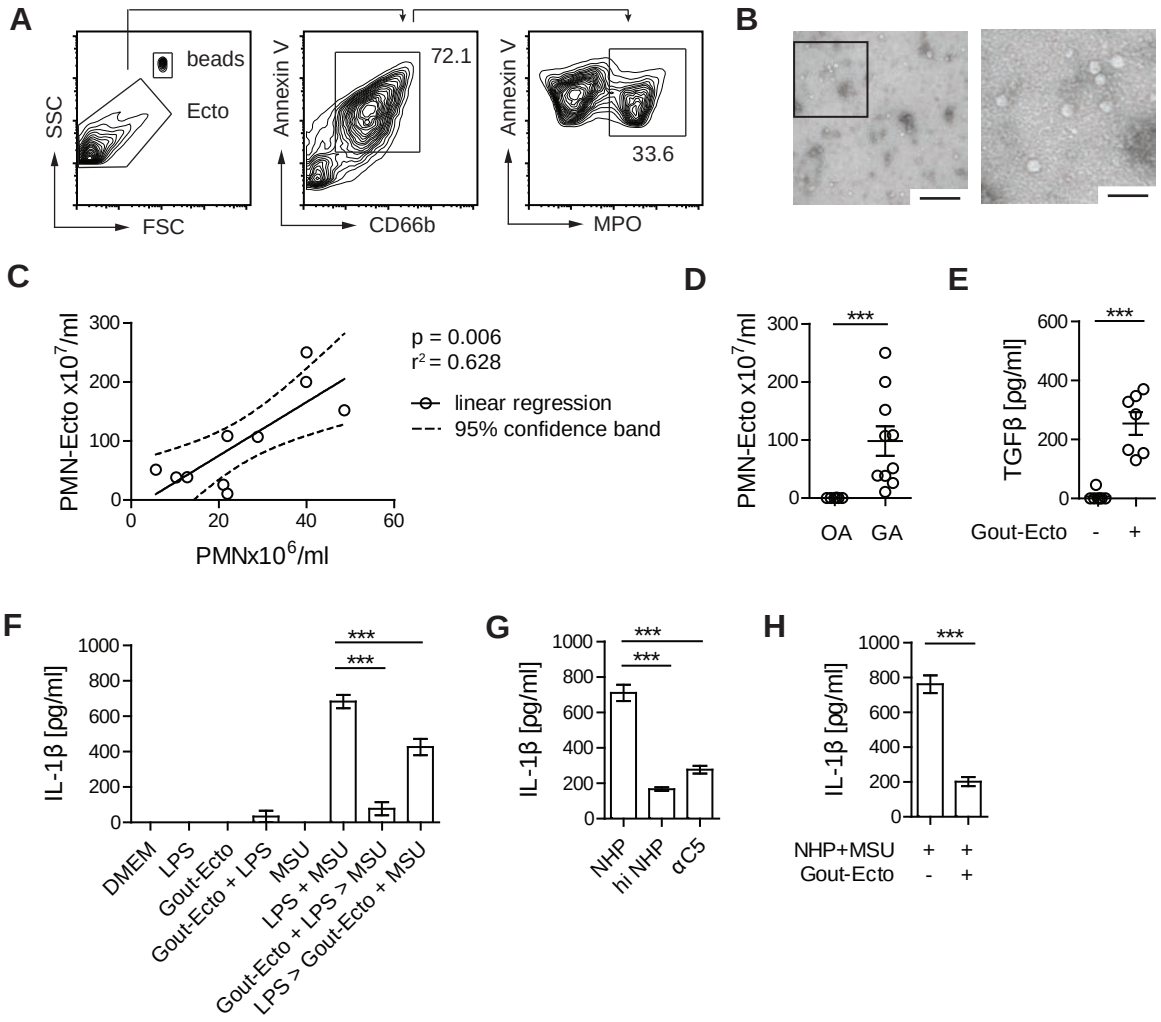
A
beads
Ecto
SSC
FSC
Annexin V
72.1
CD66b
Annexin V
33.6
MPO
B
C
PMN-Ecto x10^7/ml
PMNx10^6/ml
p = 0.006
r^2 = 0.628
linear regression
95% confidence band
D
PMN-Ecto x10^7/ml
***
OA
GA
E
TGFβ [pg/ml]
***
Gout-Ecto
F
IL-1β [pg/ml]
***
***
DMEM
LPS
Gout-Ecto
Gout-Ecto + LPS
MSU
LPS + MSU
Gout-Ecto + LPS > MSU
LPS > Gout-Ecto + MSU
G
IL-1β [pg/ml]
***
***
NHP
hi NHP
αC5
H
IL-1β [pg/ml]
***
NHP+MSU
Gout-Ecto

Supplementary Figure 1.

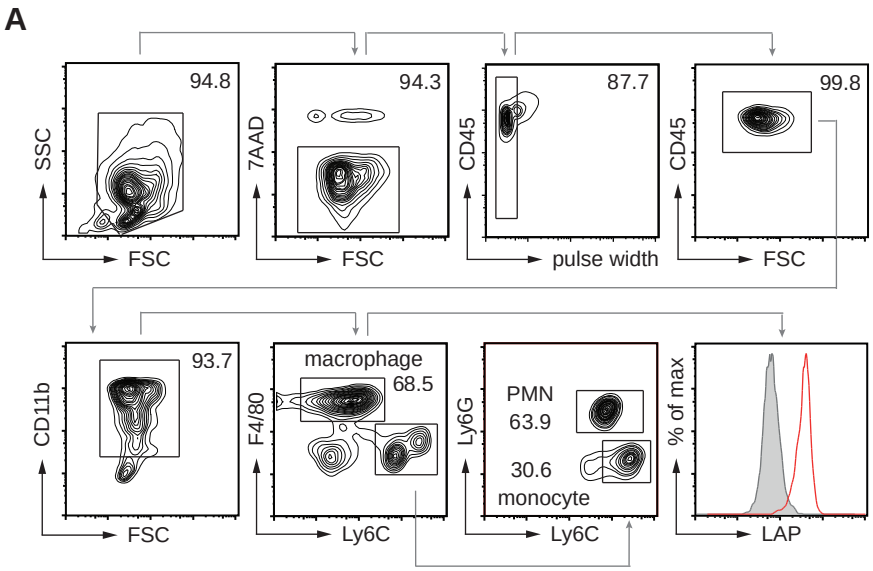

Antithymocyte globulin-induced platelet prothrombinase activity is a consequence of complement activation and platelet microvesicle release.

Arun Cumpelik[1], Estelle Gerossier[1], Julie Jin[2], Dimitrios Tsakiris[4,5], Michael Dickenmann[3], Salima Sadallah[1], Jürg A. Schifferli[1,2] and Daniel Zecher[1,2,3]

Departments of [1]Research, [2]Medicine, [3]Transplantation Immunology and Nephrology, [4]Hematology and [5]Laboratory Medicine, Basel University Hospital, Basel, Switzerland

Abstract

T cell depletion with antithymocyte globulins (ATG) can be complicated by thrombopenia and hypercoagulability. The underlying mechanism is still unclear. We found that binding of ATG to platelets caused platelet aggregation, alpha-granule release, membrane phosphatidylserine-exposure and the rapid release of platelet microvesicles (MV). Platelet activation and MV release were complement-dependent and required membrane insertion of C5b-8 but not stable lytic pore formation by C5b-9. Full platelet aggregation and activation by ATG also required the low-affinity Fc gamma receptor FcγRII. MV release, however, was FcγRII-independent. Platelet MV expressed high prothrombinase activity. Moreover, blocking C5 inhibited ATG-induced thrombin generation in platelet rich plasma. In 19 hematopoietic stem cell and kidney transplant patients, ATG treatment resulted in thrombopenia and increased plasma levels of d-dimer and thrombin-anti-thrombin-complexes. Flow cytometric analysis of complement fragments on platelet MV in patient plasma confirmed dose-dependent complement activation by ATG. However, the rapid rise in MV numbers observed in vitro was not seen during ATG treatment. *In vitro* experiments suggested that this was due to adherence of C3b-tagged MV to red blood cells via complement receptor CR1. These data suggest a clinically relevant link between complement activation and thrombin generation and offer a potential mechanism underlying ATG-induced hypercoagulability.

Introduction

Antithymocyte globulins (ATG) have been used successfully since the 1970s for the prevention of graft-versus-host disease in allogeneic hematopoietic stem cell transplantation (HSCT) (1) and to prevent or treat rejection in solid organ transplantation, most notably of kidney allografts (NTX) (2). ATG are polyclonal immunoglobulins generated by immunizing rabbits with human thymocytes (Thymoglobulin®) or the human Jurkat T cell line (ATG-Fresenius®). Its immunosuppressive effects are predominantly attributed to a profound and long-lasting depletion of T cells (3). It has been proposed that T cell depletion by ATG is achieved through various mechanisms including activation-induced apoptosis (4) and complement-dependent cytotoxicity, the latter being the dominant mechanism in blood (3, 4).

Whereas ATG-treatment is highly effective, it can be complicated by coagulation activation (5-8). The latter is commonly referred to as “non-overt disseminated intravascular coagulopathy” (9), as laboratory evidence reproducibly denotes thrombopenia and elevated plasma markers of hypercoagulability during ATG treatment (6, 10), whereas clinically apparent thrombosis or bleeding complications occur less frequently (6, 8). The exact mechanisms underlying this phenomenon are not yet known. Previous studies have suggested that ATG treatment induces a cytokine-mediated release of tissue factor (TF) into the circulation (6). Recently, Langer et al. showed that ATG binding to monocytes resulted in rapid complement-dependent TF decryption and activation of the extrinsic coagulation pathway (11). An alternative mechanism was proposed by Ankersmit et al., who reported that ATG induces platelet aggregation and activation via binding to the low affinity Fc gamma receptor FcγRII on platelets (12). Although the specific antigenic targets on platelets have not yet been identified, ATG is known to bind to platelet surfaces (13). In vitro, complement activation and deposition of the membrane attack complex C5b-9 on platelets has been shown to induce platelet activation and the translocation of phosphatidylserine (PS) from the inside to the outside of plasma membranes (14). PS can serve as a catalytic surface for the assembly of clotting factors into specific complexes. Whereas the TF:factor VIIa (FVIIa) complex is required for the initiation of hemostasis, the prothrombinase complex FVa:FXa:prothrombin is the major amplification mechanism, ultimately resulting in generation of thrombin, which is the critical step in coagulation activation. C5b-9 also induces shedding of microvesicles (MV) from the platelet surface (15). These MV display significant prothrombinase activity and have been proposed to constitute the principal catalytic surface for the prothrombinase complex (15, 16). Platelet MV can be isolated from blood of

healthy individuals (17). They have been found increased in various pathological conditions including sickle cell anemia (18), sepsis (19) and hemolytic uremic syndrome (20) and are thought to contribute to disease-related hypercoagulability (21).

On the basis of these findings, we hypothesized that the clinical phenomenon of ATG-induced hypercoagulability is a consequence of complement activation on platelets and subsequent release of procoagulant MV. To test this hypothesis, we first characterized the effects of ATG-mediated platelet activation in vitro and then studied platelet MV release during ATG treatment in HSCT and NTX patients.

Results

ATG induces aggregation and activation of platelets. We first set out to analyze the effect of ATG on platelet function by assessing the ability of ATG to induce aggregation and activation of platelets. Using light transmission aggregometry and platelet rich plasma (PRP), ATG alone had no effect on platelet aggregation (not shown). When platelets were simultaneously primed with low concentrations of ADP (0.75-1.5μM), ATG dose-dependently (10-100 μg/ml) induced strong and stable platelet aggregation. ADP alone or in combination with polyclonal rabbit IgG only caused a transient agglutination of platelets, indicating an ATG-specific effect (Figure 1A-B). Using flow cytometry, we next determined the impact of ATG on platelet activation assessing degranulation (surface expression of p-selectin) and exposure of PS (binding of annexin V). ATG bound to and dose-dependently activated platelets both in whole blood (Figure 1C,D) and PRP (Figure 1F). Platelet activation was ATG-specific as it did not occur in response to polyclonal rabbit IgG. Blocking the low affinity Fc receptor FcγRII on platelets using an anti-CD32 antibody reduced, but did not fully abolish, ATG-induced platelet aggregation (Figure 1E). Consistently, incubation of platelets with ATG following FcγRII blockade still caused significant platelet activation (Figure 1F). These findings suggested that there was a dose-dependent, FcγRII-independent activating effect of ATG on platelets.

ATG induces the release of platelet microvesicles with prothrombinase activity. We next investigated whether platelet activation by ATG resulted in the release of MV. Following incubation of whole blood with ATG, platelet MV were isolated by sequential centrifugation and characterized as well as counted by flow cytometry. We found a dose-dependent increase of CD41+ annexinV+ double-positive platelet MV in response to ATG, which was not observed with polyclonal rabbit IgG (Figure 2A-B). Blocking FcγRII on platelets prior to incubation with ATG had no effect on the number of MV released (Figure 2C). The surface of ATG-induced platelet MV was highly enriched in the coagulation factor FV/Va (Figure 2D), which is part of the prothrombinase complex. Consequently, addition of increasing amounts of platelet MV to plasma resulted in a dose-dependent activation of thrombin in a chromogenic thrombin assay (Figure 2E).

Role of complement in ATG-induced platelet activation and MV release. We next used flow cytometry to analyze platelets and platelet MV for surface deposition of complement fragments as an indicator of complement activation following ATG binding. Incubation of platelets with

rabbit IgG in the presence of normal human serum (NHS) resulted in deposition of low levels of C1q, C4d and C3b, whereas C5b-9 was undetectable. After incubation with ATG, however, there was evidence of robust complement activation on platelet membranes (Figure 3A). Platelet MV analysis resulted in three major observations (Figure 3A). First, constitutive MV (low numbers released in the absence of ATG) weakly bound C1q and C4d, but displayed considerable binding of C3b. C5b-9, however, was absent. Second, analysis of ATG-induced MV revealed strong ATG-binding and substantial deposition of all complement fragments including C5b-9. Third, fluorescence intensity of ATG and C5b-9 was higher on MV than on platelets indicating a higher density of these molecules on MV compared to platelets. In conjunction with the much smaller surface area of MV compared to platelets, these findings indicated a preferential shedding of ATG and C5b-9 from platelets by vesiculation. Moreover, these results suggested that vesiculation took place in proximity of the terminal complement complex proteins and raised the question whether complement activation was required for this platelet response. To test this, we preincubated serum with eculizumab, which blocks cleavage and activation of C5. This significantly inhibited the release of MV in response to ATG (Figure 3B). Blocking membrane insertion of C5b-7 with a monoclonal antibody targeting native C7 was equally effective (Figure 3C). Using C8-depleted serum, MV release was completely abolished (Figure 3D). In contrast, blocking C9 with a monoclonal antibody that prevents stable lytic pore formation by inhibiting incorporation of C9 into the C5b-8 complex (11), had no effect (Figure 3E). Of note, MV release paralleled PS surface exposure (Figure 3 F-G) and degranulation (not shown) of platelets, which was significantly inhibited in the absence of C8 or following blockade of C5 or C7. Consistently, blockade of C9 had no effect (Figure 3F). These results indicated that ATG-induced platelet activation and MV release required insertion of C5b-8 into the platelet membrane but not stable lytic pore formation by C5b-9.

ATG-induced platelet prothrombinase activity can be inhibited by complement blockade. We next asked whether blocking complement-dependent platelet activation would inhibit ATG-induced prothrombinase activity in PRP. ATG treatment of PRP resulted in rapid generation of thrombin in a fluorogenic thrombin assay. We found a shorter lag time and steeper increase of the fluorogenic signal following treatment with ATG compared to control IgG (Figure 3H). Endogenous thrombin potential (area under the curve), however, was comparable, potentially reflecting earlier clotting and subsequent inhibition of complement activation on platelets. Importantly, pretreatment of platelets with eculizumab reduced all parameters of thrombin

generation, indicating that complement activation was indeed required for thrombin generation and that ATG-induced hypercoagulability can be inhibited by anti-C5 treatment.

ATG cause thrombopenia, hypercoagulability and complement activation in patients. To corroborate our in vitro findings, we next analyzed blood from patients receiving ATG either prior to HSCT (n=10) or during NTX (n=9). In both patient groups, we found a rapid reduction in platelet counts detectable already at the end of the first ATG infusion (Figure 4A). Plasma levels of d-dimer and thrombin-anti-thrombin (TAT) complexes were elevated on day 1 compared to baseline (Figure 4 B-C). There was a significant correlation between the absolute drop in platelets between baseline and day 1 to TAT levels on day 1 (Spearman correlation coefficient r=0.70 p=0.002, Figure 4D). Levels of sC5b-9 increased during the course of ATG treatment, albeit to a modest degree (Figure 4F).

Kinetics of platelet MV release during ATG treatment. Next, we counted and characterized plasma platelet MV by flow cytometry during ATG treatment (Figure 5A). At baseline, there was no significant difference in CD41+ annexinV+ double-positive platelet MV counts between HSCT and NTX patients and healthy controls (Figure 5B). Of note, the three NTX patients with post-operative bleeding (n=2/9) or thrombotic complications (n=1/9) had the highest platelet MV counts at baseline (47, 136 and 222x10^5 MV/ml plasma, respectively, Figure 5B). Contrary to what we had hypothesized, we observed a decrease (defined as less than 50% of baseline) rather than an increase (defined as doubling) in platelet MV counts 15 min following the start of ATG in 50% (9/18) of the patients analyzed. Compared to baseline numbers, MV counts at later time points either remained low (HSCT patients) or varied considerably with no clear pattern identifiable (NTX patients) (Figure 5C).

Patient platelet MV stain positive for ATG and complement fragments. There was a rapid percentual increase in ATG-positive platelet MV that peaked after ATG infusion in both groups (Figure 6A). Staining for C4d showed high inter-individual variability without significant changes during ATG treatment (Figure 6B). Deposition of C3d and C5b-9 differed between the two groups. In NTX patients, deposition of both proteins increased and peaked after ATG infusion with a high correlation between these two parameters (Spearman correlation coefficient r=0.67, p<0.01). In HSCT patients, no relevant changes in C3d or C5b-9 deposition were observed over time and deposition of both proteins was significantly lower compared to NTX patients (Figure 6 C-D). Complement activation in NTX patients was due to ATG and not related to the surgical

procedure, as platelet MV from a cohort of NTX patients not treated with ATG displayed significantly less C5b-9 deposition at a comparable time point (Figure 6E). These findings indicated a higher degree of complement activation in NTX compared to HSCT patients, which was likely a reflection of the higher dose and infusion speed in the former compared to the latter. There was no significant correlation between the magnitude of complement fragment deposition at any time during ATG treatment and the plasma markers of hypercoagulability tested.

ATG-opsonized MV adhere to red blood cells in vitro. Next we tried to understand the discrepancy between the dose-dependent release of platelet MV in response to ATG in vitro and the lack thereof seen in ATG-treated patients. We hypothesized that complement fragment deposition on ATG-induced MV facilitated binding to cells carrying complement receptors (CR). We focused on red blood cells (RBC) due to their predominance in blood and the well-described phenomenon of immune-adherence of C3b-positive immune complexes to RBC via CR1(22, 23). Following incubation of CFSE-labeled ATG-negative MV with RBC, there was some binding of MV to RBC (Figure 7A) consistent with the presence of C3b on ATG-negative MV (Figure 3A). However, there was a major increase in binding when equal numbers of ATG-positive MV were incubated with RBC (Figure 7A). Blocking CR1 on RBC significantly reduced MV binding (Figure 7B), suggesting that CR1 indeed mediated this interaction. Taken together, these results suggested that plasma platelet MV numbers are under-estimated during ATG treatment due to the excess capacity of RBC to bind complement-opsonized MV via CR1.

Discussion

In this study, we describe a mechanism how immunosuppressant therapy with ATG activates platelets and establish a link between complement and coagulation activation as a potential explanation for the clinically observed phenomenon of ATG-induced hypercoagulability.

One of the major findings of the present study is that both platelet exposure of PS and MV shedding in response to ATG were dependent on membrane insertion of the complement proteins C5b-8 but that full lytic pore formation by C5b-9 was dispensable. In line with these findings, Langer et al. recently demonstrated that ATG-induced PS exposure on THP-1 monocytes required C5b-7 insertion but not full MAC assembly. The specific role of C8, however, was not addressed (11). Integration of C8 into membrane bound C5b-7 causes target cell activation by inducing an inward directed calcium flux (24). Sims et al. previously demonstrated that platelet vesiculation following membrane assembly of C5b-9 was calcium-dependent but did not address the specific contribution of C8 versus C9 (15). Our data strongly suggest that membrane insertion of C8 is the critical step triggering ATG-induced platelet activation and subsequent vesicle release.

Whereas PS is critical in supporting coagulation activation, TF has a major role in initiating it. In this regard, it is important to note that Langer et al. recently reported on rapid activation of monocyte TF by ATG (11). Whether platelets and platelet MV express TF is highly controversial. Some investigators have attributed platelet TF to monocyte-derived MV bound to platelets (21). We were not able to induce thrombin generation in PRP by ATG without addition of purified TF (unpublished observation). Therefore, it is likely that the mechanism described by Langer et al. is critical for initiation of ATG-induced hypercoagulability, whereas the mechanism described here is complementary in that it potently amplifies clotting once it has been initiated.

Previous studies have already reported on plasma MV in the context of ATG treatment (10, 25). Using flow cytometry, either total (10) or platelet (25) MV were counted before and compared to MV counts after several days of ATG treatment. These studies did not find any difference in plasma MV numbers. Based on the rapid MV release in response to ATG observed in vitro, we studied plasma platelet MV numbers within minutes to hours following the first dose of ATG, hypothesizing that this approach would allow for the detection of a temporary rise in platelet MV. The unexpected finding of an early decrease rather than increase in MV counts after starting

ATG suggested that in patients, ATG-induced platelet MV are either rapidly cleared from the circulation or adhere to circulating cells, these two mechanisms not being mutually exclusive(22). MV are cleared within minutes following intravenous injection in mice (26, 27). Various uptake mechanisms have been proposed involving PS on MV and the integrin αvβ3 on phagocytic cells (27, 28). Alternatively, uptake might involve C3b on MV and its receptor CR1 on macrophages (29). Moreover, CR1 is known to mediate binding of C3b-tagged immune complexes to RBC in the blood stream, which then shuttle these complexes to the monocyte-macrophage system in spleen and liver for degradation (22, 23). Our results do not rule out binding of C3b-opsonized MV to cells other than erythrocytes, e.g. CR1-positive neutrophils (20, 29). However, given that 95% of CR1 in the circulation can be found on RBC and that clustering of CR1 on RBC facilitates target binding (22), it is likely that the mechanism described here is relevant for immune adherence of ATG-opsonized MV. Consistent with previous reports (30), we observed complement fragment deposition on MV independent of antibody binding. Moreover, we found weak but relevant binding of ATG-negative MV to RBC. This suggests that immune adherence of MV occurs constitutively and might be a physiological means to maintain MV homeostasis. We also observed direct binding of ATG to MV shed constitutively in vitro (unpublished observation). Binding of free ATG to preexisting plasma MV and subsequent immune adherence to RBC might explain the persistently lower than baseline MV counts observed during ATG treatment especially in HSCT patients. Lastly, complement fragment deposition on MV in the absence of ATG as well as immune adherence of ATG-opsonized MV might explain the lack of correlation between MV counts or phenotype and the serological markers of hypercoagulability tested.

Our findings have several potential clinical implications. Blocking FcγRII, as previously suggested (12), might be insufficient to prevent ATG-induced hypercoagulability given that NTX patients treated with IVIG (whose primary mechanism of action is saturating Fc receptors) displayed the same degree of thrombopenia and hypercoagulability compared to HSCT patients not treated with IVIG. High baseline platelet MV counts might help identify those patients prone to ATG-induced hypercoagulability. Complement blockade during ATG treatment might prevent coagulation activation in these patients. Of note, both clinical (31, 32) and experimental (33, 34) evidence suggests that T cell depletion by ATG still occurs in the absence of terminal complement activation and therefore blocking C5 with eculizumab might be a potential therapeutic to limit ATG-induced hypercoagulability.

Taken together, we have identified how ATG activates platelets and how complement activation on target cells results in vesicle shedding and hypercoagulability. These findings might not only be relevant in the context of ATG treatment but potentially extent to other pathological conditions of focal complement activation like thrombotic microangiopathy or antibody-mediated allograft rejection. Moreover, CR1-mediated immune-adherence of C3b-coated MV might be a general mechanism contributing to the homeostasis of cell-derived MV.

Materials and Methods

Reagents and antibodies. Antithymocyte globulins (ATG-Fresenius®) were from Fresenius (Oberdorf, Switzerland), polyclonal rabbit IgG from BioXCell (West Lebanon, USA), anti-C5 (eculizumab®) from Alexion Pharmaceuticals (Lausanne, Switzerland), anti-C7 (clone A221) from Quidel (San Diego, USA), anti-C9 (X197) from Hycult Biotech (Uden, Netherlands) and C8-depleted serum was from Sigma (Buchs, Switzerland). Murine mAb V237 recognizing human FV/Va was a generous gift from Dr. Charles Esmon (OMRF, Oklahoma, USA). Anti-CD32 (FUN-1) was from Biolegend (San Diego, USA), anti-CR1 (J3D3) from Beckman Coulter (Nyon, Switzerland) and CFSE from Molecular Probes (Zug, Switzerland).

Platelet stimulation and MV release in vitro. 1 ml refludan-anticoagulated blood was incubated with ATG or rabbit IgG for 30 min at 37°C. Blood was then either used directly or was centrifuged twice at 3000x*g* for 10 min to generate plasma. Plasma was further centrifuged at 18500x*g* for 15 min to isolate MV. Alternatively, platelet rich plasma (PRP) was obtained from refludan-anticoagulated blood centrifuged 2 min at 750x*g*. PRP was diluted 1:10 in Ca-free Tyrode's buffer. 0.25 ml of this solution ($1x10^7$ platelets) were incubated for 30 min at 37°C with ATG and 10% autologous normal human serum (NHS) in a buffer containing 2.5 mM $CaCl_2$. Where indicated, PRP and NHS were preincubated with antibodies blocking individual complement proteins for 15 min at RT before adding ATG. To study the impact of C8, sepharose gel-filtered platelets were incubated with 20% NHS or C8-depleted NHS in the presence of ATG. Following washing, platelets were analyzed by flow cytometry. MV were isolated by sequentially centrifuging the platelet supernatant (10 min at 1000x*g* then 15 min at 18500x*g*). All donors gave informed consent before the blood draw.

Platelet aggregation. Aggregation of PRP ($2.5\text{-}3x10^5$ platelets/µl) was assessed photometrically using an APACT4004 aggregometer (Labitec, Ahrensburg, Germany). After 60 seconds, ADP (0.75-1.5 µM) was added alone or together with varying amounts of ATG or IgG. Aggregation was assessed over the next 9 minutes.

Thrombin generation assays. To assess MV prothrombinase activity, equal volumes of MV (generated by stimulating platelets with increasing concentrations of ATG or IgG in the presence of NHS) were incubated with 25% normal human plasma and the chromogenic substrate TH8198 (Pefachrome®, DSM, Basel, Switzerland). After thrombin-mediated cleavage of the

substrate, the amount of p-nitroaniline dihydrochloride formed was determined by kinetic measurements of absorbance at 405 nm on a Synergy H1 microplate reader (Biotek, Luzern, Switzerland). Thrombin generation in PRP was determined using the calibrated automated thrombogram (Thrombinoscope, Stago, Zürich, Switzerland) on a Thermo Fisher fluorometer. Briefly, citrated PRP ($1x10^6$ platelets/µl) was mixed with 0.1 mg/ml ATG or rabbit IgG and $CaCl_2$ (10 mM final concentration) for 5 min prior to adding 0.5 pM TF. The fluorogenic substrate amino-methyl-coumarin was then added and thrombin generation recorded over time. Where indicated, PRP was preincubated with 0.25 µg/ml anti-C5 prior to adding ATG.

Clinical study protocol. Plasma samples were obtained from patients receiving ATG between January and December 2013 at Basel University Hospital. Patients undergoing deceased donor renal transplantation were given ATG (ATG-Fresenius®, Fresenius, Oberdorf, Switzerland) at 9 mg/kg or Thymoglobulin® (Genzyme, Naarden, Netherlands) at 1.5 mg/kg body weight, respectively, over 4 hours during surgery. All patients had received 500 mg methylprednisolone and IVIG (0.4 g/kg body weight) and had been started on mycophenolate-mophetil and tacrolimus within 24 hours prior to transplantation. Patients with hematological malignancies were given ATG-Fresenius® (5 mg/kg body weight over 6 hours) on day -3 relative to HLA-identical non-related hematopoietic stem cell transplantation. These patients were simultaneously started on various conditioning chemotherapies and had received 100 mg methylprednisolone prior to the start of ATG. The study had been approved by the local ethical committee and all patients had given written informed consent prior to inclusion in the study. Blood was drawn at the following time points relative to the start of the first ATG infusion: prior to start (baseline), 15, 30, 120 min, after the infusion and 24h later prior to the second dose of ATG (day 1). Platelet counts and coagulation parameters were determined at the central laboratory of Basel University Hospital. EDTA- and heparin-plasma were frozen at -80°C within two hours of blood drawing following two centrifugations at 3000x*g* and snap freezing in liquid nitrogen. For MV analysis, heparin-plasma was thawed at 37°C, diluted in 0.22 µm filtered HBSS+Hepes and centrifuged at 16000x*g*. The pellet was resuspended in 0.25 ml for flow cytometric analysis.

Flow cytometric analysis of platelets and platelet MV. Refludan-anticoagulated whole blood, PRP, platelet MV or MV isolated from patient plasma were resuspended in 0.22 µm filtered buffers and incubated with annexin V-APC (Immunotools, Forsythe, Germany) and fluorescently-tagged antibodies against the following targets as indicated: CD41 (clone HIP8,

BD), CD235a (HI264, BD), CD62P (AK4, Biolegend), polyclonal C1q and C3d (both Dako). C5b-9 staining was performed using unlabeled mouse anti-C5b-9 (aE11, Dako) followed by anti-mouse IgG Alexa488 (Invitrogen). Monoclonal anti-C4d (A213, Quidel) was fluorescently labeled using the Lightning-Link Rapid Dylight 488 kit (Innova Biosciences). ATG binding was revealed using goat anti-rabbit IgG Alexa488 (Invitrogen). Flow cytometry was performed on a CyanADP (in vitro experiments) or a Gallios cytometer (patient samples, both Beckman Coulter). MV were gated on logarithmic FSC/SSC scale with an arbitrary SSC threshold using CyanADP and no threshold on Gallios. The number of specific MV was quantitated using Trucount® beads (BD) as follows: (number of beads x % MV of total events (FSC/SSC) x % specific population) / % beads). Data were analyzed using FloJo software (version 9.5.2, TreeStar, San Jose, USA).

MV adherence to red blood cells. Platelet MV were generated by incubating PRP with 200 µg/ml ATG (ATG+ MV) or rabbit IgG (control MV) + 10% NHS as described above. Equal numbers of MV were then incubated with 5 µM CFSE for 15 min at 37°C. Following washing, CFSE-positive MV were incubated with washed autologous red blood cells (RBC) at a ratio of 100:1 for 15 min. Following washing, MV binding to RBC was revealed by flow cytometry. Where indicated, $1x10^7$ RBC were incubated with 0.1 mg/ml unlabeled anti-CR1 for 15 min. 1/100 of this solution was then added to $1x10^7$ CFSE-labeled MV containing 0.1 mg/ml anti-CR1 and incubated for 30 min at 37°C. Following washing, binding was assessed flow cytometry.

sC5b-9 ELISA. EDTA plasma samples were analyzed for sC5b-9 using the Microvue® sC5b-9 Plus ELISA Kit (Quidel, San Diego, USA).

Statistical analysis. Data are presented as mean ± SD. Comparison between groups was done using paired or unpaired t-test or one-way ANOVA with Bonferroni's multiple comparison post testing. Analyses were performed using Prism software (version 6; GraphPad Software). Significance was set at $p < 0.05$.

Acknowledgments

D.Z. was supported by Fondation Machaon, Geneva, Switzerland and *Wissenschaftsfonds* of Basel University Hospital, Basel, Switzerland. J.A.S. was supported by the Swiss National Science Foundation.

Authorship

A.C. and D.Z. designed and performed experiments and wrote the paper. E.G. and J.J. performed experiments. D.T., M.D. and S.S. gave conceptual advice and J.A.S. supervised the project.

References

1. Kumar A, Mhaskar AR, Reljic T, Mhaskar RS, Kharfan-Dabaja MA, Anasetti C, Mohty M, and Djulbegovic B. Antithymocyte globulin for acute-graft-versus-host-disease prophylaxis in patients undergoing allogeneic hematopoietic cell transplantation: a systematic review. *Leukemia.* 2012;26(4):582-8.
2. Brennan DC, Daller JA, Lake KD, Cibrik D, and Del Castillo D. Rabbit antithymocyte globulin versus basiliximab in renal transplantation. *N Engl J Med.* 2006;355(19):1967-77.
3. Mohty M. Mechanisms of action of antithymocyte globulin: T-cell depletion and beyond. *Leukemia.* 2007;21(7):1387-94.
4. Genestier L, Fournel S, Flacher M, Assossou O, Revillard JP, and Bonnefoy-Berard N. Induction of Fas (Apo-1, CD95)-mediated apoptosis of activated lymphocytes by polyclonal antithymocyte globulins. *Blood.* 1998;91(7):2360-8.
5. Pihusch R, Holler E, Muhlbayer D, Gohring P, Stotzer O, Pihusch M, Hiller E, and Kolb HJ. The impact of antithymocyte globulin on short-term toxicity after allogeneic stem cell transplantation. *Bone Marrow Transplant.* 2002;30(6):347-54.
6. Weber M, Kröger N, Langer F, Hansen A, Zabelina T, Eifrig B, Hossfeld DK, and Zander AR. Non-overt disseminated intravascular coagulation in patients during treatment with antithymocyte globulin for unrelated allogeneic hematopoietic stem cell transplantation. *Bone marrow transplantation.* 2003;31(9):817-22.
7. Madaio MP, Spiegel JE, and Levey AS. Life-threatening thrombocytopenia complicating antithymocyte globulin therapy for acute kidney transplant rejection. Evidence of in situ immune complex formation on the platelet surface. *Transplantation.* 1988;45(3):647-9.
8. Trivedi HS, Lal SM, Gupta N, and Ross G, Jr. ATGAM associated coagulopathy in renal transplant patients: a report of two unusual cases. *The International journal of artificial organs.* 1996;19(8):448-50.
9. Taylor FB, Jr., Toh CH, Hoots WK, Wada H, Levi M, Scientific Subcommittee on Disseminated Intravascular Coagulation of the International Society on T, and Haemostasis. Towards definition, clinical and laboratory criteria, and a scoring system for disseminated intravascular coagulation. *Thromb Haemost.* 2001;86(5):1327-30.
10. Inbal A, Lubetsky A, Shimoni A, Dardik R, Sela BA, Eskaraev R, Levi I, Tov NS, and Nagler A. Assessment of the coagulation profile in hemato-oncological patients receiving

ATG-based conditioning treatment for allogeneic stem cell transplantation. *Bone marrow transplantation.* 2004;34(5):459-63.

11. Langer F, Spath B, Fischer C, Stolz M, Ayuk FA, Kröger N, Bokemeyer C, and Ruf W. Rapid activation of monocyte tissue factor by antithymocyte globulin is dependent on complement and protein disulfide isomerase. *Blood.* 2013;121(12):2324-35.
12. Ankersmit HJ, Roth GA, Moser B, Zuckermann A, Brunner M, Rosin C, Buchta C, Bielek E, Schmid W, Jensen-Jarolim E, et al. CD32-mediated platelet aggregation in vitro by anti-thymocyte globulin: implication of therapy-induced in vivo thrombocytopenia. *American journal of transplantation : official journal of the American Society of Transplantation and the American Society of Transplant Surgeons.* 2003;3(6):754-9.
13. Greco B, Bielory L, Stephany D, Hsu SM, Gascon P, Nienhuis A, and Young N. Antithymocyte globulin reacts with many normal human cell types. *Blood.* 1983;62(5):1047-54.
14. Wiedmer T, Esmon CT, and Sims PJ. On the mechanism by which complement proteins C5b-9 increase platelet prothrombinase activity. *J Biol Chem.* 1986;261(31):14587-92.
15. Sims PJ, Faioni EM, Wiedmer T, and Shattil SJ. Complement proteins C5b-9 cause release of membrane vesicles from the platelet surface that are enriched in the membrane receptor for coagulation factor Va and express prothrombinase activity. *The Journal of biological chemistry.* 1988;263(34):18205-12.
16. Sinauridze EI, Kireev DA, Popenko NY, Pichugin AV, Panteleev MA, Krymskaya OV, and Ataullakhanov FI. Platelet microparticle membranes have 50- to 100-fold higher specific procoagulant activity than activated platelets. *Thromb Haemost.* 2007;97(3):425-34.
17. Berckmans RJ, Nieuwland R, Boing AN, Romijn FP, Hack CE, and Sturk A. Cell-derived microparticles circulate in healthy humans and support low grade thrombin generation. *Thromb Haemost.* 2001;85(4):639-46.
18. Nebor D, Romana M, Santiago R, Vachiery N, Picot J, Broquere C, Chaar V, Doumdo L, Odievre MH, Benkerrou M, et al. Fetal hemoglobin and hydroxycarbamide moduate both plasma concentration and cellular origin of circulating microparticles in sickle cell anemia children. *Haematologica.* 2013;98(6):862-7.
19. Joop K, Berckmans RJ, Nieuwland R, Berkhout J, Romijn FP, Hack CE, and Sturk A. Microparticles from patients with multiple organ dysfunction syndrome and sepsis support coagulation through multiple mechanisms. *Thromb Haemost.* 2001;85(5):810-20.

20. Ståhl A-l, Sartz L, and Karpman D. Complement activation on platelet-leukocyte complexes and microparticles in enterohemorrhagic Escherichia coli-induced hemolytic uremic syndrome. *Blood.* 2011;117(20):5503-13.
21. Owens AP, 3rd, and Mackman N. Microparticles in hemostasis and thrombosis. *Circ Res.* 2011;108(10):1284-97.
22. Schifferli JA, Ng YC, and Peters DK. The role of complement and its receptor in the elimination of immune complexes. *The New England journal of medicine.* 1986;315(8):488-95.
23. Horakova E, Gasser O, Sadallah S, Inal JM, Bourgeois G, Ziekau I, Klimkait T, and Schifferli JA. Complement mediates the binding of HIV to erythrocytes. *J Immunol.* 2004;173(6):4236-41.
24. Niculescu F, and Rus H. Mechanisms of signal transduction activated by sublytic assembly of terminal complement complexes on nucleated cells. *Immunologic research.* 2001;24(2):191-9.
25. Pihusch R, Höhnberg B, Salat C, Pihusch M, Hiller E, and Kolb H-J. Platelet flow cytometric findings in patients undergoing conditioning therapy for allogeneic hematopoietic stem cell transplantation. *Annals of hematology.* 2002;81(8):454-61.
26. Willekens FLA, Werre JM, Kruijt JK, Roerdinkholder-Stoelwinder B, Groenen-Döpp YAM, van den Bos AG, Bosman GJCGM, and van Berkel TJC. Liver Kupffer cells rapidly remove red blood cell-derived vesicles from the circulation by scavenger receptors. *Blood.* 2005;105(5):2141-5.
27. Dasgupta SK, Le A, Chavakis T, Rumbaut RE, and Thiagarajan P. Developmental endothelial locus-1 (Del-1) mediates clearance of platelet microparticles by the endothelium. *Circulation.* 2012;125(13):1664-72.
28. Dasgupta SK, Abdel-Monem H, Niravath P, Le A, Bellera RV, Langlois K, Nagata S, Rumbaut RE, and Thiagarajan P. Lactadherin and clearance of platelet-derived microvesicles. *Blood.* 2009;113(6):1332-9.
29. Fearon DT. Identification of the membrane glycoprotein that is the C3b receptor of the human erythrocyte, polymorphonuclear leukocyte, B lymphocyte, and monocyte. *J Exp Med.* 1980;152(1):20-30.
30. Sadallah S, Eken C, Martin PJ, and Schifferli JA. Microparticles (ectosomes) shed by stored human platelets downregulate macrophages and modify the development of dendritic cells. *Journal of immunology (Baltimore, Md : 1950).* 2011;186(11):6543-52.

31. Stegall MD, Diwan T, Raghavaiah S, Cornell LD, Burns J, Dean PG, Cosio FG, Gandhi MJ, Kremers W, and Gloor JM. Terminal complement inhibition decreases antibody-mediated rejection in sensitized renal transplant recipients. *American journal of transplantation : official journal of the American Society of Transplantation and the American Society of Transplant Surgeons.* 2011;11(11):2405-13.
32. Goh BK, Chedid MF, Gloor JM, Raghavaiah S, and Stegall MD. The impact of terminal complement blockade on the efficacy of induction with polyclonal rabbit antithymocyte globulin in living donor renal allografts. *Transpl Immunol.* 2012;27(2-3):95-100.
33. Neff KS, Richards SM, Williams JM, Garman RD, and Ruzek MC. Murine antithymocyte globulin T-cell depletion is mediated predominantly by macrophages, but the Fas/FasL pathway selectively targets regulatory T cells. *Transplantation.* 2011;92(5):523-8.
34. Barth RF, Singla O, and Ward PA. Immunosuppressive effects of anti-lymphocyte serum in complement deficient mice. II. Evidence that activity is mediated by C3 independent antibodies. *J Immunol.* 1974;112(2):858-61.

Figure legends

Figure 1. ATG induces aggregation and activation of platelets. (**A**) Platelet rich plasma (PRP) was stimulated with low concentrations (0.75-1.5 µM) of ADP and ATG, polyclonal rabbit IgG (both 100 µg/ml) or PBS (no Ab) (arrow). (**B**) PRP was stimulated with ADP and increasing concentrations (10-100 µg/ml) of ATG. Aggregation in (**A**) and (**B**) was then assessed photometrically over nine minutes. (**C**) Flow cytometric analysis of ATG binding to platelets (using a monoclonal anti-rabbit IgG antibody), platelet surface exposure of p-selectin (using a monoclonal anti-CD62P antibody) and phosphatidylserine (PS, detected by annexin V) following incubation of whole blood with 0.5 mg/ml ATG (red) or control IgG (blue). Platelets were identified by forward-sideward-scatter characteristics and positivity for CD41. (**D**) Platelets in whole blood were incubated with increasing concentrations (0.05-0.5 mg/ml) of ATG or 0.5 mg/ml polyclonal rabbit IgG and analyzed for p-selectin and PS as in (C) (n=3). (**E**) PRP was stimulated with ADP and 100 µg/ml ATG with or without prior incubation with 5 or 25 µg/ml anti-FcγRII (anti-CD32). Aggregation was assessed as in (**A**). (**F**) Platelets were incubated with increasing doses of anti-FcγRII (anti-CD32) prior to addition of 100 µg/ml ATG and 10% NHS. Platelet activation was analyzed as in (C) (n=5-7). Mean±SD are shown. Representative experiments are shown in panels A, B, C, E. **** $P<0.0001$.

Figure 2. ATG induces the release of procoagulant microvesicles. (**A**) Whole blood was incubated with 100 µg/ml ATG for 30 min at 37°C. Platelet microvesicles (MV) were isolated by sequential centrifugation and characterized and counted by flow cytometry. Forward-sideward-scatter characteristics compared to 4.2 µm counting beads and surface staining for CD41 and PS (using annexin V). (**B**) Whole blood was incubated with ATG (0.05-0.5 mg/ml) or 0.5 mg/ml polyclonal rabbit IgG for 30 min at 37°C prior to isolation of MV (mean±SD, n=3-5). (**C**) Platelets were incubated with increasing doses of anti-FcγRII (anti-CD32) prior to addition of 100 µg/ml ATG and 10% NHS for 30 min at 37°C. MV isolation and counting was done as in (**A**) (mean±SD, n=5-7). (**D**) MV were generated as in (A). Surface expression of factor V/Va was revealed by flow cytometry using mAb V237. (**E**) Platelets were incubated with ATG (0.01-0.25 mg/ml) or 0.25 mg/ml polyclonal rabbit IgG + 10% NHS for 30 min at 37°C. MV were subsequently isolated as in (**A**). Equal volumes of MV suspensions were then incubated with normal human plasma in the presence of TH8198. Thrombin generation was recorded over time measuring OD at 405 nm. *$P<0.05$, ****$P<0.0001$, n.s. non-significant. Representative experiments are shown in panels A,D,E.

Figure 3. ATG-induced platelet activation and MV release is dependent on complement activation. (**A**) Platelets were incubated with 100 µg/ml ATG or polyclonal rabbit IgG with 10% NHS for 30 min at 37°C. Platelets and isolated platelet MV were then analyzed for binding of ATG and surface deposition of complement fragments by flow cytometry using mAbs against rabbit IgG, C1q, C4d, C3-fragments and C5b-9. Representative histograms from platelets incubated with ATG (red histograms) or IgG (blue histograms) and the respective MV are shown. Isotype controls are in gray. (**B**, **C**, **E**) Platelets + 10% NHS were incubated with 0-25 µg/ml monoclonal antibody against C5 (**B**), C7 (**C**) or C9 (**E**) prior to addition of 100 µg/ml ATG for 30 min at 37°C. (**D**) Gel-filtered platelets were incubated with C8-depleted serum instead of NHS. MV isolation and counting in (**B**-**E**) was done as in Figure 2A. N=3-4/group. (**F**, **G**). Platelets were treated as in (**B**-**E**) using 10 µg/ml of anti-complement protein antibodies or C8-depleted serum and analyzed for PS expression by flow cytometry using annexin V (n=4-8). Mean+SD is shown. *P<0.05, ***P<0.001, ****P<0.0001. (**H**) Recalcified PRP was incubated with 100 µg/ml ATG or polyclonal IgG for 5 min at RT prior to addition of 0.5 pM TF and analyzed for thrombin generation. Alternatively, PRP was incubated with 25 µg/ml anti-C5 mAb for 15 min prior to addition of ATG (PRP+aC5 >ATG). Representative experiments are shown in panels A and H.

Figure 4. ATG treatment causes thrombopenia, hypercoagulability and complement activation in hematopoietic stem cell (HSCT) and kidney (NTX) transplant patients. (**A**) Platelet counts and levels of (**B**) d-dimer and (**C**) thrombin-anti-thrombin-complexes (TAT) were measured at the indicated time points relative to the first dose of ATG in HSCT (○, n=10) and NTX (●, n=9) patients. (**D**) Correlation between TAT measured on day 1 and drop in platelet count between baseline and day 1. (**E**) Plasma levels of sC5b-9 during ATG treatment in HSCT (○, n=10) and NTX (●, n=9) patients determined by ELISA. *<0.05, **P<0.01, n.s. = not significant.

Figure 5. Characterization and quantitation of platelet MV during ATG treatment. Total plasma MV were isolated as described in *methods*. (**A**) Forward/sideward-scatter characteristics and surface staining with anti-CD41 and annexinV by flow cytometry. Co-incubation with known amounts of beads allowed for quantitation of CD41+ annexinV+ double-positive platelet MV. (**B**) Number of platelet MV prior to the start of ATG infusion in kidney transplant (NTX, n=9) and hematopoietic stem cell transplant (HSCT, n=10) patients compared to platelet MV counts in

healthy controls (n=6). (**C**) Platelet MV counts in NTX and HSCT patients before, during (15, 30 and 120 minutes after starting ATG) at the end of the first ATG infusion (after) and on day 1. n=9 and 10, respectively.

Figure 6. Dynamics of complement fragment deposition on platelet MV during ATG treatment. CD41+ annexinV+ double-positive platelet MV were analyzed by flow cytometry for surface deposition of ATG (**A**) and the complement fragments C4d (**B**), C3d (**C**) and C5b-9 (**D**) at the indicated time points. For each parameter, a representative histogram is shown (blue) including an isotype control (grey histogram). Specificity for ATG was controlled for comparing staining with anti-rabbit IgG after the end of ATG treatment (blue) to staining at baseline (red histogram). *P<0.05, **P<0.01, ***P<0.001.

Figure 7. ATG-opsonized platelet MV adhere to RBC via complement receptor 1 in vitro. (**A**) $1x10^5$ red blood cells (RBC) were incubated with $1x10^7$ CFSE-labeled ATG-positive (+ATG MV) or ATG-negative control (+ctrl MV) platelet MV for 30 min at 37°C. Following washing, binding of MV to RBC was assessed measuring CFSE-fluorescence of RBC. RBC without MV were used as controls (RBC). (**B**) RBC were pre-incubated with anti-CR1 prior to incubation with CFSE-labeled ATG MV. Binding of MV to RBC was assessed analogous to (A). Representative histograms of two independent experiments are shown.

Figure 1.

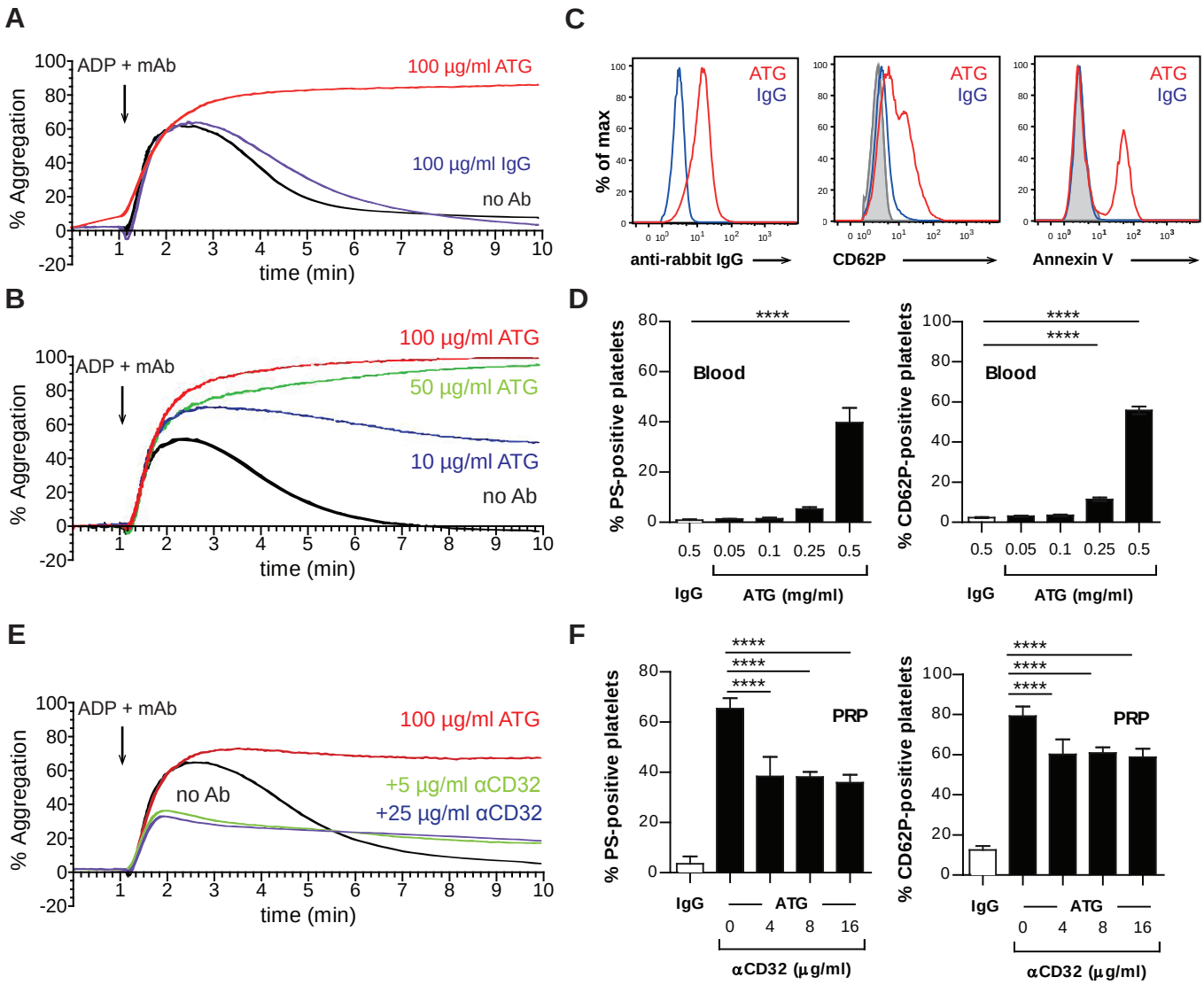
A
ADP + mAb
100 µg/ml ATG
100 µg/ml IgG
no Ab
% Aggregation
time (min)
B
ADP + mAb
100 µg/ml ATG
50 µg/ml ATG
10 µg/ml ATG
no Ab
% Aggregation
time (min)
C
ATG
IgG
% of max
anti-rabbit IgG
CD62P
Annexin V
D
Blood
% PS-positive platelets
% CD62P-positive platelets
IgG
ATG (mg/ml)
0.5 0.05 0.1 0.25 0.5
****
E
ADP + mAb
100 µg/ml ATG
no Ab
+5 µg/ml αCD32
+25 µg/ml αCD32
% Aggregation
time (min)
F
PRP
% PS-positive platelets
% CD62P-positive platelets
IgG
ATG
0 4 8 16
αCD32 (µg/ml)
****

Figure 2.

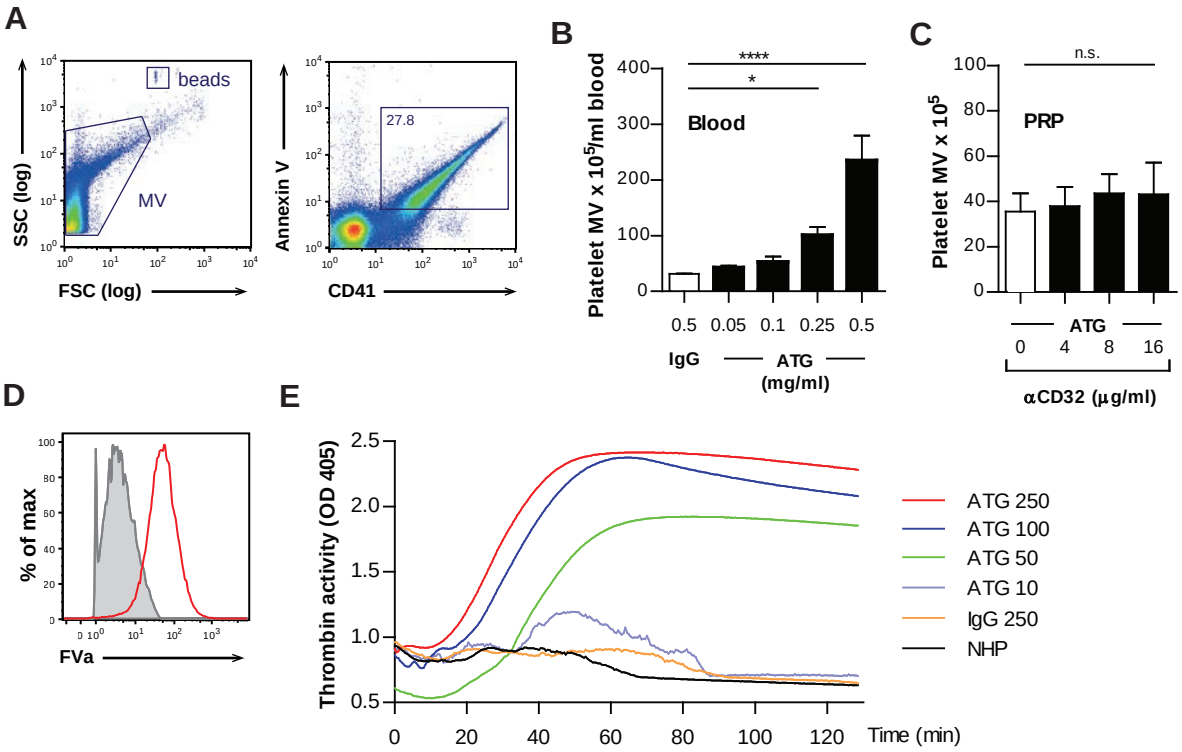
A
beads
MV
SSC (log)
FSC (log)
27.8
Annexin V
CD41
B
****
*
Blood
Platelet MV x 10^5/ml blood
0.5 0.05 0.1 0.25 0.5
IgG
ATG
(mg/ml)
C
n.s.
PRP
Platelet MV x 10^5
ATG
0 4 8 16
αCD32 (µg/ml)
D
% of max
FVa
E
Thrombin activity (OD 405)
Time (min)
ATG 250
ATG 100
ATG 50
ATG 10
IgG 250
NHP

Figure 3.

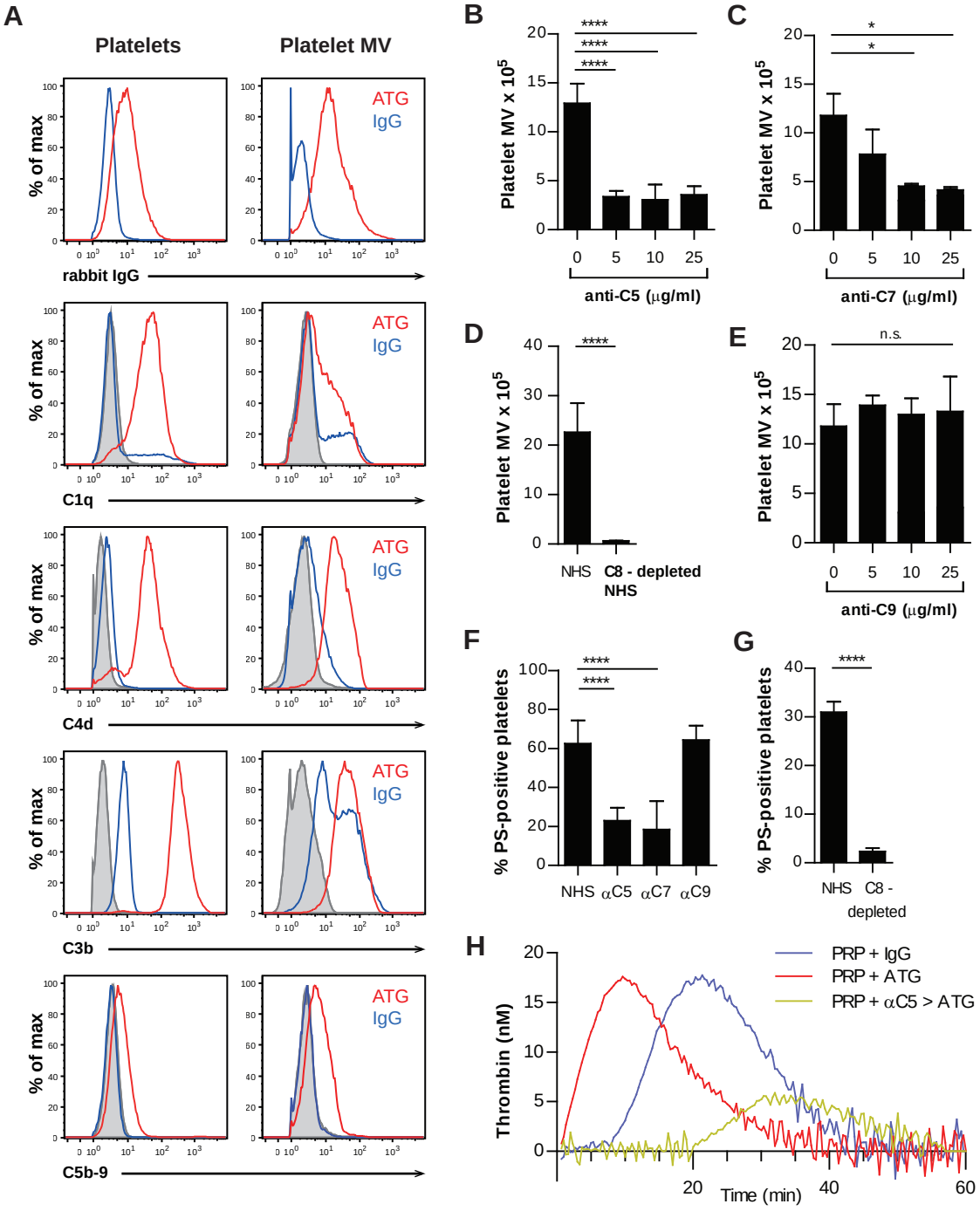
A
Platelets
Platelet MV
% of max
ATG
IgG
rabbit IgG
C1q
C4d
C3b
C5b-9
B
Platelet MV x 10^5
anti-C5 (μg/ml)
C
anti-C7 (μg/ml)
D
NHS
C8 - depleted NHS
E
n.s.
anti-C9 (μg/ml)
F
% PS-positive platelets
NHS αC5 αC7 αC9
G
NHS C8 - depleted
H
Thrombin (nM)
Time (min)
PRP + IgG
PRP + ATG
PRP + αC5 > ATG

Figure 4.

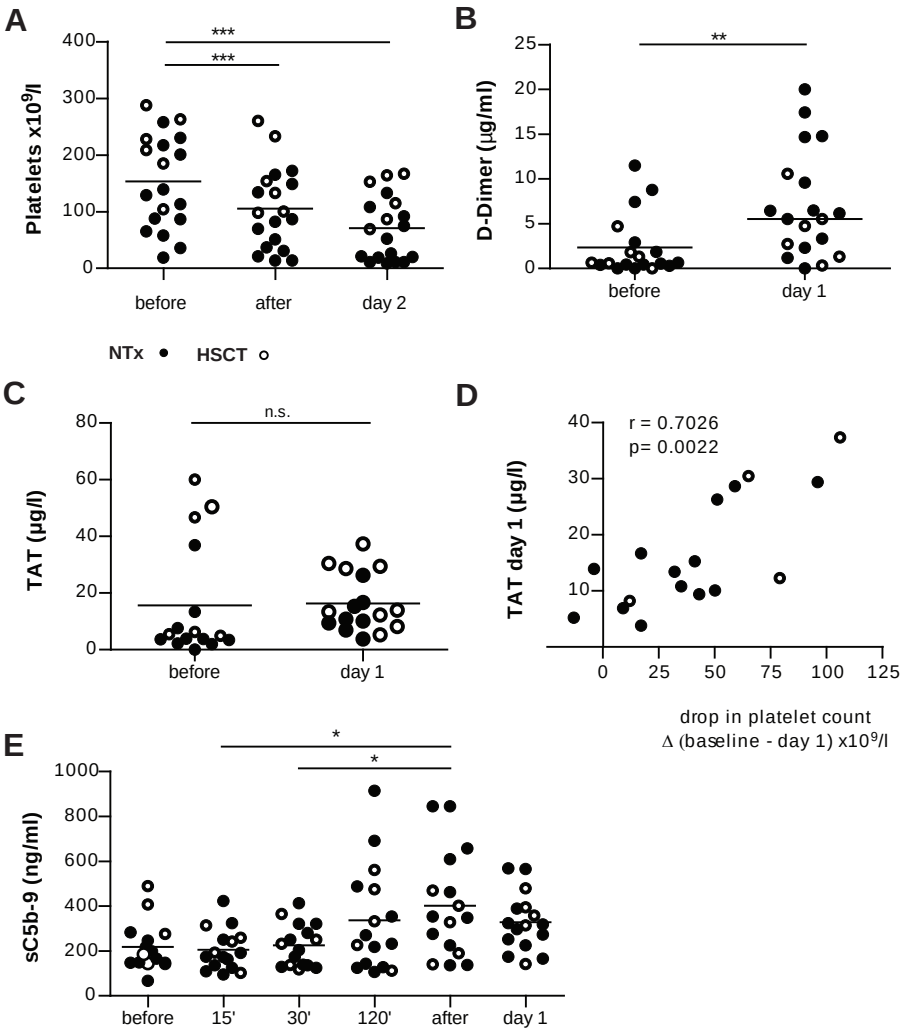
A
Platelets x10⁹/l
400
300
200
100
0
***
***
before
after
day 2
B
D-Dimer (µg/ml)
25
20
15
10
5
0
**
before
day 1
NTx
HSCT
C
TAT (µg/l)
80
60
40
20
0
n.s.
before
day 1
D
TAT day 1 (µg/l)
40
30
20
10
r = 0.7026
p= 0.0022
0
25
50
75
100
125
drop in platelet count
Δ (baseline - day 1) x10⁹/l
E
sC5b-9 (ng/ml)
1000
800
600
400
200
0
*
*
before
15'
30'
120'
after
day 1

Figure 5.

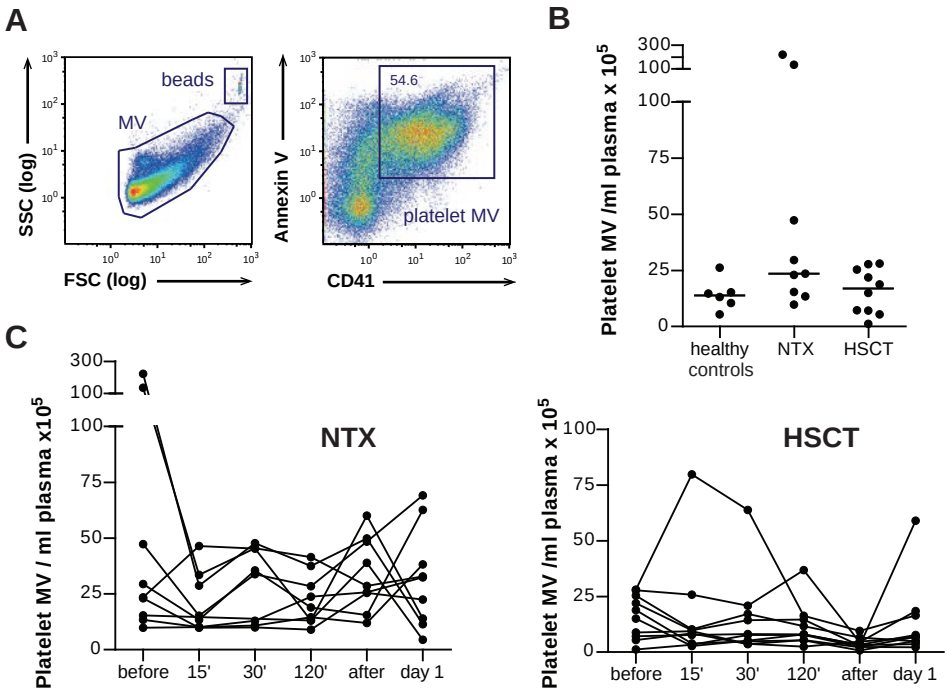
A
beads
MV
SSC (log)
FSC (log)
54.6
platelet MV
Annexin V
CD41
B
Platelet MV /ml plasma x 10^5
healthy controls
NTX
HSCT
C
Platelet MV / ml plasma x10^5
NTX
before
15'
30'
120'
after
day 1
Platelet MV /ml plasma x 10^5
HSCT

Figure 6.

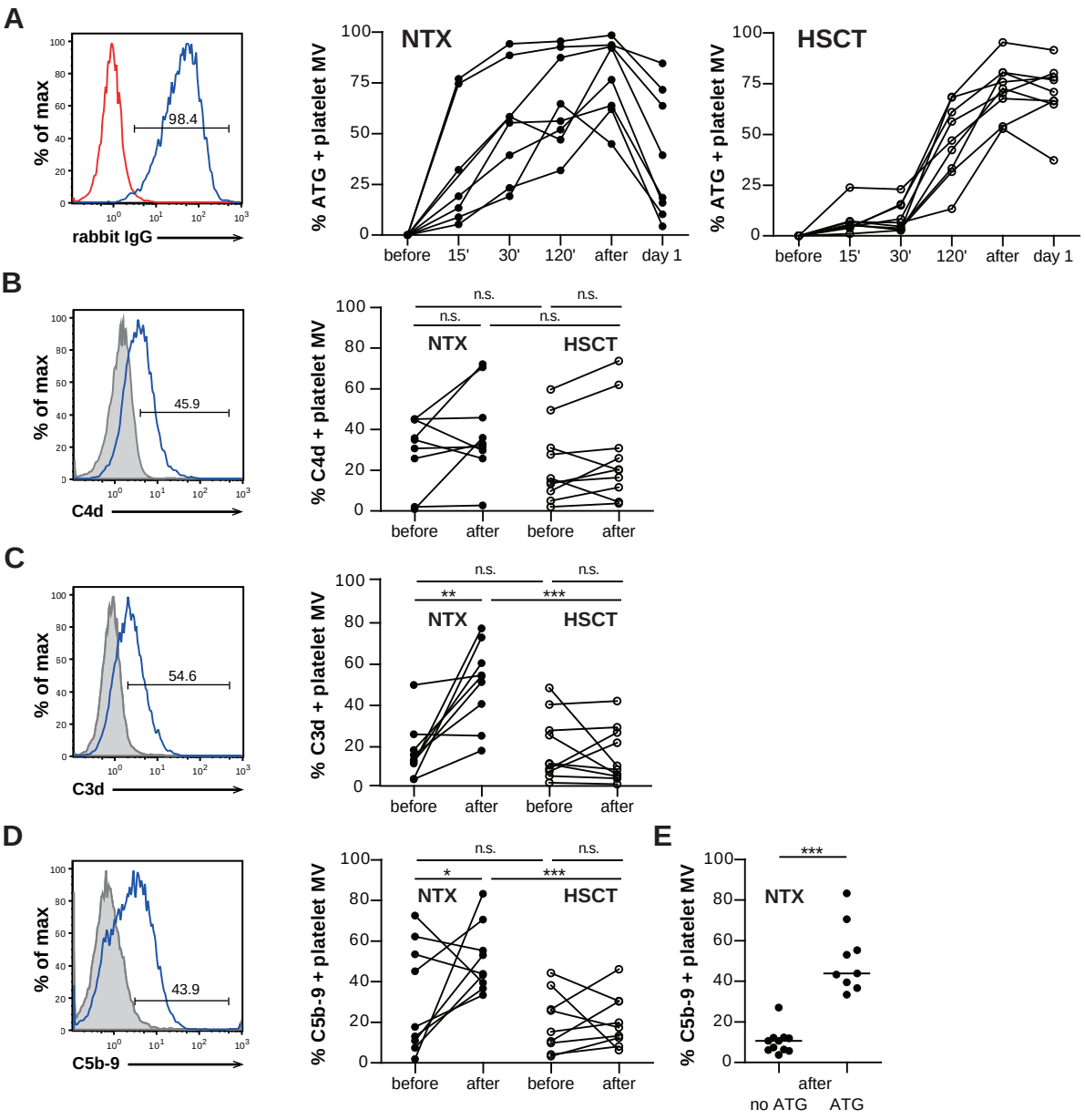
A
% of max
98.4
rabbit IgG
% ATG + platelet MV
NTX
HSCT
before
15'
30'
120'
after
day 1
B
45.9
C4d
% C4d + platelet MV
n.s.
C
54.6
C3d
% C3d + platelet MV
**
***
D
43.9
C5b-9
% C5b-9 + platelet MV
*
E
no ATG
ATG

Figure 7.

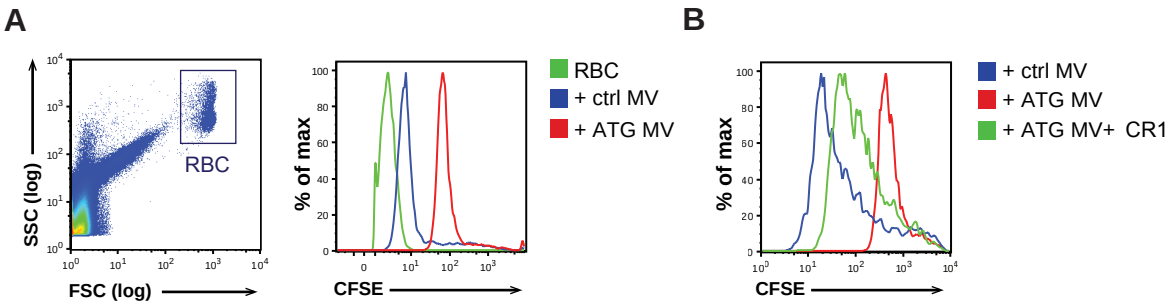

Erythrocyte-derived microvesicles amplify systemic inflammation by thrombin-dependent activation of complement

Daniel Zecher, MD[1,2,3], Arun Cumpelik, MD[1], Jürg Schifferli, MD, PhD[1,3]

[1]Department of Biomedicine, University Hospital Basel, Basel University, Switzerland [2]Department of Transplantation Immunology and Nephrology, University Hospital Basel, Switzerland [3]Department of Medicine, University Hospital Basel, Switzerland

Abstract

Objective: Transfusion of aged blood has been associated with increased morbidity and mortality in critically ill patients. During storage, erythrocytes release increasing numbers of microvesicles (RBC-MV). We hypothesized that RBC-MV mediate some of the deleterious effects of aged blood transfusions.

Approach and Results: We established a murine transfusion model using RBC-MV purified from aged mouse erythrocytes. Injection of RBC-MV into healthy mice had no effect. However, they aggravated pulmonary leukocyte sequestration and peripheral blood leukopenia induced by LPS. LPS-induced proinflammatory cytokines were significantly increased in plasma following RBC-MV injection. These effects were not seen in C5aR-deficient mice. *In vitro*, RBC-MV bound C3 fragments after incubation with plasma but failed to bind immunoglobulins, C1q or MBL. Preventing thrombin generation inhibited complement activation *in vitro* and *in vivo* and reversed the proinflammatory effects of RBC-MV in LPS-primed mice. Finally, the RBC-MV-induced phenotype was recapitulated using phosphatidylserine(PS)-expressing liposomes, suggesting that surface expression of PS by RBC-MV was mechanistically involved.

Conclusions: These results point towards a thrombin-dependent mechanism of complement activation by RBC-MV independent of the classical, lectin or alternative pathway. Besides identifying RBC-MV as potential mediators of transfusion-related morbidity, our findings may be relevant for other inflammatory disorders involving intravascular microvesicle release, e.g. sickle cell disease or thrombotic microangiopathy.

Abbreviations: RBC-MV, red blood cell-derived microvesicles; PS, phosphatidylserine; LPS, lipopolysaccharides.

Introduction

Transfusion of stored erythrocytes is one of the most common in-hospital procedures with approximately 14 million transfusions performed in the US every year (1). Up to 40% of intensive care patients receive blood products during their hospital stay with a mean of five units per patient (2). International blood bank policies allow storage for up to 42 days between erythrocyte collection and transfusion. Over the last decades, there has been substantial controversy over the question whether an increased storage time of blood products prior to transfusion is associated with higher patient morbidity and mortality (3). Whereas some studies were negative (4, 5), various other studies found increased overall mortality rates (6-9), a higher incidence of post-operative infections (10), renal failure (7) and a higher frequency of clotting disorders (11, 12) in patients that received aged compared to those that received fresh blood products and identified critically ill individuals, i.e. patients after trauma or cardiac surgery, to be the most vulnerable patient population (8, 13).

During aging, erythrocytes undergo a series of biochemical and physical changes known as the “storage lesion”. These changes include lipid and protein oxidation as well as a reduction in deformability and osmotic stability, the latter resulting in considerable hemolysis with release of free hemoglobin and iron (14). Notably, erythrocytes lose around 20% of hemoglobin and membrane surface area over time by the release of microvesicles. Erythrocyte-derived microvesicles increase significantly in number during storage (15, 16) and therefore large amounts are given to patients at the time of transfusion. Microvesicle release is a coordinate and active process coined ectocytosis to account for the fact that these vesicles (ectosomes) bud directly from the cell membrane (17). This is contrary to exocytosis that describes the release of vesicles (exosomes) following fusion of intracellular multivesicular bodies with the cell membrane. Irrespective of their cellular origin, ectosomes harbor phosphatidylserine (PS) in their membranes and were shown to have procoagulant activity *in vitro* with PS serving as a platform for thrombin generation (18). Also, human erythrocyte-derived ectosomes (termed RBC-MV hereafter) were found to bind complement fragments *in vitro* (19), suggesting that they might be proinflammatory via activation of the complement system.

Given their potential proinflammatory and procoagulant properties, we established a murine transfusion model to test the hypothesis that RBC-MV derived from aged mouse erythrocytes mediate pulmonary and extra-pulmonary pathology in mice independent of the two major constituents of blood transfusions, i.e. erythrocytes and hemoglobin.

Results

Characterization of red blood cell-derived microvesicles (RBC-MV). We first aimed at reproducing the storage lesion of human erythrocytes (RBC) in mice. After 18 days of storage, RBC-MV were isolated from the supernatant of stored RBC by sequential centrifugation and characterized by flow cytometry. Forward and sideward scatter analysis revealed a homogenous population that was >95% positive for Ter119, indicating their RBC origin. Consistent with previous reports in humans (20), between 25 and 45% of all microvesicles stained positive for AnnexinV, indicating surface expression of phosphatidylserine (Figure 1A). Electron microscopy revealed round shaped vesicles with a size approximating 200 nm (Figure 1B) a finding that was confirmed by nanoparticle tracking analysis (Figure 1C). We next compared surface expression of various complement regulatory proteins as well as the integrin-associated protein CD47 on RBC-MV to that of equally aged RBC. Whereas CD47 and Crry were highly expressed on both, DAF and CD59a showed only dim expression on RBC-MV compared to RBC, consistent with a specific sorting process of proteins underlying microvesicle shedding (Figure 1D). Lastly, we determined both kinetics and magnitude of RBC-MV release during storage over time. RBC-MV could be identified at low quantities in the supernatant of freshly harvested blood (not shown), but dramatically increased in number after 12 days of storage. After 18 days, an average of $1x10^9$ AnnexinV-positive microvesicles could be isolated from one milliliter of stored blood (Figure 1E).

Administration of RBC-MV has no effect in healthy mice. Our initial hypothesis was that systemic administration of RBC-MV causes acute lung injury in mice analogous to what has been reported following injection of anti-MHC-I antibodies (21-23). We injected $5x10^8$ RBC-MV intravenously and analyzed lung histology, lung water weight as an indicator of pulmonary edema and pulmonary leukocyte infiltration by flow cytometry four hours later. Histological analysis of lung sections showed no pathology. Also, total leukocyte as well as neutrophil (PMN) counts were similar after injection of RBC-MV compared to PBS-treated controls (Figure 2A-C). There were no signs of systemic inflammation as the proinflammatory cytokines IL-6, KC and MCP-1 in serum were undetectable (Figure 3). The latter findings also ruled out relevant contamination of RBC-MV during storage. These data indicated that RBC-MV cause neither lung pathology nor systemic inflammation in healthy mice.

RBC-MV prolong pulmonary neutrophil sequestration and peripheral blood leukopenia in LPS-primed mice. We next asked whether priming of mice with LPS prior to injection of RBC-MV resulted in lung injury analogous to the two-hit models of aged blood supernatant- and antibody-induced lung injury (21, 22, 24, 25). Two hours following intraperitoneal injection of LPS, RBC-MV were administered intravenously. Analysis of lung histology four hours later revealed increased leukocyte sequestration in small peripheral vessels compared to LPS-primed animals that had received PBS instead of RBC-MV (Figure 2A). However, histological changes consistent with parenchymal lung injury were not observed in any of the groups. There was an increase in lung water in all treated mice compared to PBS-treated controls. Compared to controls, lung water was significantly higher only in LPS-primed mice following RBC-MV injection (Figure 2B). However, values obtained for all groups were below those reported to represent overt pulmonary edema (23). We next quantified and phenotyped pulmonary leukocytes by flow cytometry. Consistent with published reports (26), LPS-primed mice showed an increase in pulmonary leukocyte counts compared to unprimed mice with the majority of these leukocytes being PMN. Administration of RBC-MV at two increasing concentrations resulted in a further significant increase in pulmonary PMN sequestration (Figure 2C) four hours later. Notably, analysis of peripheral blood leukocytes at that time revealed neutrophilia in LPS-primed mice, which was significantly reduced after addition of RBC-MV. Kinetic studies revealed a pronounced early pulmonary recruitment of PMN in response to LPS. Administration of RBC-MV resulted in a sustained pulmonary PMN sequestration over the next 2-4 hours in these mice, whereas PMN counts decreased more rapidly without infusion of RBC-MV (Figure 2D). The influx of $CD11b^{+}$ $Ly6C^{hi}$ inflammatory monocytes followed different kinetics. Whereas administration of RBC-MV had no impact on their rapid increase following priming with LPS, pulmonary monocyte sequestration was prolonged as evidenced by higher numbers four hours following RBC-MV injection (Figure 2D). In sum, administration of RBC-MV in LPS-primed mice resulted in increased pulmonary PMN sequestration without evidence of invasive lung injury.

RBC-MV amplify systemic inflammation. We next asked whether administration of RBC-MV in LPS-primed mice would amplify systemic inflammation. We observed a dose-dependent increase in serum levels of the proinflammatory cytokines IL-6, KC and MCP-1 following RBC-MV injection (Figure 3).

Role of hemoglobin and surface-expressed phosphatidylserine. Free hemoglobin (Hb) has been linked to the complications following transfusion of aged blood(27, 28). Given that RBC-MV contain significant amounts of Hb wrapped inside the vesicles during budding from RBC, we

wanted to know whether the phenotype following RBC-MV injection was specific to RBC-MV or whether it could also be elicited by the main content of RBC-MV, i.e. Hb. We therefore injected two different concentrations of free Hb from lysed aged erythrocytes into LPS-primed mice and analyzed both pulmonary phenotype and serum cytokines. The lower dose (1.8 mg) matched the Hb concentration in the RBC-MV preparation and was expected to be completely bound by haptoglobin in serum (29). The higher dose (18 mg) was hypothesized to exceed the haptoglogin-binding capacity and therefore mimic intravascular hemolysis. In LPS-primed mice, both doses of free Hb induced pulmonary PMN sequestration comparable to RBC-MV. However, whereas administration of RBC-MV resulted in a significant reduction of peripheral blood PMN counts, free Hb did not change LPS-induced peripheral blood neutrophilia (Figure S1A). At comparable Hb doses, RBC-MV induced significantly higher levels of IL-6, KC and MCP-1 compared to free Hb (Figure S1B). Next, we asked whether RBC-MV mediated their proinflammatory effects by surface-expressed phosphatidylserine (PS). We injected PS-containing liposomes in LPS-primed mice. This treatment reproduced both RBC-MV-mediated pulmonary PMN sequestration and systemic inflammation (Figure S2A and 2B, respectively), which was not the case when LPS-primed mice received phosphatidlycholine (PC)-containing control liposomes. In addition, we performed experiments blocking surface PS on RBC-MV by preincubating RBC-MV with saturating amounts of AnnexinV prior to intravenous injection in LPS-primed mice. This approach did not have a significant effect on pulmonary PMN sequestration or peripheral blood neutropenia (Figure S2C). Moreover, IL-6 levels were highly variable following blocking with some values being above and some below those measured in control animals. Importantly, IL-6 levels were increased following injection of free AnnexinV into LPS-primed mice even in the absence of RBC-MV (Figure S2D). Further *in vitro* experiments revealed that incubation of RBC-MV with AnnexinV in the presence of physiologic free calcium concentrations (1.25 mmol/l as compared to the commonly used 2.5 mmol/l) resulted in a significant reduction of AnnexinV binding (18.8 vs. 51.2%), suggesting that binding of AnnexinV to PS might not be stable *in vivo*. Taken together, these results indicated a specific effect of RBC-MV independent of Hb wrapped inside the vesicles or free Hb contaminating the RBC-MV preparations. Studies using liposomes further argued against a role for Hb but suggested a role for surface-expressed PS in mediating the RBC-MV-induced phenotype in LPS-primed mice.

RBC-MV bind complement fragments in vitro independent of the classical or alternative pathway. It has been speculated that some of the negative effects of stored red blood cells might relate to the ability of RBC-MV to activate complement via binding of natural antibodies

(30). We therefore investigated classical pathway activation by RBC-MV *in vitro*. Following incubation with plasma, we were unable to detect binding of IgM (Figure 4A) or IgG (not shown) on RBC-MV using flow cytometry. Also, there was no binding of MBL (not shown) or C1q (Figure 5B). That the latter result was not due to technical reasons became evident when we incubated RBC-MV with an antibody against the RBC-MV surface antigen Ter119 prior to adding plasma. This time, subsequent incubation with an anti-C1q antibody indicated binding of C1q, likely via binding to the anti-Ter119 antibody (Figure 4B). Notably, we could detect binding of C3 fragments using an anti-iC3b antibody (Figure 4C). That this was independent of classical pathway activation was further supported by the fact that C3 fragment binding was revealed following incubation with both wild-type and $Rag^{-/-}$ plasma, the latter being devoid of antibodies. Lastly, chelation of calcium by EGTA prevented C3 fragment binding. This effect could not be reversed following addition of magnesium, arguing against involvement of the alternative pathway (Figure 4D).

C5aR is critical for the RBC-MV-induced phenotype in vivo. We next assessed plasma levels of C5a in our *in vivo* model and found a rapid rise in C5a following injection of RBC-MV in LPS-primed mice compared to LPS-treated controls (Figure 4E). To test whether C5a was mechanistically involved, we applied our *in vivo* protocol to Balb/c mice comparing pulmonary PMN sequestration and serum cytokines between wild-type mice and mice unable to respond to the complement fragment C5a due to a targeted mutation in the gene encoding the C5a receptor ($C5aR^{-/-}$). We observed the same phenotype in Balb/c wild-type compared to B6 mice, indicating a strain-independent phenomenon (Figures 4F and G). Strikingly, we found that both the RBC-MV-induced increase in pulmonary PMN sequestration and the increase in proinflammatory cytokines were completely abolished in LPS-primed mice in the absence of C5aR (Figures 4F and G) suggesting that the presence of C5aR is critical for the proinflammatory effects mediated by RBC-MV *in vivo*.

Inhibition of thrombin prevents complement activation in vitro and in vivo and reverses the RBC-MV-induced proinflammatory phenotype in LPS-primed mice. Microvesicles from platelets but also erythrocytes were shown to have procoagulant properties *in vitro* with surface expression of phosphatidylserine serving as a platform for thrombin generation (18). Moreover, thrombin can function both as a C5 and C3 convertase (31-33) and therefore can activate complement independent of the classical or alternative pathway. Consistent with these studies, C3 fragment binding following incubation of RBC-MV with plasma *in vitro* could be completely prevented

when plasma was used from mice anticoagulated with either heparin (not shown) or refludan, a specific thrombin inhibitor (Figure 5A). As mentioned earlier, binding of C3 fragments to RBC-MV was also inhibited in the presence of EGTA (Figure 4D). Given the effect of thrombin-inhibition on C3 fragment binding, this finding was consistent with calcium being a necessary cofactor for thrombin activation. *In vivo*, injection of RBC-MV resulted in increased serum levels of thrombin compared to LPS-treated controls (Figure 5C). Refludan prevented RBC-MV-induced pulmonary PMN sequestration (Figure 5D), reversed peripheral blood neutropenia (not shown) and abolished RBC-MV-induced pro-inflammatory cytokines, most notably IL-6 (Figure 5E). Importantly, refludan also reduced plasma levels of C5a, directly linking thrombin generation to complement activation (Figure 5B).

Discussion

In this study we established a murine transfusion model to ask whether RBC-MV derived from the supernatant of aged erythrocytes have proinflammatory properties when injected intravenously into mice. We found that infusion of RBC-MV into healthy mice did not result in any pathology. When we extended our studies to LPS-primed mice (mimicking the clinical condition of sepsis), we found that under inflammatory conditions, RBC-MV amplified both pulmonary neutrophil sequestration and peripheral blood neutropenia and induced higher serum levels of proinflammatory cytokines. Mechanistic *in vitro* and *in vivo* studies revealed that these effects were due to activation of both the complement and the coagulation system. RBC-MV induced thrombin-dependent complement activation *in vitro* and *in vivo*. Moreover, RBC-MV lost their proinflammatory effects in mice unresponsive to the anaphylatoxin C5a and in mice that had received the specific thrombin-inhibitor refludan. Studies using liposomes suggested that the proinflammatory effects of RBC-MV involve surface expression of PS. Taken together, these findings suggest that thrombin can function as a C3 and/or C5 convertase *in vivo* independent of the classical, lectin or alternative complement pathway.

The impetus for this work was the clinical observation that transfusion of aged erythrocytes is associated with increased morbidity and mortality in the critically ill, the pathophysiology and triggering factors of this phenomenon still being incompletely understood. The results of our study are in accordance with several clinical observations. First, aged blood is more harmful in critically ill patients compared to healthy individuals, consistent with the observation that RBC-MV in our model were only harmful in endotoxemic mice whereas healthy mice withstood the harmful effects. Second, studies exploring the pathophysiology of anti-HLA antibody-induced TRALI (21-23, 34) do not explain why aged blood carries a higher risk of adverse reactions than younger blood, given that the amount of antibody in the transfusion bags is not expected to change over time. Moreover, these studies do not explain the non-pulmonary complications observed in these patients, notably higher rates of multi-organ failure, infections or thromboembolic complications (10, 11, 13). The findings presented here offer a possible antibody-independent mechanism of transfusion-related pathology.

For the generation of mouse RBC-MV, we aimed at mimicking human RBC purification and storage conditions. However, several factors in our protocol differed from human blood banking conditions. This included dextran sedimentation for RBC enrichment and MV purification from

RBC aged longer than what is thought to be equivalent to the human maximum storage time of 42 days (35). These differences might impact both quality and quantity of mouse RBC-MV. Although these differences should not preclude the mechanistic findings of our manuscript, a direct translation of our findings to human RBC transfusions warrants caution.

Previous animal studies have already suggested that the supernatant of aged erythrocytes can mediate transfusion-related complications (24, 25, 36). Hod et al. recently found free iron released from damaged stored RBC to amplify LPS-induced inflammation in a murine transfusion model (37). Despite differences in RBC purification and storage conditions between our study and the work by Hod and coworkers (35, 37), several findings are consistent. First, the amount of stored RBC we used to prepare RBC-MV was comparable to that used by Hod et al. for injection of stored RBC supernatants or hemolysates. Second, in the absence of LPS-priming, neither RBC-MV in our study nor the supernatant (containing RBC-MV) or hemolysate of stored RBC used by Hod et al. induced inflammation. These results also support that our method to generate RBC-MV did not result in a more proinflammatory effect per se. In the presence of LPS-priming, infusion of free hemoglobin from aged erythrocytes (likely containing iron) did amplify pulmonary PMN sequestration and resulted in an increase in proinflammatory cytokines in our model. However, when equal doses of hemoglobin were infused, the proinflammatory effects of RBC-MV were significantly more pronounced. Together with the data obtained using PS-positive liposomes (that lack hemoglobin), these results suggested that there is a hemoglobin-independent proinflammatory effect of RBC-MV, likely via surface expression of PS. It is important to note, however, that the evidence using PS-positive liposomes is associative. To test for causality, we performed blocking experiments preincubating RBC-MV with AnnexinV prior to intravenous injection and found no significant effect on pulmonary phenotype and proinflammatory cytokines (Figures IIC-D). Given that injection of AnnexinV in LPS-primed mice increased inflammation in the absence of RBC-MV and considering that blocking surface PS with AnnexinV might not be stable *in vivo*, the results from these experiments do not allow a final conclusion on the role of PS on RBC-MV in our model. Further experiments will have to be done to establish causality.

A crosstalk between the complement and the coagulation system has long been suggested, although *in vivo* evidence is limited. *In vitro* studies found complement activation products, i.e. C3a and C5a, following incubation of serum with clotting factors, notably thrombin (32, 33). Recently, Huber-Lang et al. found evidence for thrombin-mediated cleavage of C5 in a mouse

model of immune-complex mediated lung injury (31), linking coagulation to complement activation and systemic inflammation *in vivo*. The procoagulant properties of erythrocyte- and platelet-derived microvesicles are well described in the literature and are mainly based on solid-phase *in vitro* assays of thrombin generation (18, 38). As in our model, the specific thrombin inhibitor refludan was able to prevent both RBC-MV-induced complement activation *in vitro* (assessed by binding of C3 fragments to RBC-MV) and *in vivo* (evidenced by reduced C5a levels in the presence of refludan), our findings support the concept of thrombin-induced complement activation.

Outside the context of RBC transfusions, various other diseases like thrombotic microangiopathy (TMA) and sickle cell anemia are characterized by hypercoagulability (39), systemic complement activation (40) and increased blood levels of microparticles (41-43). Stahl et al. recently reported the presence of complement fragments on platelet and monocyte-derived microparticles in patients with shigatoxin-induced hemolytic uremic syndrome, a form of TMA (42)., suggesting a pathogenetic role of microvesicles in these conditions.

Taken together, we have identified RBC-MV to mediate transfusion-related pathology by thrombin-dependent activation of the complement system in a mouse transfusion model. These findings might not only be relevant for RBC storage and transfusion allocation strategies but describe a proinflammatory amplification loop with potential relevance for other conditions characterized by intravascular microvesicle release.

Materials and Methods

Mice. C57BL/6 (B6), Balb/c and B6 Rag$^{-/-}$ mice were bred at the institution's animal facility or purchased from Charles River (Sulzfeld, Germany). C.129S4(B6)-C5ar1^{tm1Cge}/J (C5aR$^{-/-}$) on a Balb/c background were from the Jackson Laboratories (Bar Harbor, USA). All mice were housed in a specific pathogen-free environment and were used between 7 and 12 weeks of age. Animal care and experimentation were performed in accordance with national guidelines (Federal Veterinary Office) and had been approved by the local government authorities.

Reagents and monoclonal antibodies. Fluorochrome-tagged mAbs against CD11b (clone M1/70), CD45 (30-F11), CD47 (miap301), CD59a (mCD59.3), Ly6C (AL-21), Ly6G (1A8), Ter119 (Ly-76), DAF (RIKO-3), Crry (512), IgG (Poly4053), IgM (RMM-1) and purified anti-CD16/32 (2.4G2) were from Biolegend (San Diego, USA), eBioscience (Vienna, Austria) or BD Pharmingen (Allschwil, Switzerland). Anti-iC3b (3.26) and anti-MBL-C (8G6) were from Hycult Biotech (Uden, the Netherlands). FITC-conjugated anti-C1q (RmC7H8) was from Cedarlane (Burlington, Canada), AnnexinV-APC from Immunotools (Friesoyte, Germany) and 7-AAD from Invitrogen (Zug, Switzerland).

Generation and analysis of red blood cell-derived microvesicles (RBC-MV). Mouse RBC-MV were generated by aging. Briefly, blood was obtained by cardiac puncture following sacrifice. Erythrocytes (RBC) were purified by dextran sedimentation. RBC were stored between 16 and 18 days at a ratio of 2:1 in the human erythrocyte-storage solution PAGGSM at 4˚C in polystyrene tubes (BD). Storage time was chosen empirically to maximize yield of RBC-MV and simultaneously minimize concurrent hemolysis. Preliminary experiments had shown significant hemolysis (hematocrit < 75% from baseline) in samples stored for longer than 18 days. Following storage, supernatants were diluted with PBS and sequentially centrifuged at 250g, 1210g and 13000g. The final pellet containing RBC-MV was diluted in PBS, stored at 4˚C and used within 24 hours. RBC-MV were analyzed by flow cytometry in 0.22 µm-filtered buffers. Trucount beads (BD) were used for quantitation. RBC-MV were gated on logarithmic FSC/SSC with an arbitrary threshold set on SSC. RBC-MV were further identified as double positive for Ter119 and AnnexinV. The number of AnnexinV-positive RBC-MV/ml was calculated as follows: (number of Trucount beads x % RBC-MV of total events (FSC/SSC) x % AnnexinV+ of total Ter119+) / % Trucount beads. Flow cytometry was performed using a CyanADP cytometer

(Beckman Coulter, Nyon, Switzerland). Data were analyzed using FlowJo Software (TreeStar, San Jose, USA).

Generation of liposomes. Unilamellar liposomes, composed of either L-α-phosphatidylcholine (PC) alone or PC together with equimolar concentrations of L-α-phosphaditylserine (PSPC, both Avanti Polar Lipids, Alabaster, USA) were prepared according to the repeated freeze–thawing method and extruded using nucleopore polycarbonate filters (VWR, San Diego, USA) (44). Final liposome concentration was 16 mM as measured by a standard phosphate assay. Liposome diameter was approximately 200 nm as determined by electron microscopy.

Two-hit experimental protocol. Mice were primed with an intraperitoneal (i.p.) injection of Lipopolysaccharides (LPS from Escherichia coli 055:B5 used at 1 mg/kg, Cat. Nr. L2880, Sigma, Buchs, Switzerland) followed two hours later by intravenous (i.v.) injection of $5x10^8$ or $1x10^9$ RBC-MV in a total volume of 200µl PBS via the tail vain. At the indicated times, mice were sacrificed with thiopental and organs were harvested. Where indicated, LPS-primed mice received 200µl of hemoglobin (Hb) at 9 mg/ml or 90 mg/ml i.v. prepared from stored erythrocytes instead of RBC-MV. Hb was obtained by freeze-thawing 18 day-old RBC followed by centrifugation at 13000g for 1 hour. Supernatants were analyzed for Hb concentration measuring absorbance at 405 nm with known concentrations of human Hb (Sigma) as standard. Hb content of RBC-MV was determined accordingly. Alternatively, LPS-primed mice received equimolar amounts of PC- or PSPC-liposomes i.v. instead of RBC-MV. Where indicated, the specific thrombin inhibitor refludan (Celgene, Boudry, Switzerland)) was given i.p. at 2 mg/kg 15 min prior to and again two and four hours following injection of LPS, respectively.

Electron microscopy. RBC-MV were fixed in 1% glutaraldehyde and adsorbed to parlodion-coated copper grids. After washing, samples were stained with 2% uranylacetate and analyzed using a Philips Morgani 268D transmission electron microscope operated at 80 kV.

Lung histology. Lungs were fixed in 4% paraformaldehyde and embedded in paraffin. 10 µm sections were stained with H&E and analyzed on an Olympus BX61 microscope.

Determination of lung water. Left lungs were removed intact, weighed and dried for > 24 hours. Following drying, lungs were weighed again. The percentage of lung weight accounted for by water was determined as follows: ((pre- minus post-drying weight)/ pre-drying weight) x100.

Analysis of blood and tissue leukocytes. Peripheral blood was obtained by cardiac puncture. To obtain lung-infiltrating leukocytes, right lungs were excised without prior perfusion and digested for 30 min at 37°C in RPMI-2.5% FCS + 2 mg/ml Collagenase IV + 0.1 mg/ml DNAse I (both Sigma). RBC were removed by hypotonic lysis. Blood leukocytes were counted using GLASSTIC® slides (Hycor, USA), the total cell number of the pulmonary homogenate was counted with an automated cell counter (Beckman Coulter). Pulmonary neutrophil numbers were calculated by multiplying the total cell number of the right lung homogenate by % $CD45^+$ $CD11b^+$ $Ly6C^+$ $Ly6G^+$ cells following exclusion of doublets and dead ($7\text{-}AAD^+$) cells as determined by flow cytometry. Pulmonary monocyte numbers were calculated accordingly with monocytes being $CD45^+$ $CD11b^+$ $Ly6C^{high}$ $Ly5G^-$.

ELISA and thrombin assay. Serum concentrations for IL-6, KC and MCP-1 were analyzed by ELISA following the manufacturers instructions (IL-6 and MCP-1 BD OptEIA, KC R&D Systems). For plasma C5a levels and thrombin activity, blood was drawn into tubes containing 10 mM EDTA. For C5a, ELISA plates were coated with purified monoclonal mouse C5a-specific IgG (5 µg/ml, BD). Following blocking with 10% FCS in PBS, plasma was added. C5a was revealed using a biotinylated monoclonal mouse C5a-specific antibody (0.5 µl/ml, BD) and SA-HRP. Recombinant human C5a (BD) was used as a standard. Thrombin activity was determined using fresh plasma and TH8198 (Pefachrome®, DSM, Basel, Switzerland) as substrate. After thrombin-mediated cleavage of the substrate, the amount of *p*-nitroaniline dihydrochloride formed was measured by absorbance at 405 nm. The assay was performed in the presence of aprotinin (Sigma). Unspecific absorbance was corrected for by subtracting absorbance in the absence of TH8198 from absorbance in the presence of TH8198 for each individual plasma sample (ΔOD).

In vitro complement binding studies. Blood from $Rag^{-/-}$ or wild-type mice was obtained by cardiac puncture and immediately put on ice. Plasma was harvested following centrifugation (10 min, 3000g). Anticoagulated plasma was obtained from mice injected 100µg refludan i.p. 5 min prior to cardiac puncture the blood being aspirated into syringes containing 100µg refludan. 5 µl RBC-MV were incubated with 10% plasma for 30 min at 37°C. Where indicated, 5 mM EGTA with or without 1 mM Mg were added to RBC-MV during incubation. Samples were then washed at 13000g for 10 min. To reveal binding of IgG, IgM, C1q or iC3b, RBC-MV were incubated with the respective flourochrome-tagged mAbs, washed and analyzed by flow cytometry.

Statistical analysis. All data are presented as mean ± SEM. Depending on data distribution, comparisons between treatment groups were performed using one-way ANOVA with Bonferroni's multiple comparison post-testing or using a two-tailed Mann-Whitney U test as indicated (Prism; GraphPad Software). Significance was set at $p < 0.05$.

Acknowledgements

We thank D. Tsakiris and A. Buser (both Dept. of Hematology, Basel University Hospital) for providing reagents and helpful discussions, M. Courtet and Estelle Gerossier for excellent technical assistance, B. Schneider for performing histology and V. Olivieri from the Microscopy Core Facility at *Biozentrum*, Basel University, for performing electron microscopy.

Authorship

D.Z. and A.C. designed, performed and analyzed all the experiments. D.Z., A.C. and J.A.S. wrote the manuscript.

References

1. Sullivan MT, Cotten R, Read EJ, and Wallace EL. Blood collection and transfusion in the United States in 2001. *Transfusion.* 2007;47(3):385-94.
2. Vincent JL, Baron JF, Reinhart K, Gattinoni L, Thijs L, Webb A, Meier-Hellmann A, Nollet G, and Peres-Bota D. Anemia and blood transfusion in critically ill patients. *JAMA.* 2002;288(12):1499-507.
3. van de Watering L. Pitfalls in the current published observational literature on the effects of red blood cell storage. *Transfusion.* 2011;51(8):1847-54.
4. van de Watering L, Lorinser J, Versteegh M, Westendord R, and Brand A. Effects of storage time of red blood cell transfusions on the prognosis of coronary artery bypass graft patients. *Transfusion.* 2006;46(10):1712-8.
5. Edgren G, Kamper-Jorgensen M, Eloranta S, Rostgaard K, Custer B, Ullum H, Murphy EL, Busch MP, Reilly M, Melbye M, et al. Duration of red blood cell storage and survival of transfused patients (CME). *Transfusion.* 2010;50(6):1185-95.
6. Wang D, Sun J, Solomon SB, Klein HG, and Natanson C. Transfusion of older stored blood and risk of death: a meta-analysis. *Transfusion.* 2012;52(6):1184-95.
7. Weinberg JA, McGwin G, Jr., Marques MB, Cherry SA, 3rd, Reiff DA, Kerby JD, and Rue LW, 3rd. Transfusions in the less severely injured: does age of transfused blood affect outcomes? *J Trauma.* 2008;65(4):794-8.
8. Koch CG, Li L, Sessler DI, Figueroa P, Hoeltge GA, Mihaljevic T, and Blackstone EH. Duration of red-cell storage and complications after cardiac surgery. *N Engl J Med.* 2008;358(12):1229-39.
9. Weinberg JA, McGwin G, Jr., Griffin RL, Huynh VQ, Cherry SA, 3rd, Marques MB, Reiff DA, Kerby JD, and Rue LW, 3rd. Age of transfused blood: an independent predictor of mortality despite universal leukoreduction. *J Trauma.* 2008;65(2):279-82; discussion 82-4.
10. Offner PJ, Moore EE, Biffl WL, Johnson JL, and Silliman CC. Increased rate of infection associated with transfusion of old blood after severe injury. *Arch Surg.* 2002;137(6):711-6; discussion 6-7.
11. Spinella PC, Carroll CL, Staff I, Gross R, Mc Quay J, Keibel L, Wade CE, and Holcomb JB. Duration of red blood cell storage is associated with increased incidence of deep vein thrombosis and in hospital mortality in patients with traumatic injuries. *Crit Care.* 2009;13(5):R151.

12. Hendrickson JE, Shaz BH, Pereira G, Atkins E, Johnson KK, Bao G, Easley KA, and Josephson CD. Coagulopathy is prevalent and associated with adverse outcomes in transfused pediatric trauma patients. *J Pediatr.* 2012;160(2):204-9 e3.
13. Zallen G, Offner PJ, Moore EE, Blackwell J, Ciesla DJ, Gabriel J, Denny C, and Silliman CC. Age of transfused blood is an independent risk factor for postinjury multiple organ failure. *Am J Surg.* 1999;178(6):570-2.
14. Card RT. Red cell membrane changes during storage. *Transfus Med Rev.* 1988;2(1):40-7.
15. Rumsby MG, Trotter J, Allan D, and Michell RH. Recovery of membrane micro-vesicles from human erythrocytes stored for transfusion: a mechanism for the erythrocyte discocyte-to-spherocyte shape transformation. *Biochem Soc Trans.* 1977;5(1):126-8.
16. Rubin O, Crettaz D, Canellini G, Tissot JD, and Lion N. Microparticles in stored red blood cells: an approach using flow cytometry and proteomic tools. *Vox Sang.* 2008;95(4):288-97.
17. Stein JM, and Luzio JP. Ectocytosis caused by sublytic autologous complement attack on human neutrophils. The sorting of endogenous plasma-membrane proteins and lipids into shed vesicles. *Biochem J.* 1991;274 (Pt 2)(381-6.
18. Sweeney J, Kouttab N, and Kurtis J. Stored red blood cell supernatant facilitates thrombin generation. *Transfusion.* 2009;49(8):1569-79.
19. Sadallah S, Eken C, and Schifferli JA. Erythrocyte-derived ectosomes have immunosuppressive properties. *J Leukoc Biol.* 2008;84(5):1316-25.
20. Salzer U, Zhu R, Luten M, Isobe H, Pastushenko V, Perkmann T, Hinterdorfer P, and Bosman GJ. Vesicles generated during storage of red cells are rich in the lipid raft marker stomatin. *Transfusion.* 2008;48(3):451-62.
21. Sachs UJ, Wasel W, Bayat B, Bohle RM, Hattar K, Berghofer H, Reil A, Bux J, Bein G, Santoso S, et al. Mechanism of transfusion-related acute lung injury induced by HLA class II antibodies. *Blood.* 2011;117(2):669-77.
22. Looney MR, Su X, Van Ziffle JA, Lowell CA, and Matthay MA. Neutrophils and their Fc gamma receptors are essential in a mouse model of transfusion-related acute lung injury. *J Clin Invest.* 2006;116(6):1615-23.
23. Strait RT, Hicks W, Barasa N, Mahler A, Khodoun M, Kohl J, Stringer K, Witte D, Van Rooijen N, Susskind BM, et al. MHC class I-specific antibody binding to nonhematopoietic cells drives complement activation to induce transfusion-related acute lung injury in mice. *J Exp Med.* 2011;208(12):2525-44.

24. Silliman CC, Voelkel NF, Allard JD, Elzi DJ, Tuder RM, Johnson JL, and Ambruso DR. Plasma and lipids from stored packed red blood cells cause acute lung injury in an animal model. *J Clin Invest.* 1998;101(7):1458-67.
25. Kelher MR, Masuno T, Moore EE, Damle S, Meng X, Song Y, Liang X, Niedzinski J, Geier SS, Khan SY, et al. Plasma from stored packed red blood cells and MHC class I antibodies causes acute lung injury in a 2-event in vivo rat model. *Blood.* 2009;113(9):2079-87.
26. Andonegui G, Bonder CS, Green F, Mullaly SC, Zbytnuik L, Raharjo E, and Kubes P. Endothelium-derived Toll-like receptor-4 is the key molecule in LPS-induced neutrophil sequestration into lungs. *Journal of Clinical Investigation.* 2003;111(7):1011-20.
27. Donadee C, Raat NJ, Kanias T, Tejero J, Lee JS, Kelley EE, Zhao X, Liu C, Reynolds H, Azarov I, et al. Nitric oxide scavenging by red blood cell microparticles and cell-free hemoglobin as a mechanism for the red cell storage lesion. *Circulation.* 2011;124(4):465-76.
28. Baek JH, D'Agnillo F, Vallelian F, Pereira CP, Williams MC, Jia Y, Schaer DJ, and Buehler PW. Hemoglobin-driven pathophysiology is an in vivo consequence of the red blood cell storage lesion that can be attenuated in guinea pigs by haptoglobin therapy. *J Clin Invest.* 2012;122(4):1444-58.
29. Kickler TS, Gong PF, Johnson GF, and Solomon HM. Kinetic determination of serum haptoblobin with a centrifugal analyzer. *Clin Chem.* 1976;22(12):1962-7.
30. Weinberg JA, Barnum SR, and Patel RP. Red blood cell age and potentiation of transfusion-related pathology in trauma patients. *Transfusion.* 2011;51(4):867-73.
31. Huber-Lang M, Sarma JV, Zetoune FS, Rittirsch D, Neff TA, McGuire SR, Lambris JD, Warner RL, Flierl MA, Hoesel LM, et al. Generation of C5a in the absence of C3: a new complement activation pathway. *Nat Med.* 2006;12(6):682-7.
32. Spath P, and Gabl F. Critical role of the conversion of the third complement component C3 (beta 1C/beta 1A) for its immunochemical quantitation. *Clin Chim Acta.* 1976;73(1):171-5.
33. Amara U, Flierl MA, Rittirsch D, Klos A, Chen H, Acker B, Bruckner UB, Nilsson B, Gebhard F, Lambris JD, et al. Molecular intercommunication between the complement and coagulation systems. *J Immunol.* 2010;185(9):5628-36.
34. Fung YL, Kim M, Tabuchi A, Aslam R, Speck ER, Chow L, Kuebler WM, Freedman J, and Semple JW. Recipient T lymphocytes modulate the severity of antibody-mediated transfusion-related acute lung injury. *Blood.* 2010;116(16):3073-9.

35. Gilson CR, Kraus TS, Hod EA, Hendrickson JE, Spitalnik SL, Hillyer CD, Shaz BH, and Zimring JC. A novel mouse model of red blood cell storage and posttransfusion in vivo survival. *Transfusion.* 2009;49(8):1546-53.
36. Vlaar AP, Hofstra JJ, Levi M, Kulik W, Nieuwland R, Tool AT, Schultz MJ, de Korte D, and Juffermans NP. Supernatant of aged erythrocytes causes lung inflammation and coagulopathy in a "two-hit" in vivo syngeneic transfusion model. *Anesthesiology.* 2010;113(1):92-103.
37. Hod EA, Zhang N, Sokol SA, Wojczyk BS, Francis RO, Ansaldi D, Francis KP, Della-Latta P, Whittier S, Sheth S, et al. Transfusion of red blood cells after prolonged storage produces harmful effects that are mediated by iron and inflammation. *Blood.* 2010;115(21):4284-92.
38. Bidot L, Jy W, Bidot C, Jr., Jimenez JJ, Fontana V, Horstman LL, and Ahn YS. Microparticle-mediated thrombin generation assay: increased activity in patients with recurrent thrombosis. *J Thromb Haemost.* 2008;6(6):913-9.
39. Shah N, Thornburg C, Telen MJ, and Ortel TL. Characterization of the hypercoagulable state in patients with sickle cell disease. *Thromb Res.* 2012;130(5):e241-5.
40. Chudwin DS, Papierniak C, Lint TF, and Korenblit AD. Activation of the alternative complement pathway by red blood cells from patients with sickle cell disease. *Clin Immunol Immunopathol.* 1994;71(2):199-202.
41. Jimenez JJ, Jy W, Mauro LM, Horstman LL, Soderland C, and Ahn YS. Endothelial microparticles released in thrombotic thrombocytopenic purpura express von Willebrand factor and markers of endothelial activation. *Br J Haematol.* 2003;123(5):896-902.
42. Stahl AL, Sartz L, and Karpman D. Complement activation on platelet-leukocyte complexes and microparticles in enterohemorrhagic Escherichia coli-induced hemolytic uremic syndrome. *Blood.* 2011;117(20):5503-13.
43. Camus SM, Gausseres B, Bonnin P, Loufrani L, Grimaud L, Charue D, De Moraes JA, Renard JM, Tedgui A, Boulanger CM, et al. Erythrocyte microparticles can induce kidney vaso-occlusions in a murine model of sickle cell disease. *Blood.* 2012;120(25):5050-8.
44. Szoka F, Olson F, Heath T, Vail W, Mayhew E, and Papahadjopoulos D. Preparation of unilamellar liposomes of intermediate size (0.1-0.2 mumol) by a combination of reverse phase evaporation and extrusion through polycarbonate membranes. *Biochim Biophys Acta.* 1980;601(3):559-71.

Figure legends

Figure 1. Characterization of red blood cell-derived microvesicles (RBC-MV). Flow cytometric analysis of MV after 18 days of storage (**A**, **D**). Forward/sideward-scatter characteristics compared to 4.2 µm control beads (*) and surface staining for Ter119 and Annexin V (**A**). Differential surface expression of the indicated molecules on RBC-MV compared to red blood cells (RBC) both aged for 18 days (**D**). Transmission electron microscopy of RBC-MV reveals round shaped vesicles with a size of around 200 nm. Left size bar 1 µm, right size bar 200 nm (**B**). Nanoparticle Tracking Analysis (NTA) of RBC-MV reveals a homogenous population with a mean diameter of 200 nm (**C**). Kinetics of RBC-MV release during storage. Data are mean±SEM from 3-8 independent experiments per time point (**E**).

Figure 2. Systemic administration of RBC-MV amplifies pulmonary neutrophil sequestration and peripheral blood leukopenia in LPS-primed mice. B6 mice were primed with an i.p. injection of LPS followed by the i.v. injection of $5x10^8$ or $1x10^9$ RBC-MV (LPS+RBC-MV) two hours later. Alternatively, mice were given LPS i.p. followed by PBS i.v. (LPS). Control groups received PBS instead of LPS for priming followed by $5x10^8$ RBC-MV i.v. (RBC-MV) or were given PBS i.p. and i.v. (PBS). 4 hours later, lungs were harvested and lung sections stained by H&E. Magnification 100 x, inset 600 x. Pictures are representative of at least four mice analyzed per group (**A**). % water weight of lungs of the indicated groups determined as outlined in the methods sections. n=3 (PBS, RBC-MV only), 12 (LPS) and 15 (LPS+RBC-MV) pooled from several independent experiments (**B**). Accumulation of $CD45^+$ leukocytes and $CD11b^+$ $Ly6C^{int}$ $Ly6G^+$ neutrophils (PMN) in right lungs as well as peripheral blood leukocyte and PMN counts of the indicated groups as determined by flow cytometry. n=4-6/group (lung) and 5-7/group (blood) pooled from two representative experiments (**C**). Kinetics of pulmonary $CD45^+$ leukocyte, PMN, and $CD11b^+$ $Ly6C^{hi}$ $Ly6G^{neg}$ inflammatory monocyte sequestration in LPS vs. LPS+$5x10^8$ RBC-MV treated mice. N=4-6/group and time point (**D**). * $P < 0.05$ using one-way ANOVA and Bonferroni's post-test. Mean±SEM is shown.

Figure 3. Dose-dependent amplification of LPS-induced systemic inflammation by RBC-MV. Serum levels of IL-6, KC and MCP-1 four hours after i.v. injection of PBS or RBC-MV in unprimed (PBS and RBC-MV, respectively) or LPS-primed B6 mice (LPS, LPS+$5x10^8$ RBC-MV, LPS+$1x10^9$ RBC-MV, respectively) as determined by ELISA. N =6-16/group pooled from at least

three independent experiments. * $P < 0.05$, ** $P < 0.01$, *** $P < 0.001$ using a nonparametric Mann-Whithey test. Mean±SEM is shown.

Figure 4. Involvement of complement. RBC-MV bind C3 fragments independent of classical or alternative pathway activation *in vitro*. B6 RBC-MV were incubated with wild-type or $Rag^{-/-}$ plasma or heat-inactivated (HI) control wild-type serum *in vitro*. Binding of IgM (**A**), C1q (**B**) or iC3b fragments (**C**) was subsequently revealed by flow cytometry following incubation with fluorochrome-tagged anti-IgM, anti-C1q or anti-C3b mAbs, respectively. For (**B**), RBC-MV were incubated with an antibody specifically binding to surface glycophorin-A (Ter119) prior to incubation with plasma. Binding of C1q was then revealed following incubation with anti-C1q mAb (1º α-Ter119, 2º plasma). To test for alternative pathway activation *in vitro*, RBC-MV were incubated with plasma in the presence or absence of EGTA, the latter with (EGTA+Mg) or without (EGTA) addition of magnesium. iC3b fragment binding was revealed as in (**C**) and (**D**). Results are representative of >2 independent experiments (**A**-**D**). Increased levels of C5a in LPS-primed B6 mice 15 min after i.v. injection of RBC-MV (n=5-6) (**E**). Amplification of pulmonary phenotype and cytokine production by RBC-MV in LPS-primed mice depends on complement receptor C5aR. Balb/c wild-type and C5aR-deficient mice were treated as described in Figure 2. 4 hours later, pulmonary PMN sequestration (n=7-8) (**F**) as well as serum cytokines (n=7-11) (**G**) were determined. * $P < 0.05$, ** $P < 0.01$, *** $P < 0.001$ using one-way ANOVA and Bonferroni's post-test (pulmonary PMN counts) or a nonparametric Mann Whitney test (cytokines). n.s. = non-significant. Mean±SEM is shown.

Figure 5. RBC-MV induced effects can be reversed by inhibition of thrombin *in vitro* and *in vivo*. iC3b binding to RBC-MV *in vitro* after incubation with plasma can be reversed by refludan (**A**). B6 RBC-MV were incubated with plasma, heat-inactivated control serum or plasma from mice that had been anticoagulated with refludan prior to sacrifice. iC3b binding was revealed following incubation with an anti-iC3b mAb by flow cytometry (**A**). Plasma levels of C5a and thrombin are reduced in the presence of refludan. LPS-primed B6 mice anticoagulated with refludan (+) or not (-) were given $1x10^9$ RBC-MV i.v. 15 min later, plasma was obtained and C5a levels (**B**) and thrombin activity (**C**) were determined by ELISA and a thrombin assay, respectively, as indicated in *Methods*. Amplification of pulmonary PMN sequestration (**D**) and systemic inflammation (**E**) in LPS-primed B6 mice 4 hours after injection of RBC-MV can be reversed by refludan. N=6-8/group pooled from at least three independent experiments (**B-E**). *

P < 0.05, ** *P* < *0.01* using one-way ANOVA and Bonferroni's post-test (**C**, **D**) or a nonparametric Mann-Whitney test (**B**, **E**). n.s. = not significant. Mean±SEM is shown.

Figure S1. Effect of free hemoglobin on pulmonary phenotype and serum cytokines in LPS-primed mice. LPS-primed B6 mice received an i.v. injection of PBS (LPS), 1.8 mg hemoglobin (LPS+1.8 mg Hb), 18 mg hemoglobin, or 1x109 RBCMV containing 1.8 mg hemoglobin. 4 hours later, pulmonary and peripheral blood PMN counts (**A**) as well as serum cytokines (**B**) were determined. N=5-6/group pooled from >2 independent experiments each. * *P* < 0.05, ** *P* < 0.01 using one-way ANOVA and Bonferroni's post-test (**A**). N=5-7/group pooled from at least three independent experiments. * *P* < 0.05, ** *P* < 0.01 using a nonparametric Mann Whitney test (B). n.s. = non-significant. Mean±SEM is shown.

Figure S2. The RBC-MV-induced effects can be mimicked by phosphatidylserine-positive liposomes. RBC-MV-induced pulmonary phenotype (**A**) and amplification of proinflammatory cytokines (**B**) in LPS-primed B6 mice can be mimicked by i.v. injection of liposomes containing phosphatidylcholine (PC) and phosphatidylserine (PS) at a 1:1 ratio (L+PSPC). Injection of PSPC in the absence of LPS (PSPC) or control PC-liposomes in LPS-primed mice (L+PC) had no effect. N=7-9/group from at least three independent experiments (**A**-**B**). Blocking of PS on RBC-MV by preincubation with saturating amounts of AnnexinV prior to i.v. injection in LPS-primed mice does not reverse the RBC-MV-induced pulmonary phenotype (**C**) and results in highly variable serum levels of IL-6 (**D**). N=3-5/group from two independent experiments (**C**-**D**). * *P* < 0.05, ** *P* < 0.01 using one-way ANOVA and Bonferroni's post-test (**A**) or a nonparametric Mann-Whitney test (**B**). n.s. = not significant. Mean±SEM is shown.

Figure 1.

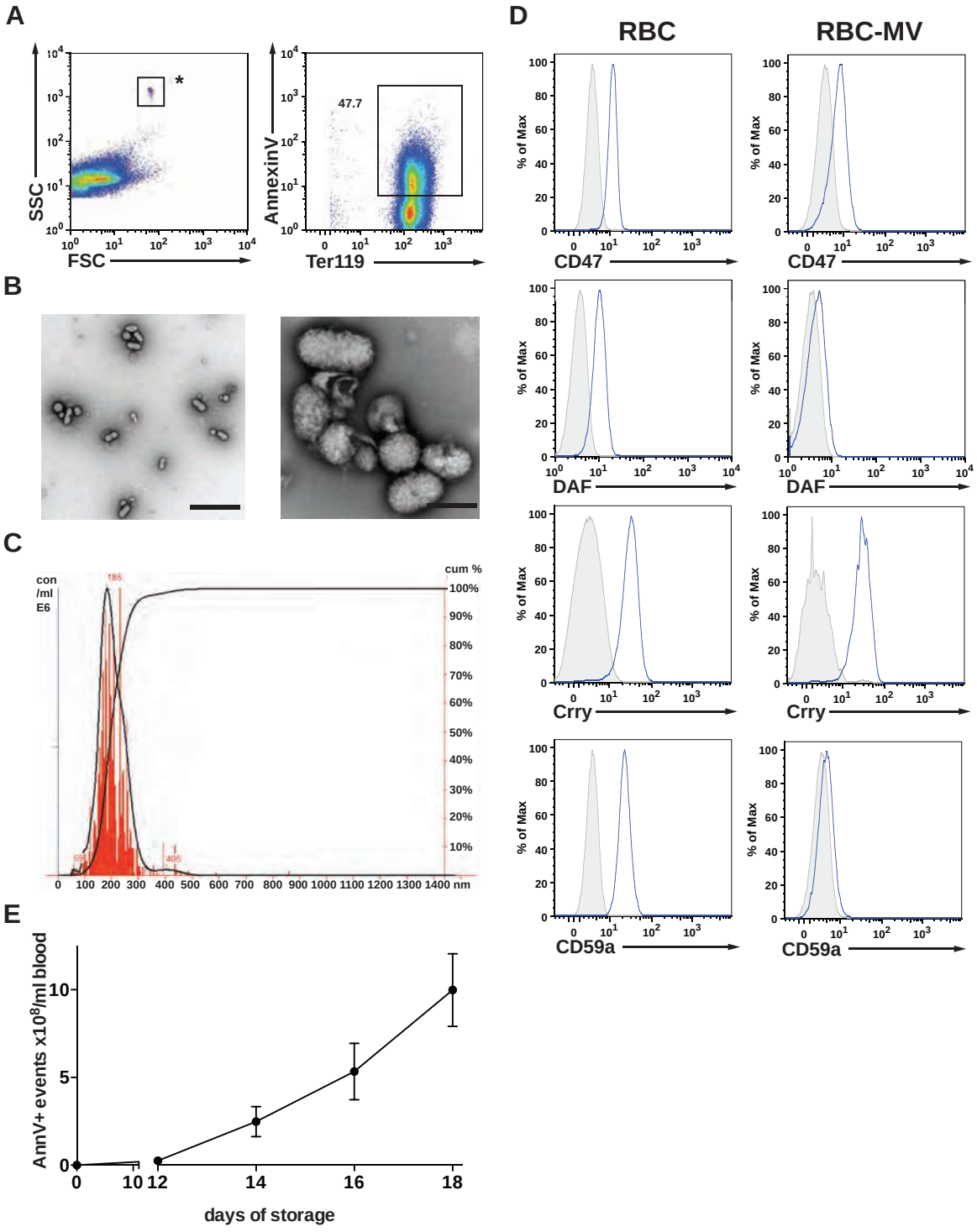
A
SSC
FSC
AnnexinV
Ter119
47.7
B
C
con /ml E6
cum %
days of storage
D
RBC
RBC-MV
% of Max
CD47
DAF
Crry
CD59a
E
AnnV+ events x10^8/ml blood
days of storage

Figure 2.

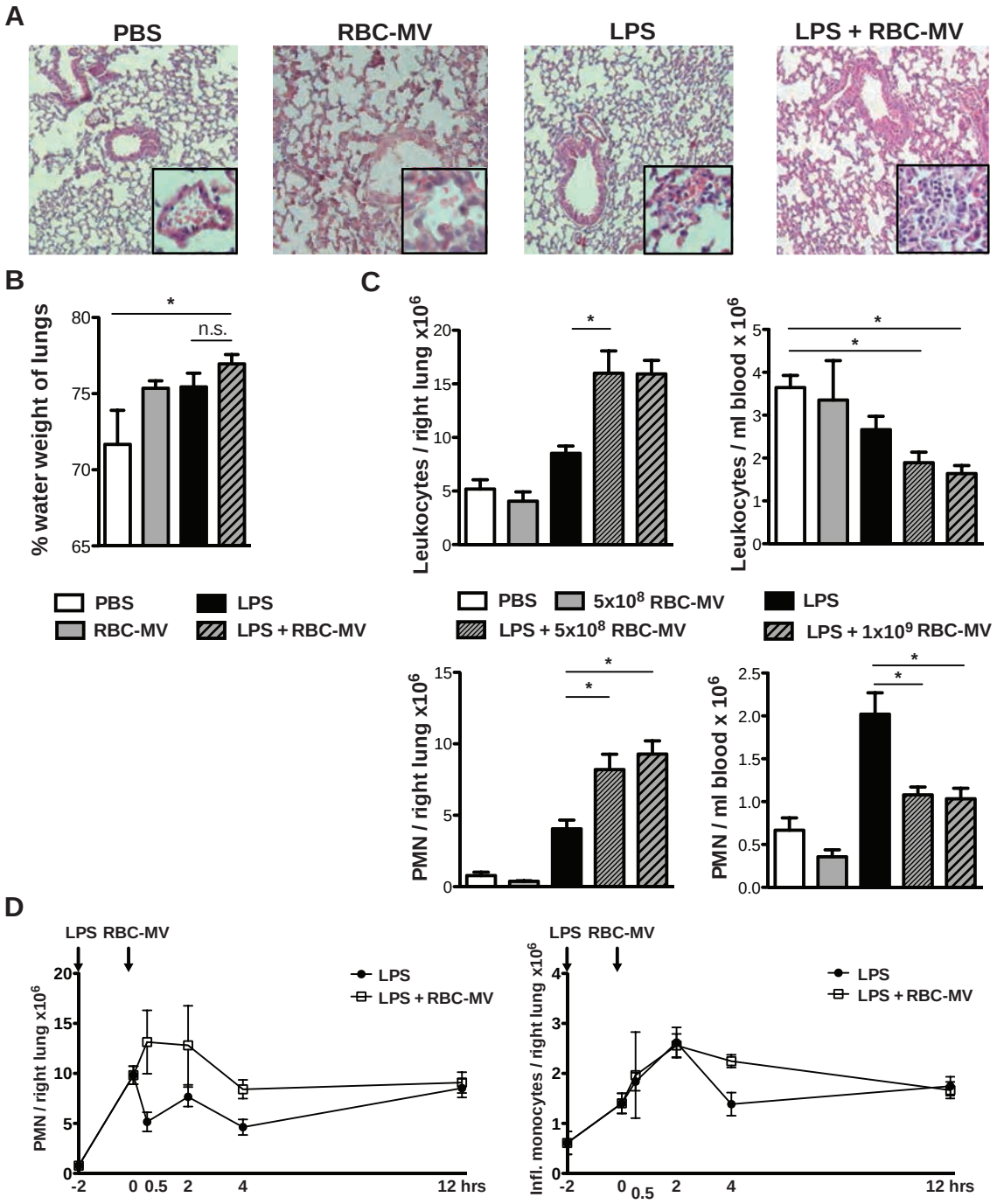
A
PBS
RBC-MV
LPS
LPS + RBC-MV
B
% water weight of lungs
80
75
70
65
*
n.s.
C
Leukocytes / right lung x10^6
20
15
10
5
0
*
Leukocytes / ml blood x 10^6
5
4
3
2
1
0
*
*
PBS
RBC-MV
LPS
LPS + RBC-MV
PBS
5x10^8 RBC-MV
LPS + 5x10^8 RBC-MV
LPS
LPS + 1x10^9 RBC-MV
PMN / right lung x10^6
15
10
5
0
*
*
PMN / ml blood x 10^6
2.5
2.0
1.5
1.0
0.5
0.0
*
*
D
LPS RBC-MV
PMN / right lung x10^6
20
15
10
5
0
LPS
LPS + RBC-MV
-2
0
0.5
2
4
12 hrs
LPS RBC-MV
Infl. monocytes / right lung x10^6
4
3
2
1
0
LPS
LPS + RBC-MV
-2
0
0.5
2
4
12 hrs

Figure 3.

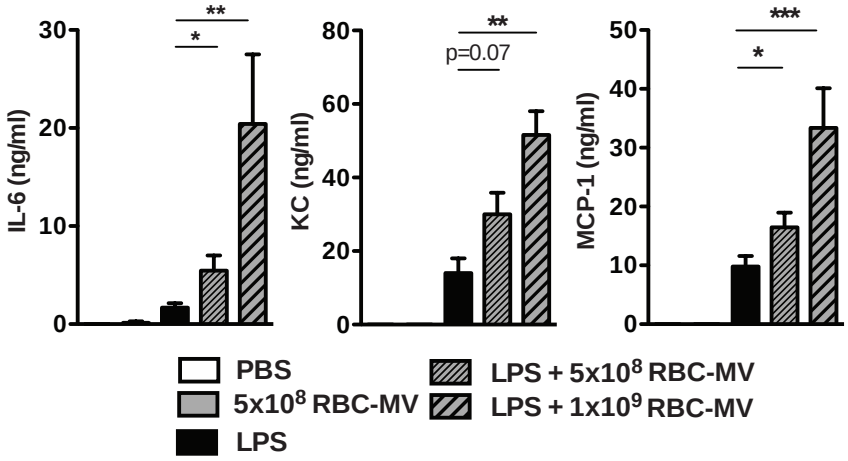
IL-6 (ng/ml)
KC (ng/ml)
MCP-1 (ng/ml)
p=0.07
PBS
5x10^8 RBC-MV
LPS
LPS + 5x10^8 RBC-MV
LPS + 1x10^9 RBC-MV

Figure 4.

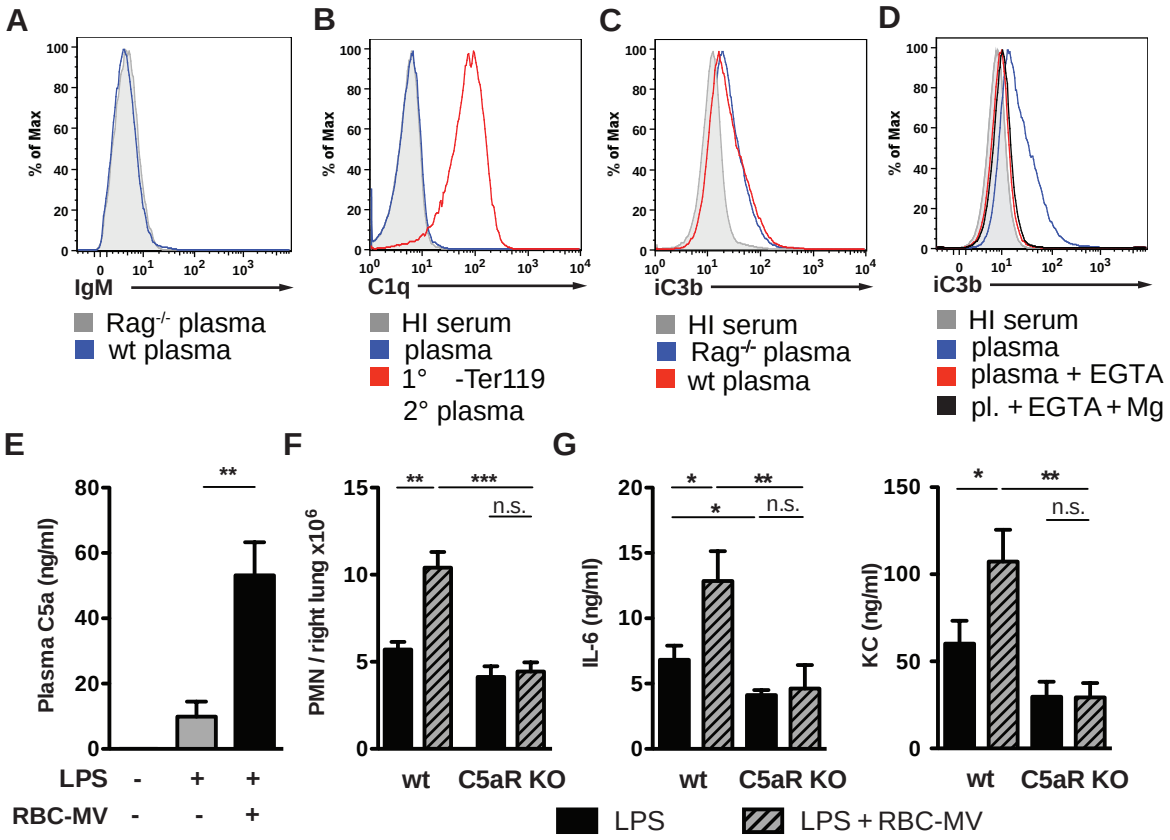
A
B
C
D
% of Max
IgM
C1q
iC3b
iC3b
Rag-/- plasma
wt plasma
HI serum
plasma
1° -Ter119
2° plasma
HI serum
Rag-/- plasma
wt plasma
HI serum
plasma
plasma + EGTA
pl. + EGTA + Mg
E
F
G
Plasma C5a (ng/ml)
PMN / right lung x10^6
IL-6 (ng/ml)
KC (ng/ml)
LPS - + +
RBC-MV - - +
wt
C5aR KO
n.s.
LPS
LPS + RBC-MV

Figure 5.

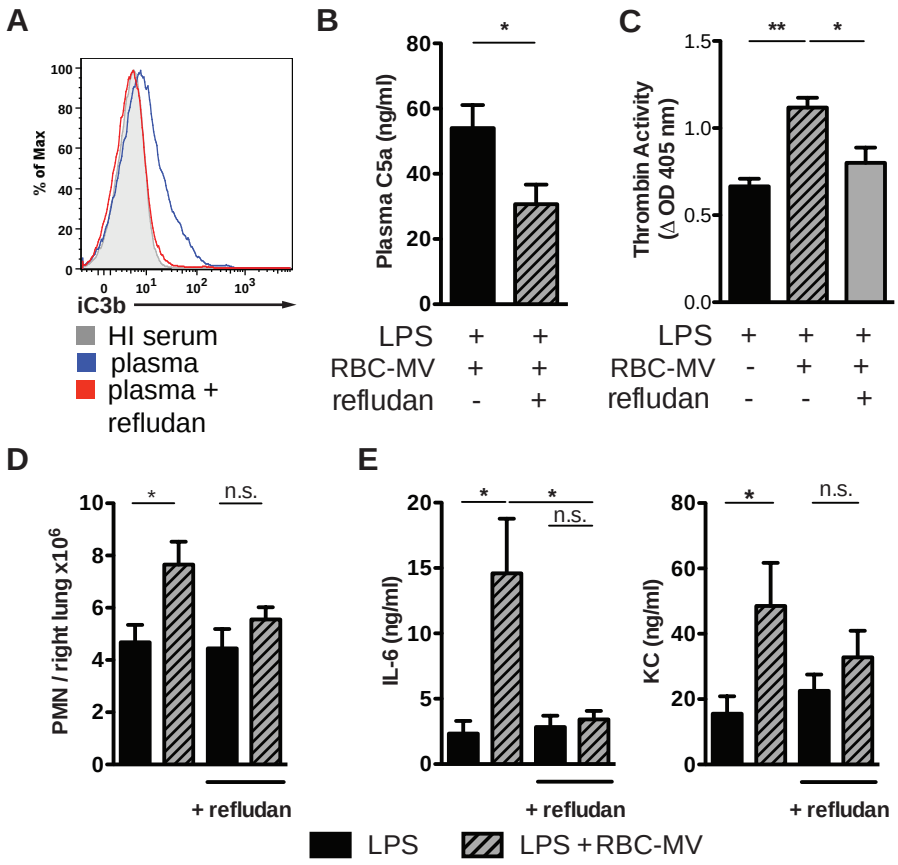
A
% of Max
iC3b
HI serum
plasma
plasma + refludan
B
Plasma C5a (ng/ml)
LPS + +
RBC-MV + +
refludan - +
C
Thrombin Activity (Δ OD 405 nm)
LPS + + +
RBC-MV - + +
refludan - - +
D
PMN / right lung x10^6
n.s.
+ refludan
E
IL-6 (ng/ml)
KC (ng/ml)
n.s.
+ refludan
LPS
LPS + RBC-MV

Figure S1.

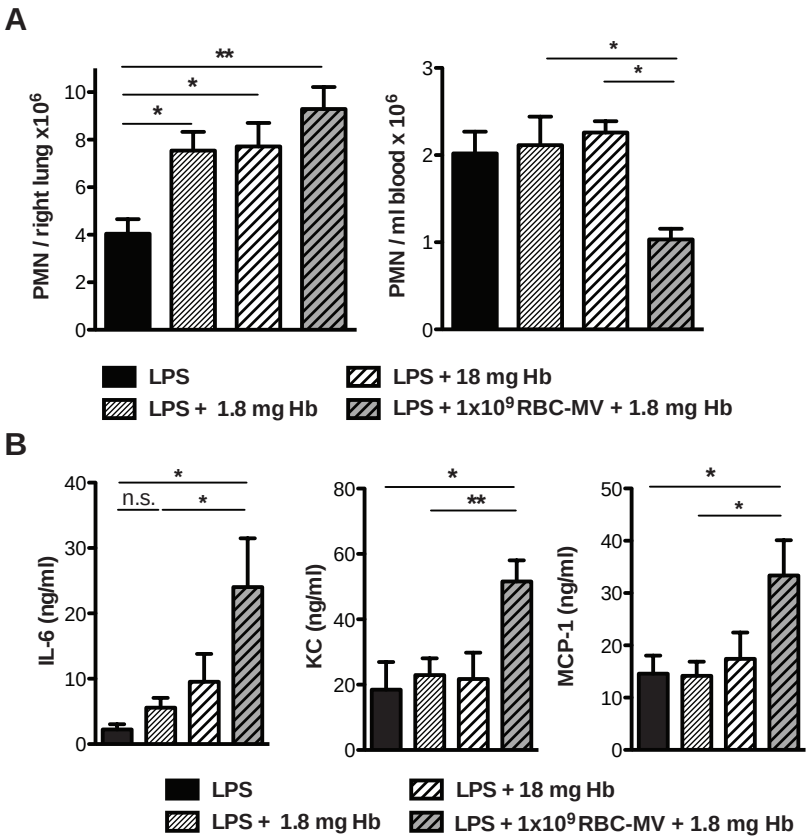
A
PMN / right lung x10^6
PMN / ml blood x 10^6
LPS
LPS + 1.8 mg Hb
LPS + 18 mg Hb
LPS + 1x10^9 RBC-MV + 1.8 mg Hb
B
IL-6 (ng/ml)
KC (ng/ml)
MCP-1 (ng/ml)
n.s.
LPS
LPS + 1.8 mg Hb
LPS + 18 mg Hb
LPS + 1x10^9 RBC-MV + 1.8 mg Hb

Figure S2.

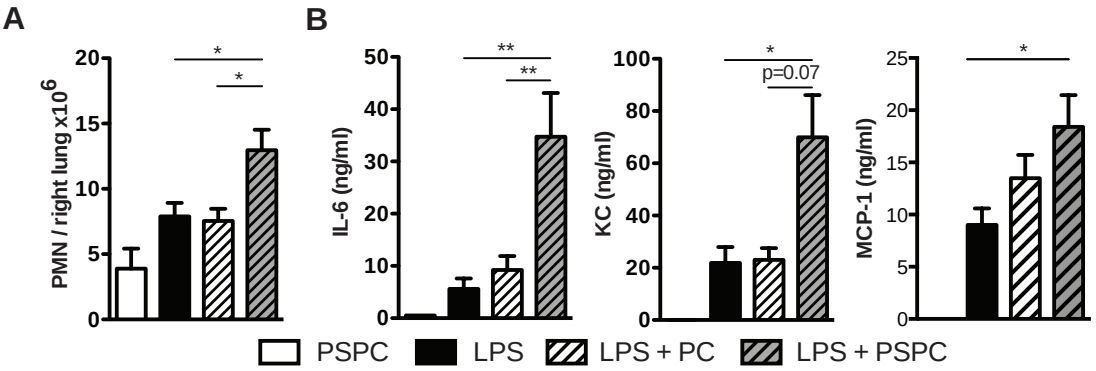
A
B
PMN / right lung x10^6
IL-6 (ng/ml)
KC (ng/ml)
MCP-1 (ng/ml)
p=0.07
PSPC
LPS
LPS + PC
LPS + PSPC

Critical points and Future perspectives

PMN-Ecto

In our MSU peritonitis model we could demonstrate that PMN-Ecto actively resolve inflammasome mediated inflammation by engaging the PS-MerTK axis. PMN-Ecto were released early on by infiltrating PMN and render cells unresponsive to pro-inflammatory stimuli. There are, however, several aspects of the MSU peritonitis model and PMN-Ecto mediated resolution that remain un-resolved.

Various stimuli have been suggested to induce PMN-Ecto release. These stimuli include fMLP, C5a, C5b-9 deposition, Ca-ionophores and PMA (1-3). Although these stimuli are structurally diverse and activate different signaling pathways, all share the ability to induce rapid Ca^{2+} influx (3-8). The mechanism triggering Ecto release therefore most likely relies on changes in intracellular Ca^{2+} concentrations. Ca^{2+} influx or the release of Ca^{2+} from intracellular stores is a feature in many signaling cascades, making Ecto release a general phenomena of cell activation, rather than a specific process linked to a particular stimulus or signaling cascade. Which stimulus is the most relevant depends on the circumstance. In gout, C5a is likely the most potent trigger for neutrophil vesiculation.

Among the various mechanism suggested to resolve gouty inflammation, some may apply to PMN-Ecto and foster their ability to inhibit IL-1β release. A group of plasma proteins called Annexins bind to PS expressing surfaces. Annexin A1 (AnA1) was shown to bind to PMN-Ecto and hinder neutrophil recruitment in response to IL-1β in an murine air pouch model (9). AnA1 act by inhibiting phospholipase A2, which in turn is responsible for the synthesis of pro-inflammatory lipid mediators derived from arachidonic acid (prostanoids and leukotriens). We could confirm low levels of AnA1 on PMN-Ecto isolated from gout exudates (Gout-MV). Interestingly, the same group reported that PMN-Ecto induce the synthesis of anti-inflammatory resolvins (RV1-2, RVE2) by macrophages (10). Resolvins are distal product of phospholipase A2 metabolites. It is not yet clear whether PMN-Ecto carry AnA1 and if so, how can they induce they synthesis resolvins and inhibit phospholipase A2 at the same time. This conflict was not discussed by the group.

There are various receptors that have the capacity to recognize PS. These include Tim4, BAI1, Stabilin 2, scavenger receptors (CD36, SRA-1), αv integrins and TAM receptors (of which Axl and Mer are expressed by immune cells). By using the MerTK$^{-/-}$ we could confirm the involvement of TAM receptors in the biological effect of PMN-Ecto. Since the loss of MerTK alone was sufficient to cancel the effect of PMN-Ecto, the contribution of Axl is unlikely. The use of an Axl$^{-/-}$ would elucidate the relative contribution of each TAM receptor. Although we saw MerTK-dependent changes in SOCS1 and 3 expression, the evidence for SOCS1/3 involvement remains associative.

PMN-Ecto have the tendency to recruit enzymes from azurophilic (myeloperoxidase, proteinase3 and neutrophil elastase) and specific (matrix metalloproteinase-9) granules once they are released during neutrophil activation (1). This has several important biological implications. PMN-Ecto induce the release of pre-stored TGFβ, but do not initiate its de novo synthesis. The mechanism of TGFβ release by PMN-Ecto is poorly understood. Matrix metalloproteinase-9 (MMP-9) and neutrophil elastase (NE) have broad substrate specificities and are known to cleave latent TGFβ (11). Specifically MMP-9 targets the protease-sensitive hinge region of LAP. Once LAP is cleaved TGFβ is released. We could demonstrate that the release of TGFβ requires phagocytosis of PMN-Ecto and is in part dependent on MMP-9 and NE. NE adsorbed on PMN-Ecto induce the release TGFβ from macrophages much faster than free NE. This was arguably due to the fact that the uptake of free NE is unspecific and relies on macro-pinocytosis, whereas the clearance of NE on PMN-Ecto is incentivized by PS. In this respect, PMN-Ecto function as an effective delivery mechanism for MMP-9 and NE.

In our model TGFβ was dispensable in the PMN-Ecto mediated resolution of acute gout. TGFβ was non-essential on 3 counts. Firstly, In the MerTK$^{-/-}$ mice PMN-Ecto failed to achieve suppression despite the significant release of TGFβ. Secondly, PMN-Ecto suppression was not antagonized by TGFβ blocking. Thirdly, recombinant active mouse TGFβ on its own did not suppress inflammation when given instead of PMN-Ecto. Interestingly TGFβ was anti-inflammatory in vitro. In vitro, recombinant mouse TGFβ inhibited inflammasome priming by specifically suppressing the upregulation of NALP3, but did not inhibit pro-IL-1β production. TGFβ therefore limits inflammasome activation in macrophages by maintaining their high activation threshold for inflammasome stimuli. This may not be the limiting factor in the acute phase of gout, but may control the recurrence of subsequent attacks.

These findings are contrary to some of the previously published studies. The conclusion that TGFβ plays a role in gout is largely based on two studies that pre-date the discovery of the inflammasome. In one of the studies TGFβ was shown to be anti-inflammatory in an MSU rat air pouch model, where extraneous TGFβ suppressed cell influx (12). In the other in vitro study MSU treated human macrophages released TGFβ, which suppressed endothelial cell and monocyte activation (13). We could not confirm the in vitro findings that macrophages release TGFβ when stimulated by MSU, but in accordance with the study, TGFβ impaired macrophage and monocyte response to LPS.

PMN-Ecto recruit myeloperoxidase (MPO) and proteinase 3 (PR3) to their surface (1). Both of these antigens are target antigens for autoimmune diseases defined by the presence of anti-neutrophil cytoplasmic antibodies (ANCA). ANCA antibodies against MPO (pANCA) and PR3 (cANCA) cause small vessel inflammation, a vasculitis, affecting the lungs and kidney. What initiates ANCA vasculitis is not yet understood, but it is hypothesized that patients with a predisposition to autoimmune disease (impaired apoptotic cell clearance) lose tolerance against MPO or PR3 during an infection. In particular Staphylococcus aureus carriers infected by Gram-negative bacteria contribute to induction and persistence of ANCA-associated vasculitis (14). Neutrophils are one of the first cell to respond and accumulate at the site of infection. They infiltrate in great numbers and typically have short life spans in the course of an immune response dying off by an apoptotic or necrotic cell death. While apoptotic cells tolerize the immune system to self-antigens, they remain apoptotic only for a short time frame and if not cleared undergo secondary necrosis. The potential for anti-inflammatory effect of apoptotic cells is therefore limited. In patients with defects in apoptotic clearance this mechanism of ensuring peripheral tolerance is less effective. PMN-Ecto generated during neutrophil activation on the other hand carry all the abilities of apoptotic cells with respect to their anti-inflammatory effects, but are released earlier and do not undergo secondary necrosis. It is plausible to hypothesize that recruitment of MPO and PR3 from fluid phase onto PMN-Ecto and the combined effect of PS and TGFβ may represent a mechanism for maintain tolerance for self-antigens susceptible to an auto-immune response. This hypothesis could be tested on an established model for pANCA vasculitis based immunization with MPO and allow us to establish PMN-Ecto release as means of maintaining peripheral tolerance .

PLT-Ecto

In our in vitro model, ATG recognized platelets and in the presence of serum induced platelet activation and release of pro-coagulant PLT-Ecto. Platelet activation and PLT-Ecto release relied on classical complement pathway activation and required C5b-7 insertion. In hematopoietic stem cell (HSCT) and kidney transplant (NTX) patients, ATG treatment brought about a state of heightened coagulation (d-dimer, TAT) and complement activation (soluble C5b-9). Although ATG induced the release of PLT-Ecto in vitro, PLT-Ecto count isolated from HSCT and NTX patients declined after ATG treatment due to opsonization and adsorption of PLT-Ecto to CR1 on erythrocytes.

Given that this was a translational project, the aim was not only to explain clotting (sub-clinical DIC) and inflammatory (SIRS, cytokine storm) complication during ATG therapy, but also suggest potential targets for prophylaxis. At present ATG pre-medication comprises of glucocorticoids (prednisone), anti-histamines, NSAID (acetaminophen) and anti-coagulants (heparin). The addition of eculizumab (anti-C5 depleting antibody) inhibited vesicle release, platelet activation and consequently pro-thrombinase activity in response to ATG in vitro and could ameliorate adverse effects of ATG therapy.

The shedding of C5b-9 complexes in the form of vesicles seems to be a generalized mechanism for evading complement mediated lysis. Vesiculation by endothelial cells may explain the phenomenon of accommodation in ABO-incompatible NTX, where kidney grafts do not undergo antibody mediated rejection despite the presence anti-ABO antibodies. To make ABO incompatible NTX possible and avoid hyper-acute rejection, recipients undergo plasmapharesis and both donor and recipient receive B-cell depleting antibodies (rituximab). Once anti-ABO antibody titers drop, the NTX can take place. Over the period of 3 months, however, recipient anti-ABO antibodies gradually return, but do not cause antibody mediated rejection. Kidney grafts undergo the so called process of accommodation formally defined as the deposition of C4d, but the absence of late complement fragments (C5b-9) on the graft (15). Hypothetically the shedding of C5b-9 complexes by graft endothelial cells during the gradual rise of anti-ABO antibodies and subsequent sub-lytic complement attack may explain the mechanism underlying graft accommodation. Alternatively, during antibody mediated rejection, the release of pro-coagulant endothelial MVs may accelerate thrombotic microangiopathy and further compromise graft microcirculation (16).

RBC-Ecto

In our murine transfusion model the injection of RBC-Ecto purified from aged erythrocytes amplified systemic inflammation in endotoxemic mice. RBC-Ecto treated mice had elevated levels of pro-inflammatory cytokines in plasma, peripheral blood leukopenia and lung leukocyte sequestration. These effects were C5aR dependent and could be reversed by inhibiting thrombin generation both in vitro and vivo. While PS liposomes were able to reproduce inflammatory effects of RBC-Ecto, systemic injection of hemoglobin contained in aged RBC-Ecto did not amplify inflammation. This suggested that PS expressed on the surface RBC-Ecto amplifies systemic inflammation by thrombin dependent generation of C5a. There are, however, several aspects of both the model and mechanism of RBC-Ecto mediated inflammation that still need to be explained.

RBC-Ecto amplified inflammation in LPS treated mice, but did not affect healthy mice. This went against our initial hypothesis where we expected inflammation with RBC-Ecto transfusion alone. There might be several reason why RBC-Ecto amplified inflammation in septic mice. Sepsis induces an acute phase response, which up-regulates critical components of the coagulation and complement cascade. With heightened sensitivity to exogenous insult, the mice were more likely to respond to RBC-Ecto transfusion. Furthermore, redistribution of leukocytes from the periphery to the lungs was more likely to occur in LPS treated mice which have activated leukocytes (C5aR expression) and lung endothelial cells (p-selectin expression). Lastly LPS treatment may have ensured longer half-life of transfused RBC-Ecto by down-regulating clearance mechanisms of the reticulo-endothelial system. It may have been necessary to saturate the clearance capacity for RBC-Ecto to allow pathology to unfold. In this respect $1x10^9$ RBC-Ecto, derived from 1ml of murine blood, needed to be transfused to achieve saturation. The amount of blood required to generate RBC-Ecto by ageing is likely an overestimation due to the fact that RBC-Ecto isolation from aged blood was very inefficient. RBC-Ecto yields from ionophore stimulated murine erythrocytes and human aged erythrocytes were substantially higher.

In retrospect we neglected to measure C5a and thrombin generation in the $C5aR^{-/-}$ mice. The proof of heightened C5a and thrombin activation in $C5aR^{-/-}$ would formally confirm that RBC-Ecto effects rely on the C5aR.

The motivation to analyze lung pathology came from a clinical observation in patients undergoing dialysis on cuprophan membranes (17, 18). These membranes had a tendency to activate complement (C5a) and patients undergoing dialysis frequently complained about shortness of breath. This was due to lung edema caused by systemic complement activation and transient leukocyte sequestration in the lung. Expecting C5a as the major culprit in the transfusion model we analyzed lung leukocyte sequestration and edema. The functional impact of RBC-Ecto transfusion on lung physiology could be further assessed by measuring blood gases and by body pletysmography. Impaired microcirculation of various other organs, such as the kidneys, is reported in septic states and may have been compromised as well.

Correlating clotting and inflammatory parameters to the amount of RBC-Ecto isolated from peripheral blood in transfused patients over time would have been a valuable addition to the project. Other conditions, such as hemolytic uremic syndrome or sickle cell crisis, could have been also included.

References

1. Gasser O, Hess C, Miot S, Deon C, Sanchez JC, and Schifferli JA. Characterisation and properties of ectosomes released by human polymorphonuclear neutrophils. *Exp Cell Res.* 2003;285(2):243-57.
2. Gasser O, and Schifferli JA. Activated polymorphonuclear neutrophils disseminate anti-inflammatory microparticles by ectocytosis. *Blood.* 2004;104(8):2543-8.
3. Stein JM, and Luzio JP. Membrane sorting during vesicle shedding from neutrophils during sublytic complement attack. *Biochem Soc Trans.* 1989;17(6):1082-3.
4. Veldkamp KE, Heezius HC, Verhoef J, van Strijp JA, and van Kessel KP. Modulation of neutrophil chemokine receptors by Staphylococcus aureus supernate. *Infect Immun.* 2000;68(10):5908-13.
5. Heinemann A, Ofner M, Amann R, and Peskar BA. A novel assay to measure the calcium flux in human basophils: effects of chemokines and nerve growth factor. *Pharmacology.* 2003;67(1):49-54.
6. Monk PN, and Partridge LJ. Characterization of a complement-fragment-C5a-stimulated calcium-influx mechanism in U937 monocytic cells. *Biochem J.* 1993;295 (Pt 3)(679-84.
7. Ribeiro CM, and Putney JW. Differential effects of protein kinase C activation on calcium storage and capacitative calcium entry in NIH 3T3 cells. *J Biol Chem.* 1996;271(35):21522-8.
8. Andrews DA, Yang L, and Low PS. Phorbol ester stimulates a protein kinase C-mediated agatoxin-TK-sensitive calcium permeability pathway in human red blood cells. *Blood.* 2002;100(9):3392-9.
9. Dalli J, Norling LV, Renshaw D, Cooper D, Leung KY, and Perretti M. Annexin 1 mediates the rapid anti-inflammatory effects of neutrophil-derived microparticles. *Blood.* 2008;112(6):2512-9.
10. Dalli J, and Serhan CN. Specific lipid mediator signatures of human phagocytes: microparticles stimulate macrophage efferocytosis and pro-resolving mediators. *Blood.* 2012;120(15):e60-72.
11. Yu Q, and Stamenkovic I. Cell surface-localized matrix metalloproteinase-9 proteolytically activates TGF-beta and promotes tumor invasion and angiogenesis. *Genes Dev.* 2000;14(2):163-76.

12. Lioté F, Prudhommeaux F, Schiltz C, Champy R, Herbelin A, Ortiz-Bravo E, and Bardin T. Inhibition and prevention of monosodium urate monohydrate crystal-induced acute inflammation in vivo by transforming growth factor beta1. *Arthritis Rheum.* 1996;39(7):1192-8.
13. Yagnik DR, Evans BJ, Florey O, Mason JC, Landis RC, and Haskard DO. Macrophage release of transforming growth factor beta1 during resolution of monosodium urate monohydrate crystal-induced inflammation. *Arthritis Rheum.* 2004;50(7):2273-80.
14. Kallenberg CG. Pathogenesis of ANCA-associated vasculitis, an update. *Clin Rev Allergy Immunol.* 2011;41(2):224-31.
15. Lynch RJ, and Platt JL. Accommodation in renal transplantation: unanswered questions. *Curr Opin Organ Transplant.* 2010;15(4):481-5.
16. Hamilton KK, Hattori R, Esmon CT, and Sims PJ. Complement proteins C5b-9 induce vesiculation of the endothelial plasma membrane and expose catalytic surface for assembly of the prothrombinase enzyme complex. *J Biol Chem.* 1990;265(7):3809-14.
17. Craddock PR, Fehr J, Dalmasso AP, Brighan KL, and Jacob HS. Hemodialysis leukopenia. Pulmonary vascular leukostasis resulting from complement activation by dialyzer cellophane membranes. *J Clin Invest.* 1977;59(5):879-88.
18. Hammerschmidt DE, Craddock PR, McCullough F, Kronenberg RS, Dalmasso AP, and Jacob HS. Complement activation and pulmonary leukotasis during nylon fiber filtration leukapheresis. *Blood.* 1978;51(4):721-30.

Acknowledgements

The work presented in this thesis was performed in the Immunonephrology Lab at the University Hospital Basel, Department of Biomedicine, under the guidance of Prof. Jürg A. Schifferli.

First and foremost I would like to thank Prof. Schifferli who gave me the opportunity to do a PhD in his lab. I am thankful for his reassuring patience, kind guidance and above all, his enthusiasm for science and medicine.

I owe a lot to Daniel Zecher, who initiated in vivo experiments in the lab and helped me immensely with all my projects.

I would also like to thank Ed Palmer for his advice and encouragement.

I thank my parents for their love and support.